Self-aligned, Capillarity-assisted Lithography for Electronics (SCALE), a New Strategy for Printed Electronics

A DISSERTATION
SUBMITTED TO THE FACULTY OF THE GRADUATE SCHOOL
OF THE UNIVERSITY OF MINNESOTA
BY

Motao Cao

IN PARTIAL FULFILLMENT OF THE REQUIREMENTS
FOR THE DEGREE OF
DOCTOR OF PHILOSOPHY

Advisors: C. Daniel Frisbie and Lorraine F. Francis

September 2019

Acknowledgements

At the beginning of this thesis, I would like to give my sincere thanks to all the people who have helped me through my graduate school. First of all, I want to thank both of my advisors, Prof. Daniel Frisbie and Prof. Lorraine Francis for their guidance and support in my research. I would like to thank Dan for giving me the freedom of exploration in research and Lorraine for her encouragement and understanding throughout my graduate study.

I want to thank Prof. Kumar for his suggestions on my research work in the printed electronics meetings. I also want to thank Prof. Sarah Swisher for allowing me to use her lab and for the valuable discussions. Many thanks to my collaborators, Prof. Jennifer Lewis and Dr. Brett Walker at Harvard University for providing me with the silver ink.

I would like to thank all my colleagues in Frisbie and Francis groups. I want to thank Dr. Wei Xie, Dr. Ankit Mahajan, Dr. Scott White and Dr. Bryce Williams for helping me get started in my research. I want to thank all the group members, Dr. Woo Jin Hyun, Krystopher Jochem, Dr. Fazel Zara Bidoky and Dr. Donghoon Song, who work together with me on the SCALE project for your generous help. I also want to give special thanks to Xinglong Ren for being a good co-worker and friend. Many thanks to Dr. Tao He, Dr. Zuoti Xie, Yan Wang, Matthew Thomas, Dr. Zhuoran Zhang, Dr. Quyen Nguyen, Xiaochen Ma, Venkatesh Paidi, Yuxin Wang and Demetra Adrahtas from Frisbie group, and Dr. Yan Wu, Dr. Yuyang Du, Dr. Tuoqi Li, Noah Holzman, Vincent Pang, Jyun-Ting Wu, Shashank Kamdar, Chengjian Zhang, Dr. Pallavi Arod and Dr. Alireza Mohammad Karim from Francis group. I also want to thank Wieslaw Suszynski for his help with

equipment training and his advice on my research. I’m very lucky to have worked with you all.

I want to give my thanks to staff members in Charfac and Minnesota Nanofabrication Center including Bing Luo, Nick Seaton, Seema Thakral, Fang Zhou, Paul Kimani and Mark Fisher for helping me with my characterization experiments and microelectronic fabrication.

At last, I want to thank all my friends for making my time at UMN a joyful and memorable journey. I want to thank my boyfriend, Tianqi Wang, for going through all the ups and downs with me in the past years. I couldn’t be where I am today without you. I want to thank my parents, Dawei Cao and Kaixia Sun for their care, love and full support in my life.

Dedication

This dissertation is dedicated to Dawei Cao, Kaixia Sun and Tianqi Wang

Abstract

With the impending development of the Internet of Things (IOT) and wearable technology, the consumer electronics market is subject to enhanced demand for flexible circuits. Printing of electronic inks is regarded as a promising route to realize low-cost, high-throughput manufacturing of flexible electronic devices for a variety of novel applications. Roll-to-roll printing, in particular, can significantly improve the throughput and further reduce production costs. Although several printing techniques, such as inkjet printing, aerosol jet printing and gravure printing, are compatible with roll-to-roll processing, there are several key technical challenges when making flexible circuits with excellent electrical performance and high yield by roll-to-roll printing. First, materials registration is a significant challenge when building multi-layer devices by printing on a moving web. Misalignment of different material layers may degrade device performance or cause electrical shorts. Patterning small features less than 10 μm is another technical challenge for printed electronics. These two challenges limit the industrial application of roll-to-roll printing.

To address these two challenges, a novel method termed SCALE (Self-aligned, Capillarity-Assisted Lithography for Electronics) has been developed to fabricate multiple components of integrated circuits. SCALE utilizes micro-imprinting to create a complex network of circular ink receivers and small capillary channels on the top surface of a plastic substrate. When inks are printed into the receivers by a drop-on-demand inkjet printhead, they spontaneously flow under capillary forces into all the capillary channels connected to the receivers. Film deposition occurs upon drying of the inks. Different films can be layered on top of one another by delivering each ink sequentially into receivers

with overlapping ink receivers or capillary channels. Since receivers have diameters on the order of 100 μm, the precision required to deliver ink is substantially relaxed. Consequently, this process is more suitable for printing on a moving web and more compatible with high-throughput, roll-to-roll processing.

In this thesis, fabrication of fully-printed resistors and low-pass RC filters via this self-aligned strategy is presented. Poly(3,4-ethylene dioxythiophene):poly(styrene sulfonate) (PEDOT:PSS) was used as the resistive material, and silver was used for the electrodes. Using SCALE, fully inkjet-printed, self-aligned resistors were achieved with resistance values ranging over five orders of magnitude while keeping the overall dimensions of the devices constant. SCALE was then employed to build low-pass RC (resistor-capacitor) filters with cutoff frequency from 0.4 - 27 kHz and excellent operational stability.

Self-aligned, fully printed diodes on plastic substrates were also demonstrated using SCALE in this thesis. A new pattern design for devices in a vertically stacked structure is reported, which incorporated flow control structures to realize better control of ink flows and to improve device yield. Printed diodes exhibited outstanding rectification ratios ($>10^4$) and excellent stability against repeated bending. Overall, the work in this thesis expands the potential of self-aligned inkjet printing for producing fully printed electronic circuits.

Table of Contents

List of Tables

List of Figures

Chapter 1 Introduction

1.1 Motivation and Background

The information revolution we are witnessing today has tremendously changed our life. This new era of information has boosted the demand for low-cost electronic devices. It also added new requirements for flexible circuits or large area circuits in order to meet special needs for some application scenarios such as wearable device, robot movement and large area displays. The forecasted annual revenues by the early 2020s ranges from $75 billion to $190 billion depends on the market for flexible electronic products [4]. To meet the growing demands of flexible electronic market, finding a way to fabricate flexible circuits at low cost and large quantities becomes more and more attractive for the semiconductor industry.

The use of printing strategies for production of flexible circuits on plastic or paper substrates is preferred for several reasons including the compatibility of printing with continuous, roll-to-roll processing, scalability to large areas at lower cost, and reduced materials waste by eliminating subtractive etching steps [5]. Silicon crystal research in microelectronics has focused on scaling down device dimensions requiring considerable improvement in device performance and integration density [6]. However, newly emerging applications such as flexible electronics require unique form factors (flexibility, thinness, lightweight) for circuit design. Envisioned applications of flexible circuit include sensors [7], large area sensor arrays [8], wearable electronics [9], displays [10], smart labels [11], and medical diagnostics [12-13]. It was found by IDTechEx Research that the total market for printed, flexible and organic electronics will increase to $77.3 billion in 2029 [14]. The main applications of that, as summarized by IDTechEx, is OLEDs, printed biosensors, and printed conductive inks. Besides, other innovative applications such as stretchable electronics, flexible energy storage devices and touch sensors also have strong growth potential [14]. Unlike semiconductor chips manufactured using traditional microfabrication methods, flexible electronic devices have less stringent requirements on device performance and dimensions. Therefore, the boosting flexible electronic market is searching for a reliable route to realize lower production costs in order to produce devices with competitive market prices.

Printed electronics offers a possible solution for large area electronics fabrication at low-cost. The production cost of circuits depends on the prices of raw materials and cost of fabrication equipment and materials processing. In printing processes, desired patterns can be directly deposited by printing in place of lithography. So, printing electronics can

considerably reduce the cost and increase the throughput by simplifying the fabrication process and eliminating unnecessary material waste. A variety of electronic materials have been reported to be printable, including conductors [15-16], semiconductors [17-18] and dielectric materials [19]. Besides, the advent of printing technology has also facilitated rapid and low-cost prototyping of circuit designs. The use of digital printing methods can significantly improve the efficiency of the development of electronic devices by reducing the turnaround time.

Among printing techniques, inkjet printing has been widely used for printed electronics demonstrations due to its numerous positive aspects including digital control, non-contact operation, materials compatibility, minimal material waste, and widespread commercial acceptance [20-34]. However, its application in high-throughput roll-to-roll processing of multilayered microelectronic circuits is limited currently by poor resolution and materials registration challenges. Printing resolution and registration are crucial in the production of functional electronic components. The current spatial resolution (> 10 μm) is insufficient for high-precision electronics [35]. Besides, the requirement for materials registration precision is at micron level for multilayered devices with excellent electrical performance.

To address these two problems, a novel inkjet-based printing method termed self-aligned capillarity-assisted lithography for electronics (SCALE) has been developed [1]. This method involves imprinting an open network of receivers, capillaries and device structures on a flexible substrate, inkjet printing electronically functional inks into the receivers and using capillarity to fill features to create electronic components. A variety of printed circuit elements fabricated via the SCALE strategy have been reported to have good electrical

performance, including transistors [1-3, 36], resistors [1] and capacitors [1, 37]. However, production of printed resistors with a wide range of resistances using this roll-to-roll compatible method has never been showed. Besides, a multilayer device with a stacked structure such as a diode has been hard to achieve using the SCALE process.

This thesis aims to present a continuing development of the SCALE strategy and further expand the applications of this technique by adding new device structures and process designs to the SCALE toolbox. This thesis describes a reliable method to fabricate self-aligned inkjet printed resistors on roll-to-roll imprinted flexible substrates with resistances ranging over five orders of magnitude. Inkjet-printed low pass RC filters with predictable and stable dynamic performance were also successfully fabricated using the SCALE process. This thesis also demonstrates a new design for fully printed and flexible diodes and diodes with a rectification ratio as high as 5×10^4 were achieved. The SCALE method appears to be a promising way to facilitate the fabrication of flexible circuits by roll-to-roll processing.

1.2 Thesis Outline

This thesis focuses on printed electronics and ways of improving the manufacturing process of circuit elements by exploring new ways to solve the existing engineering problems in roll-to-roll printing, including increasing printing resolution and realizing materials registration.

- Chapter 2 gives an introduction of printed electronics. This chapter covers trending applications of printed electronics and common printing techniques that can be employed in fabrication of semiconductor devices. Then, roll-to-roll printing, a

production method that is promising for large-scale manufacturing of electronic devices, is illustrated with its advantages and major technical challenges highlighted.

- In Chapter 3, a novel printing method termed “SCALE” is introduced aiming at addressing the technical challenges in roll-to-roll printing. The advantages of this new strategy are first discussed. This is followed by an illustration of the process flow. Then a summary of recent developments in SCALE is presented and the existing challenges are pointed out.
- Chapter 4 gives an example of electronic components fabricated via the SCALE process. Fully printed resistors with a wide range of resistances and low-pass *RC* filters with tunable cut-off frequency were created using this roll-to-roll compatible method. Details about design improvement and ink material optimization are discussed. Then, device performances for both the resistor and the *RC* filters are displayed and discussed.
- Chapter 5 continues with the research work on the development of the SCALE process. A new device pattern design is introduced to print multilayer devices in a vertically stacked structure. The new design involves multiple flow control structures to manipulate flow distance and direction. Printed diodes based on this new design are shown to have good electrical performance. Dynamic performances of printed diodes are also evaluated along with their mechanical durability against bending.
- Chapter 6 focuses on the outlook of the SCALE process. Four possible future directions are discussed in detail, including shrinking the device footprint, a new

design for multilayer devices, improving the device flexibility and fabrication of functional circuits.

Chapter 2 Printed Electronics

Printing technologies were invented for storage and exchange of information and are extensively used in publishing industry. Recently, printing techniques have moved to new areas of manufacturing, for example, semiconductor industry. The use of printing strategies for production of flexible circuits on plastic or paper substrates is attractive for several reasons including the compatibility of printing with continuous, roll-to-roll processing, scalability to large areas at lower cost, and reduced materials waste by eliminating subtractive etching steps [5]. These positive attributes have motivated the rapid development of printed electronics.

2.1 Applications of Printed Electronics

With the rapid progress of internet of things (IOT) [38] and wearable technology [39-40], the consumer electronics market is subject to witness an enhanced demand for flexible circuits. There is a prominent rise in the usage of flexible electronic devices in the information age, and work has been done to lower the cost of those ubiquitous devices. Printed electronics is regarded as a promising route to realize a dramatic reduction in the production cost of flexible electronic devices, which can find applications in a variety of new areas, including smart labels [11, 41], wearable sensors [42], displays [43-44], flexible batteries [45-46], and medical diagnostics [12-13].

2.1.1 Flexible displays

The breakthrough in organic light emitting diodes (OLEDS) has led to widely application of OLED techniques in consumer electronics market. Although most of the OLED products in the market right now are fabricated using traditional vacuum deposition methods, printing provides a promising way to substantially lower the production cost and make OLED products accessible to a larger population. Printing techniques can be utilized to manufacture both OLED pixels and the backplane circuits based on thin film transistors (TFTs) designed to drive the pixels, so it is promising for printing to overcome production challenges in order to manufacture the OLED TVs in volume.

TFT circuit-based backplanes are a critical part of displays. Fully printed and flexible active-matrix backplane has been successfully fabricated using carbon nanotube TFTs [47]. In displays, high current densities are preferred, which demand high performance thin film

transistors. Shorter electrode separation and semiconductor films with higher mobility lead to higher switching speed of transistors. When it comes to fully printed transistors, it is important to increase the printing resolution and improve the quality of printed films.

One existing challenge in fabricated printed OLED pixels is to print films with uniform thicknesses, which is very important for their application in displays. OLED pixels are usually printed in confined grooves. Printed films typically have a higher film thickness variation compared with vacuum evaporated films due to the drying behavior of drops. [48] Optimization of drying conditions and ink properties is required to improve the printed film quality.

2.1.2 RFID tags

Distributed electronics is important power sources for the idea of "Internet of Everything (IOE)". Among them, RFID (radio-frequency identification) tags are important to realize item-level tracking of products [49]. RFID has broad applications in our daily life including retail, pharma and payments and may become ubiquitous when the age of "Internet of Everything" arrives. For example, RFID tags can store more information when integrated to packages. IDTechEx forecasted that 28 billion RFID tags will be sold in 2020 [50]. Among them, disposable RFID tags are highly demanded for applications including smart packages and medication. So, it is required to produce RFID tags in large quantities at low cost to make the price competitive.

Printing RFID tags in large quantities is a promising pathway to realize low fabrication cost. There are several reports showing that fully printed RFID tags can operate at a frequency above 13.56 MHz, making it realistic for near field communication [41, 51-54]. A

fully printed humidity sensor fabricated by roll-to-roll gravure and roll-to-roll coating has been reported with the ability of wireless communication [54]. In this work, antenna, diodes, capacitors and humidity sensors were printed on PET films, and electrochromic signage units were deposited by roll-to-roll coating. Another report on printed RFID tags used roll-to-roll gravure printing (Figure 2.1) to fabricate antenna, rectifiers, and ring oscillators on plastic substrates [51]. Printed RFID tags (Figure 2.1 (a)) can operate at a frequency of 13.56 MHz. So, it is promising to produce RFID tags at ultralow cost and large quantities.

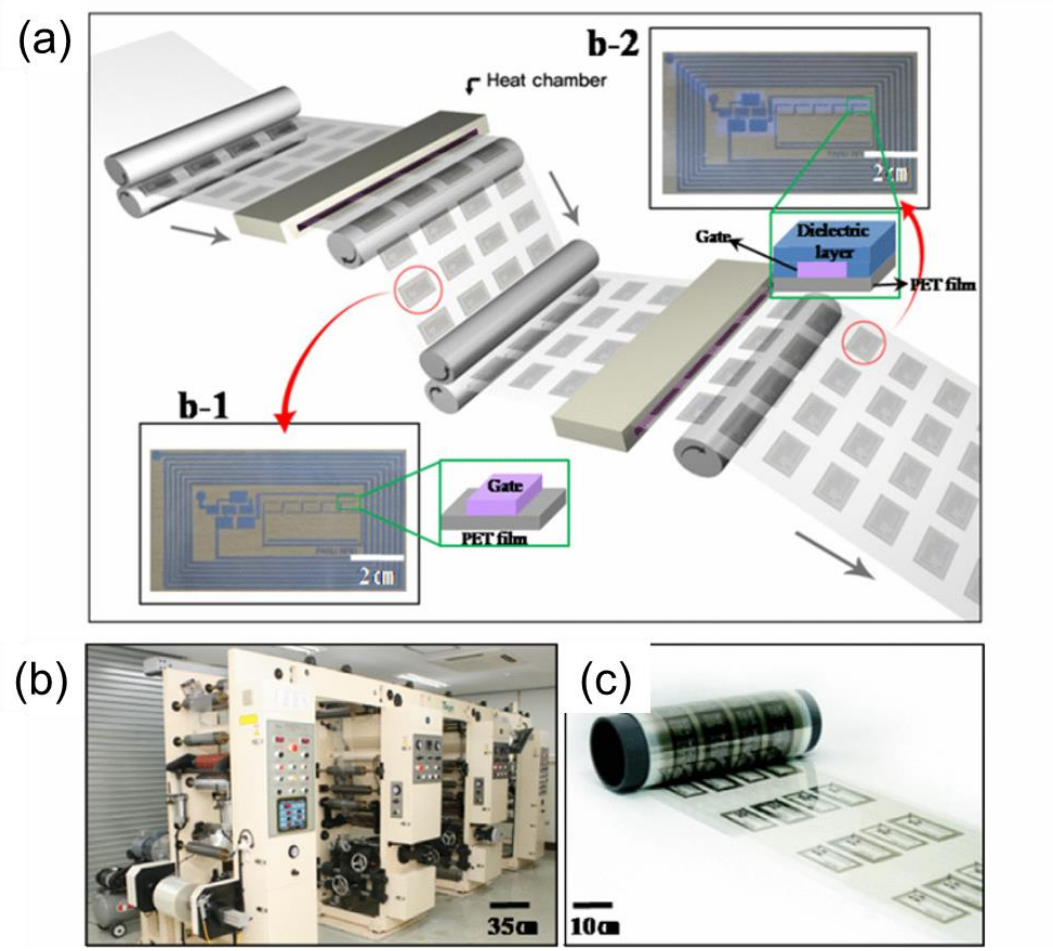

Figure 2.1 (a) Schematic illustration of roll-to-roll gravure printing, (b) picture of gravure printer, (c) Roll image of the completed R2R gravure-printed components for 13.56-MHz-operated 1-bit RF tags. Adapted from [51]

2.1.3 Stretchable electronics

The advent of wearable electronics has created a high demand for stretchable electronic devices. Stretchable electronics allow us to put function into clothes by, for example, embedding solar cells or heating circuits into fabric [55]. In medical area, metallic thin-film based flexible circuit can serve as heating smart patch for thermotherapy [56]. Besides, stretchable electronic devices can provide flex to rigid integration by connecting rigid devices on silicon to flexible components on flexible substrates. These novel applications of stretchable electronics can provide innovative solutions to problems in our daily life by overcoming the limitations of rigid substrates in traditional silicon-based electronic products.

Employing flexible substrates such as plastic and textile makes it hard to deposit and pattern films using traditional semiconductor manufacturing processes. Printing methods are more suitable because they can easily accommodate different kinds of substrates. The processing temperature in printing processes is also lower, which is compatible with inexpensive plastic substrates. Besides, conducting polymers are a promising material system for applications of stretchable electronics due to their inherent flexibility. A variety of organic electronic materials has exhibited excellent solubility, printability and electrical performance, which makes printing methods more attractive for stretchable electronics applications [57].

Current challenges of making stretchable electronic devices come from the degradation of electronic materials during long term operation. Repeatable bending and stretching may lead to cracking and delamination of films from the substrate or other defects that may

introduce instability in device performance. Resistance against washing is another concern of clothes imbedded with circuits.

2.1.4 Sensors

Sensors are an essential part of the concept of Internet of Everything (IOT) and are widely used in our daily life. Sensors are capable of responding to various types of external stimuli and can be integrated into monitoring systems to detect their ambient environment. Sensors can be utilized for environmental, healthcare and industrial applications. For example, optical sensor is an attractive application that has been studied for decades. Optical sensors are preferred for remote detection. They have the ability to instantly respond to changes of various properties of light including frequency, intensity and polarization [58]. Up to now, sensors fabricated on rigid silicon substrates still dominate the market, but several disadvantages associated with them limit their application in some emerging areas. The fabrication cost of silicon-based sensors is high, and they are subject to mechanical damage when bended. So, when it comes to novel applications such as disposable sensor patches, wearable devices and robot arm sensors, the usage of a cheaper and more flexible sensor is preferred.

Printing techniques are known for compatible with a wide range of flexible substrates. Besides, the low-cost feature of printing makes it more attractive for fabricating disposable sensors. A wearable sweat-based sensor has been printed to provide a new way of measuring glucose, monitoring heart rate and other vital signals by analyzing user's sweat [59]. Recently, printed sensors based on carbon nanotube (CNT) has been extensively investigated for applications including electrochemical sensors [60], strain sensors [61] and

tactile sensors [62]. CNT was chosen as the functional material due to its specific advantages like high flexibility, good dispersity after functionalization and biocompatibility. Although research in printed sensors are developing rapidly, further improvement in sensitivity and sustainability lies in increase of printing resolution and optimization of material system such as eliminating of insulating component in the sensing layer.

2.2 Overview of Printing Techniques

Printing technology refers to a patterning method by selectively depositing a solution or ink onto a substrate. Printing technology was invented in around 3500 BCE and was extensively used in publishing industry. Recently, the application of printing technologies has moved into new areas of manufacturing and printing starts to play a vital role among all the semiconductor fabrication techniques targeting low-cost and large-scale manufacturing. In microfabrication area, printing allows fast deposition of electronic materials without further patterning. Printing significantly simplifies the steps of creating a pattern compared with traditional photolithography-based methods. Printing also endows semiconductor manufacturers with the additional capability to reduce material waste and to lower fabrication cost. Compared with vacuum deposition, the requirements on deposition environment and deposition equipment are lower because printing is usually done in air. So, this feature can significantly reduce the cost coming from purchasing and operating the deposition tools. In addition, printing is a more environmental-friendly fabrication method. Some photoresists and their developers are classified as harmful to human health or even very toxic on single exposure. Printing is an additive manufacturing method, which means it can decrease the disposal of photoresists and hazardous solvents

by eliminating the photolithography and the lift-off steps in circuit fabrication. So, printing provides a considerable number of advantages including low-cost, simpler processing, less stringent requirements on deposition environment, reduction of hazardous waste and flexibility of process design.

Printing methodologies can be classified into two categories, contact and non-contact. Contact printing, including screen printing, gravure printing and stencil printing, involves the use of a mask or a stamp for patterning. Contact printing usually have a higher printing speed and suitable for large-area electronics. Non-contact printing techniques, including inkjet printing and aerosol jet printing, enable mask-free fabrication in an additive rather than subtractive manner and avoid the film defects generated in the delamination process of contact printing. The choice of a printing technique for a certain application depends on the requirement of printing resolution, material selection, the scale of production and commercial availability.

2.2.1 Inkjet printing

Inkjet printing is a non-contact, digital printing technique which was invented in 1960s. It is designed to deliver small and finite amounts of ink onto a substrate on a variety of substrates including paper, plastic and fabric. Inkjet printheads, which are used for the generation and ejection of the ink drops, are mounted on a carrier. A 2D-pattern can be converted into the instructions that drive the movement of the printhead or the substrate or both to create a printed pattern drop by drop. It is easier to adjust the pattern created by inkjet printing compared with other printing methods such as gravure printing which relies on a physical mold or mask for patterning.

Existing inkjet printing techniques can be classified into two categories based on the delivery of the drops, continuous inkjet printing (CIJ) or droplet on demand printing (DOD) (Figure 2.2). Depending on the way the droplets are generated, inkjet printing can also be categorized into electrohydrodynamic jet printing and piezoelectric inkjet printing (Figure 2.2). In electrohydrodynamic jet printing, ions created by an electrical field applied between the nozzle and the substrate accumulate at the liquid surface. The liquid meniscus changes into a conical shape due to the Coulombic repulsion of ions. So, droplet size is much smaller than the nozzle orifice, which can reduce the printed feature size down to less than 1 μm [63]. The work in this thesis was done using a piezoelectric drop-on-demand inkjet printer. The deposition of individual drops was realized by pressure pulses created by a piezoelectric transducer. When an external voltage is applied to the piezoelectric transducer, it deforms and leads to a sudden reduction of the ink chamber volume. This sudden reduction starts a shockwave within the ink in the chamber, causing the ejection of a drop out of the nozzle [64]. The drop volume is around picoliter [65] and can be adjusted by modifying the voltage waveform applied to the piezoelectric transducer. The drop then spreads to a diameter of several decades of μm on the substrate. Surface tension and viscosity of inks and surface energy of the substrate will determine the spreading of the printed features. Ink spreading, along with the nozzle orifice, will influence the printing resolution.

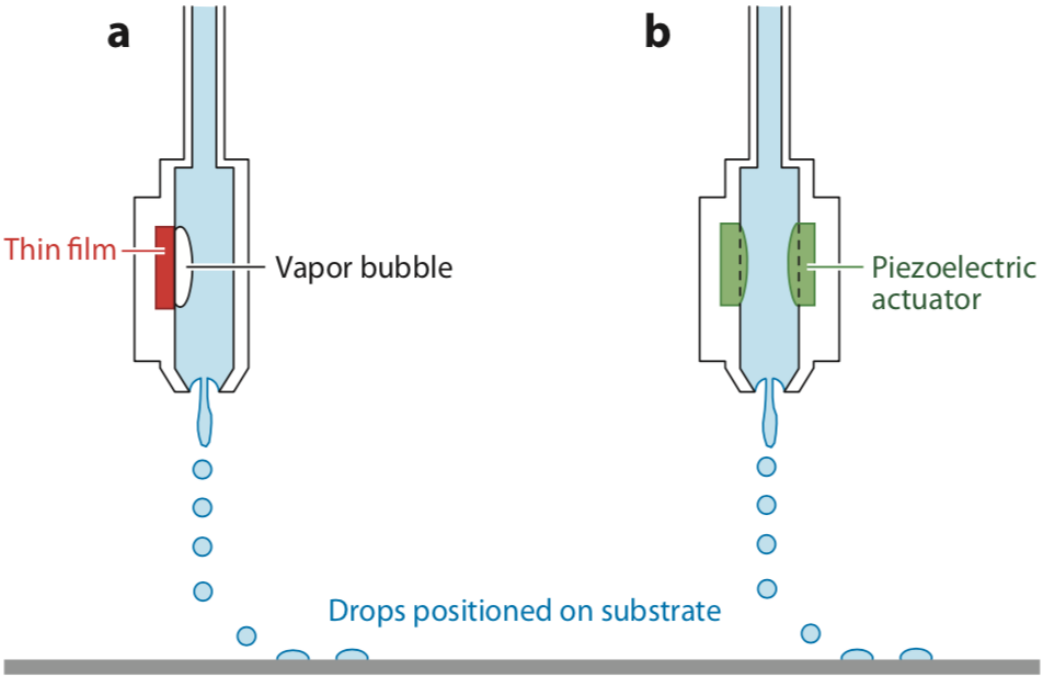

Figure 2.2 Schematic illustration of drop-on-demand inkjet printing. (a) thermal inkjet printing and (b) piezoelectric inkjet printing. Adapted from [66]

This technique is compatible with a variety of electronic inks, including conducting polymers, metal oxide, metal and carbon-based materials [25, 30, 67-68]. Also, a lot of commercial inks formulated for inkjet printing are available now in the market. In the near future, incorporating inkjet printers into a production line is a promising route to commercialize this technique and to realize large-scale production of printed circuits.

2.2.2 Aerosol jet printing

Aerosol jet printing (AJP) is also a digital non-contact printing method. Aerosol jet printing can achieve featured sizes as small as 10 μm by using a focusing sheath gas. This flowing gas also prevents clogging in the printer head allowing aerosol jet printing to accommodate a wide range of ink viscosities.

Aerosol jet printing can tolerate a wider range of ink viscosity and achieve a higher spatial resolution compared to alternatives such as inkjet printing. The aerosol jet printing process is shown in Figure 2.3 (a) where it is broken down into three steps. First, liquid ink is atomized and a dense aerosol is created. Then the aerosol is transported to the print head by an inert carrier gas through a plastic tube. Finally, aerosol stream is focused by a sheath gas and ejected at a high velocity [69]. Process parameters have a definitive influence on the morphology of printed films, which has been systematically studied [69-70]. This technique can define a line as narrow as 10 µm. A variety of inks have been aerosol jet printed into thin films including conductors [70], semiconductors [71] and insulators [72]. Aerosol jet printing can also be applied to fabricate transistors, bio-sensors and display circuits, [72-74].

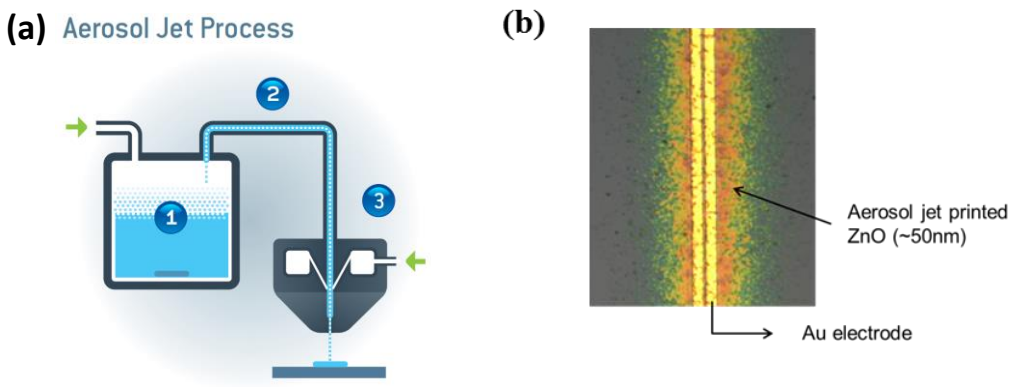

Figure 2.3 Aerosol jet printing. (a) AJP process, from aerosol jet printing 200 data sheet by Optomec® and (b) An example of aerosol jet printed lines.

However, application of aerosol jet printing is hindered by the roughness and porosity of printed film. One drawback of aerosol jet printing is when nanoparticle inks are printed, they tend to form porous films with low density and conductivity, which can significantly impact the electrical performance of printed devices. This drawback to some extent limits

the range of available inks for aerosol jet printing. Overspray is another issue involved in the aerosol jet printing process. The overspray widens the printed feature and results in a pattern with rough edge, which is shown in Figure 2.3 (b).

2.2.3 Screen Printing

Screen printing is a contact printing method which is currently used in textile industry. In screen printing, ink materials are pushed through a screen onto the substrates. Excess ink is removed afterwards by a squeegee. In screen printing, the emulsion is supposed to keep from drying in the screen due to solvent evaporation. Instead, the ink is dried by heat or light exposure after the printing. Screen printing is preferred for its inherent scalability and its simplicity of materials registration because layer-to-layer alignment is performed in a parallel-plate manner [47, 75]. The integration of screen printing as a scalable method to roll-to-roll processing is also possible by replacing the plenary screen with a cylindrical screen.

The possibility to screen print on large-area and flexible substrates at a faster speed compared to digital printing methods has made it attractive for a variety of applications. All screen-printed transistors, resistors and diodes [47, 75-78] has been reported up to now. The bottle neck of screen-printed electronic circuits lies in the difficulty to further improve the printing resolution. One method to improve the resolution is by developing new screen masks because the resolution of screen printing is dictated by the quality of the mask. Screen printed graphene with a silicon stencil has been reported to be able to print a feature of 5 um [79]. Transistors with screen printed graphene as the electrodes were also

demonstrated to have excellent electrical performance. Silver lines with a width down to 22 μm was also achieved in the same way [76].

2.2.4 Gravure Printing

Gravure printing is also a contact printing method. It began in the early fifteen century and was used in the printing of publications, packaging and special products. In gravure printing, the pattern was etched on the surface of a gravure cylinder. Etched cells are recessed into the cylinder and are used to hold the inks. The unetched area of the surface is at the original level. When printing starts, the rotating cylinder is dipped slightly into the ink to feed ink into the recessed cells. And the ink attached to the unetched area of the surface is wiped or removed by a doctor blade. Then the substrate is pressed against the inked gravure cylinder by the impression cylinder. Ink was transferred partially from the cells on the gravure cylinder to the substrate. The process is depicted schematically in Figure 2.4 [80].

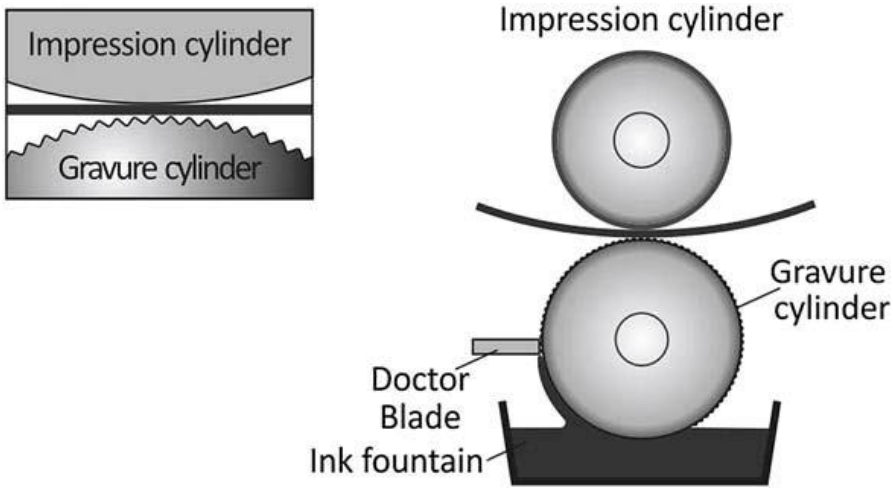

Figure 2.4 Schematic drawing of the gravure printing process. Adapted from [80].

Gravure printing is preferred for the ability of producing high-quality printing patterns at a high speed. Besides, this technique is ideal for extremely long runs since metal cylinders can last for several million impressions. In printed electronics, gravure printing is attracting a lot of attention due to its advantages including high resolution (smallest line width around 20 μm) [81], compatibility with low viscosity inks, solvent resistance of the gravure cylinder and long-run stability at high printing speeds (around several meters per min) [82]. In order to further improve the printing resolution to meet the requirements of electronic circuit production, laser technologies are utilized for engraving cylinder surfaces instead of traditional electromechanical engraving. Up to now, gravure printing has demonstrated the ability to print conductive features [82], capacitors [83], RFID antenna [84], and OLEDs [85].

2.3 Roll-to-roll Printing and Current Challenges

The development of economically viable electronic devices demands high throughput processes. Roll-to-roll printing, which combines roll-to-roll processing and printing techniques, is a promising fabrication approach for the manufacture of large-scale and flexible circuits at low cost (Figure 2.5). Roll-to-roll printing integrates several printing and annealing units together in sequence into a production line, which provides a viable way to significantly boost the productivity and reduce the cost of making large area electronic systems.

Integrating gravure printing with roll-to-roll processing is relatively easy among all the printing techniques, which has been demonstrated [81, 86]. Rotary screen printer in a roll-to-roll line has also been reported to print polymer solar cells [87]. Hosel, et al. have demonstrated roll-to-roll flexographic, inkjet, flatbed, and rotary screen printing and

evaluated their application in printing metal electrodes for solar cells [88]. Among them, roll-to-roll flexographic printing was highlighted because it represents the lowest cost, lowest materials consumption and fastest processing speed. However, printed solar cells usually has less stringent requirements for resolution or alignment. So, when it comes to other devices such as transistor, other printing techniques with higher resolution may be preferred in a roll-to-roll line.

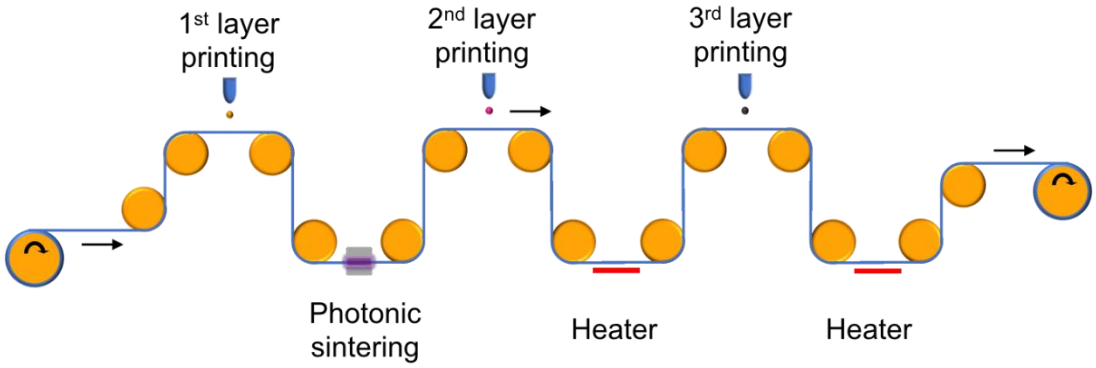

Figure 2.5 Schematic illustration of a roll-to-roll printer with printing and annealing units integrated

Heating units are also necessary in a roll-to-roll printing line because drying and annealing steps are needed to form a high-quality film after printing. Photonic sintering and IR heating are preferred annealing methods for roll-to-roll printing. Photonic sintering is a roll-to-roll process where the thin film is rapidly heated by absorbing intense light from a flash lamp. The printed semiconductor films have a higher absorbance of the radiant energy from the flash lamp compared to the underlying plastic substrates, which results in a lower temperature in substrates. Moreover, each pulse only lasts for several milliseconds, and therefore the heat transfer to the underlying polymer substrate is limited, preventing severe damage to the substrate. From a processing standpoint, this ultrafast annealing technique can reduce the thermal processing time down to a few minutes. Additionally, this process can be performed under ambient conditions eliminating the need for an inert

environment. IR heating is another promising annealing method for roll-to-roll printing. IR heating is suitable for sintering metal particles to improve film conductivity [89].

Although roll-to-roll printing has shown promising future, some major engineering problems has to some extent limited its viability in mass production of electronic circuits. When printing technologies are applied in the manufacturing of electronic circuits, the requirements of printing quality are far beyond satisfying a resolution of human eye, which is the major demand of traditional publishing industry. The application of printing in high-throughput roll-to-roll processing of multilayered circuits is limited currently by poor resolution and materials registration challenges. Printing resolution is very important for making electronic circuit. For example, reducing the distance between the source and drain electrodes of a transistor can significantly increase the operating speed of a transistor, which is an important metric of a printed transistor. Besides, smaller features are preferred to achieve higher device density. However, resolution less than 10 μm is not easy to achieve by printing techniques alone. Modification of the substrate is usually needed to increase the resolution.

Besides, the materials registration is not precise enough to create a multi-layer device with satisfactory electrical performance, especially for printed transistors. As the device size shrinks, the requirement for alignment precision also increases. Both the limitations of the printing technique and substrate deformation impact the alignment precision. In inkjet printing, for example, the alignment precision is influenced not only by the mechanical alignment of the printhead to the target, but also by the deviation of the ink drop from the original path. These problems become more severe when the printing process is done on a

continuously moving web. And the deformation of plastic substrates makes the alignment issue more complicated. These problems must be addressed before roll-to-roll printing can really be used for large-scale production in electronics industry. Much effort is taken to improve printing resolution and to investigate reliable routes to assist layer to layer alignment.

Chapter 3 Self-aligned, Capillarity assisted Lithography for Electronics (SCALE)

This chapter depicts the background, design, process flow and existing challenges of a novel printing method termed SCALE. As has been discussed in preceding chapters, Printed electronics is an emerging area for large-scale manufacturing of electronic circuits at low cost. But future development of massive production of printed electronic devices is limited by resolution and registration accuracy of current printing techniques. SCALE, a novel printing method which combines inkjet printing and imprinting, was developed in our group to address these two concerns. Here, SCALE is short for Self-aligned, Capillarity-assisted Lithography for Electronics.

3.1 Background

To address the challenges with roll-to-roll printing, research has been going on to search for novel printing routes. This part presents a brief overview of the existing self-aligned technologies and resolution improving methods of printing.

3.1.1 Overview of self-aligned technologies

One strategy of self-aligned printing is taking advantage of the ink dewetting on a chemically modified surface. Sirringhaus group invented a self-aligned printing (SAP) process that is capable of defining submicron critical features using inkjet printing [90]. Sub-100-nm channel length between source and drain electrodes can be fabricated for a transistor. This process relies on a good control of the contact angle of the ink on the chemically modified feature and a short drying time. In another report on self-aligned printing techniques, a top-contact self-aligned carbon nanotube thin film transistor was printed with a sub-micron channel length (Figure 3.1). In this report, the semiconductor layer and one electrode were printed first, followed by a self-assembly monolayer. When the second electrode was deposited over the semiconductor layer, the dewetting of the ink left a sub-micron separation between the two electrodes, which were the source and drain electrodes [91].

Another strategy of self-aligned printing utilizes a mechanical self-alignment mechanism to replace the optical alignment. Syms, et al. built a multilevel microcontact printing (μCP) system [92]. Figure shows the alignment process schematically. In this case, desired features and protrusions were pre-patterned on a PDMS stamp. Self-alignment

between layers was realized by mating the protrusions on the PDMS stamps onto corresponding grooves on the substrate. An average misalignment of 5 – 10 μm was claimed between layers. Using backside photolithography is another promising route to achieve layer-to-layer alignment. This process involves printing a UV-blocking mask layer with the desired pattern on a UV-transparent substrate. Then a UV-sensitive material is coated on top of the mask layer and also over the rest area of the substrate. After a UV-exposure from the backside of the substrate, the property of part of the UV-sensitive layer that doesn't have blocking layer underlying changes due to the UV illumination. The part of the UV-sensitive material right on top of the blocking layer remains unchanged. In the subsequent developing step, the unexposed part can either be washed off or remain on the substrate depends on the polarity of the UV-sensitive layer. So, a pattern can be created on the second layer and it is self-aligned to the bottom layer. Both the UV-blocking and the UV-sensitive layer can serve as functional layers in an electronic device or a dummy material to construct a groove. For example, Korvink et. al used a similar method to form electroplated thick-layered conductive features by inkjet printing a Ag-nanoparticle layer and then using the patterned seed layer as a shadow mask when back-exposing the negative photoresist layer on top of it [93]. After developing the photoresist, unexposed part of the photoresist, which was the area overlay with the Ag pattern, was washed off. Then a thick Cu film grew on top of the Ag seed layer and within the trench formed by the photoresist. After stripping all the residual photo resist, a thick and patterned Ag-Cu film was obtained, which was used as micro-coils in magnetic resonance microscopy. A similar method was used to successfully fabricated Ag/Cu electrodes for a transistor [94]. The electrodes were covered by a passivation layer, which was patterned by backside exposure, to reduce the

parasitic capacitance of the printed transistor. This backside photolithography method can also be used in the alignment of multiple layers in a transistor, which is much harder to achieve than fabricating a conductive layer.

Although several techniques have been approved to achieve self-alignment, it is still a challenge to self-align all the layers of a multi-layer device. Besides, these techniques are not completely roll-to-roll compatible, making it hard to upscale the fabrication to mass production. Some steps still involve alignment of the printhead to a small existing feature. A rigid mask, which cannot be used in roll-to-roll printing, is needed in some cases to achieve required precision. More investigation is needed to develop a reliable roll-to-roll compatible fabrication method.

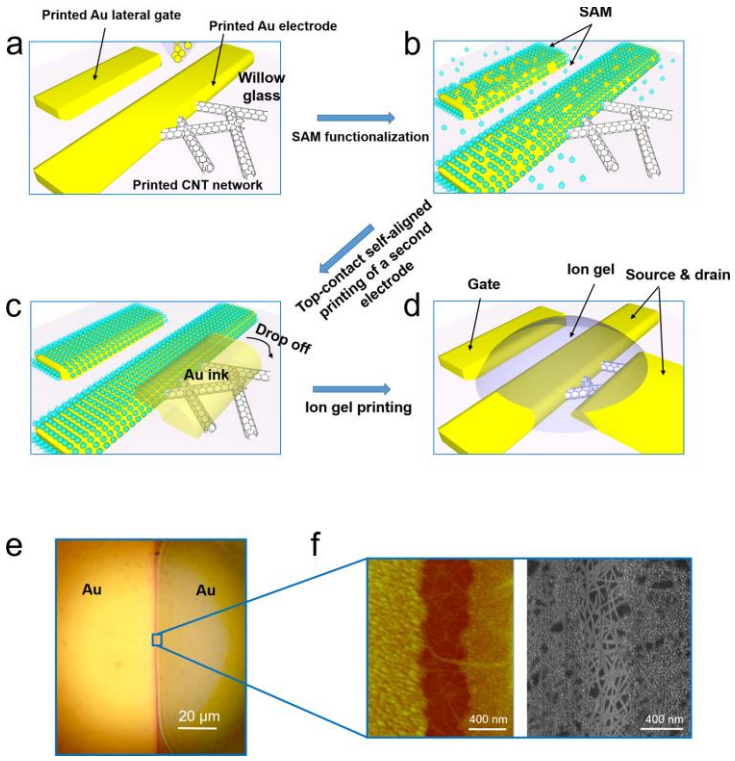

Figure 3.1 Process of self-aligned printing of CNT TFTs. (a) Printing the first Au electrode on pre-coated CNT network. (b) Medication of the surface by a self-assembly layer. (c) Printing the second Au electrode which is self-aligned to the first electrode due to contact line receding on the modified surface. (d) printing the dielectric layer. (e,f) the gap between two Au electrode. Adapted from [91]

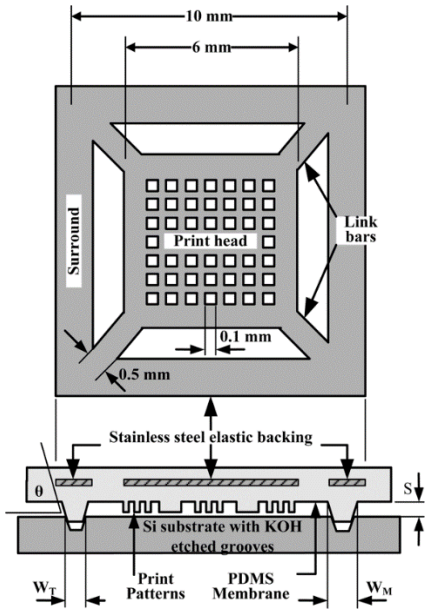

Figure 3.2. Self-aligned μCP system. Adapted from [92]

3.1.2 Overview of resolution improvement methods

Patterning resolution, which is an important metric for semiconductor manufacturing, is critical for the both device performance and device density. Without the help of photolithography, however, resolution that can be achieved using printing techniques only is relatively low for producing electronic devices that requires high resolution patterning. In general, features less than 10 μm are hard to print reproducibly. Besides, small gaps that are defined uniformly between two features are hard to print due to the scalloped or wavy edges.

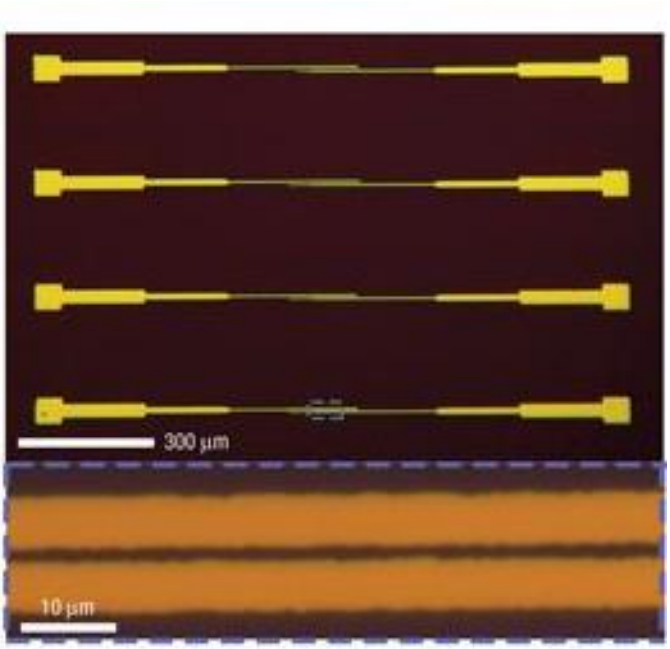

Figure 3.3 Array of source/drain electrodes with a separation of around 1 μm fabricated by electrohydrodynamic printing of photoresist layer, etching of the electrodes and removing the resist. Adapted from [63]

The resolution of printing highly depends on the specific printing method, ink properties and substrates [66]. For example, researchers have been working on updating the printing apparatus in electrohydrodynamic printing to improve the printing resolution. Wang et.al. improved the printing resolution of an electrohydrodynamic printer by introducing a triboelectric nanogenerator to provide the driving signal for droplet generation [95]. Rogers et. al also employed electrohydrodynamic printing and achieved sub-micron gap between two linear electrodes (shown in Figure 3.3) using microcapillary nozzles [63].

Similar to self-aligned strategies, surface modification can facilitate printing small features by controlling the ink spreading and the final deposition. Sirringhaus and co-workers utilized heterogeneous surfaces to exerted forces on printed droplets on the substrate [96]. Small distance less than 100 nm between two electrodes was achieved by controlling the motion of the receding contact line. Soft lithography can also be used for increasing printing resolution. IBM demonstrated a high-resolution printing method which utilized soft lithography [97]. A resist-forming ink was first coated onto a patterned elastomer stamp and then transfer printed onto a gold film. In the subsequent etching step, dried resist-forming ink served as a mask to protect the gold below it and patterning of the gold layer was achieved. A resolution compared to optical lithography (~100 nm) was achieved using this method. Although the photolithography step is replaced by transfer printing, one drawback of this transfer printing method is that a subsequent etching step is still needed.

Another method to improve the resolution is by introducing tracks of inks on substrates to guide ink flows. Schubert et.al patterned plastic substrates with grooves or microfluidic channels having widths ranging from 5 – 15 μm by hot embossing [98]. Ag features were

printed by dispensing Ag inks and allowing inks to flow along the tracks. These tracks provided geometric confinement and realized printing features smaller than the size of droplets by inkjet printing.

Despite these reports on reducing printed feature sizes, most of the existing strategy still requires alignment of the print head to a small feature. Besides, finding a reliable method to achieve both small features and small and uniformly defined gaps at the same time still remains a challenge in printed electronics.

3.2 SCALE

As has been discussed in the previous part, surface modification by embossing the substrate with microfluidic channels is a promising route to get around the existing problems. In fact, miniaturized fluidic systems has been used as fluid handling system in biology area for a long time, and liquid flows in microfluidic channels has also been extensively investigated [99]. Microfluidic system can help address the existing resolution and registration challenges with roll-to-roll printing. The idea and past experience of microfluidic system design and fabrication can be borrowed and employed in printed electronics.

In this case, a novel inkjet-based printing method called self-aligned capillarity-assisted lithography for electronics (SCALE) has been developed [1]. The SCALE process starts with imprinting a multi-level network of open receivers, capillaries, and device cavities in a UV curable coating on a flexible substrate. Imprinting and UV-curing techniques were used to develop the pre-patterned flexible substrates where a UV-curable resin was molded and

solidified on a piece of PET sheet. Subsequent materials deposition and layer-to-layer alignment is achieved by inkjetting electronic inks sequentially into the easy-to-hit reservoirs, followed by spontaneous capillary flow of the inks via open channels into cavities shaping discrete electronic components. In this thesis, a contact receiver is defined as a circular depression where inks are delivered in order to form an external contact pad for a device; a device receiver is a circular cavity in which the delivered ink dries and forms an active layer of a device. Drying and annealing steps are performed between printing of different inks to facilitate film formation. Employment of inkjet printing allows for precise deposition of a certain amount of ink. Since the open capillary channels are much thinner than the ink reservoirs, the SCALE process thus combines imprint lithography with inkjet printing to enhance printed resolution - linewidths of 1 μm are readily achievable - while simultaneously simplifying materials registration, as shown in Figure 3.4

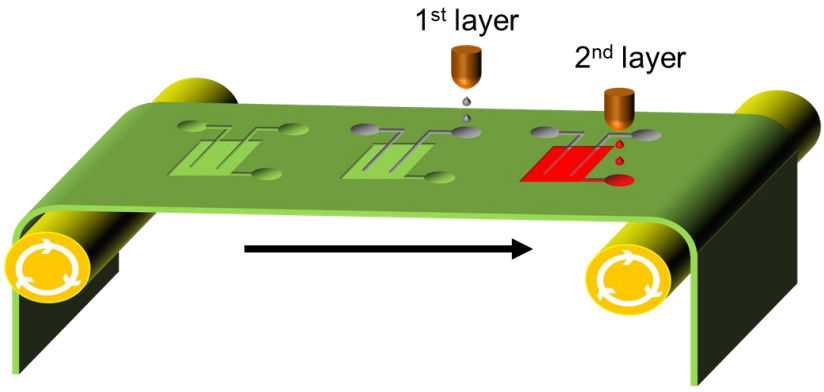

Figure 3.4 3D schematic plot showing the integration of the SCALE process to roll-to-roll processing

An additional benefit of SCALE is that crisp, well-defined line edges characteristic of conventionally photopatterned materials are readily obtainable, which is not typical of inkjet printing [100-101]. This feature to some extent reduces the negative influence on inkjet

printing resolution coming from ink spreading. What's more, a self-aligned printing process is realized by putting complex topography onto the substrate, which lowers the requirement for ink delivery precision in position. In this way, SCALE can decrease the sizes of both the printed features and the gaps between them and realize self-alignment between layers at the same time. Another appeal of this technology lies in its compatibility with roll-to-roll printing. Every step of SCALE can be potentially integrated into a roll-to-roll production line. The imprinting of pre-patterned substrate has already been realized on a roll-to-roll line with high fidelity [102].

3.3 Process Flow of SCALE

The fabrication process flow of SCALE consists of four steps, which is shown pictorially in Figure 3.5 . In the first step, the silicon master template was patterned using traditional photolithography. Then the pattern was replicated to flexible PDMS (Polydimethylsiloxane) stamps by soft lithography. In the third step, the pattern is transferred onto a plastic substrate by roll-to-roll imprinting, which can prepare large quantities of these imprinted substrate. In the last step, electronic inks were delivered into device cavities and receivers sequentially through inkjet printing. Deposition of a film was realized by additional annealing steps before the deposition of the next layer. In this way, several materials were deposited on top of one another to form multilayer devices. Experimental details and processing parameters are shown in experimental sections in Chapter 4 and 5.

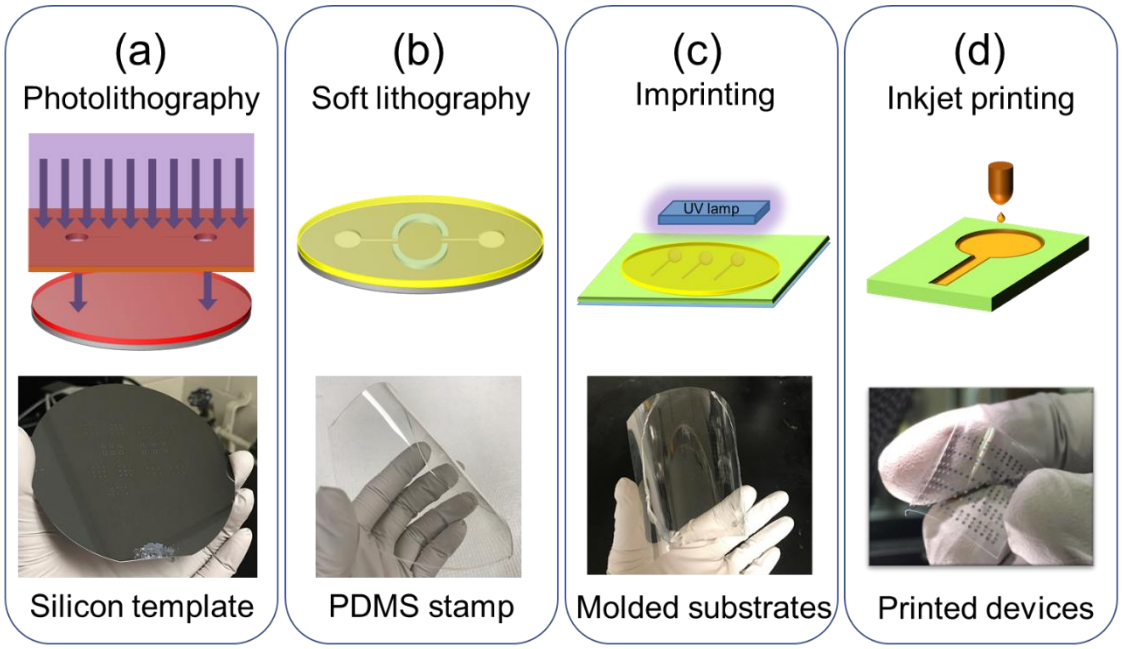

Figure 3.5 Process flow of the SCALE strategy with a schematic illustration of each step shown in the figures in the upper row and the product of each step shown in the optical images in the bottom row. (a) Patterning of a silicon template by photolithography. (b) Pattern transfer from silicon template to a PDMS stamp by soft lithography. (c) Preparation of molded substrates in large quantities by roll-to-roll imprinting. (d) Ink jet printing of an array of devices.

In the first step (Figure 3.5 (a)), photolithography was used to pattern the silicon master template to achieve precise alignment between different layers of the pattern and to create small features down to 2 μm. After developing the photoresist, a plasma etcher was utilized to etch the exposed area of the silicon wafer to create indented or raised features. A deep trench etcher was used when a feature needed vertical walls. And a STS etcher was used if a feature required tapered walls. Lines thinner than 2 μm were patterned using E-beam lithography or focused ion beam (FIB).

In the second step (Figure 3.5 (b)), a mixture of curing agent and Polydimethylsiloxane (PDMS) was casted onto the silicon wafer. After solidification by heating, the transparent PDMS stamp were peeled off from the silicon wafer, so the patterns were transferred to the PDMS stamp. PDMS is a silicone material which is commonly used in soft lithography. It

is flexible and transparent to UV light. So, it can be wrapped around an imprinting drum and allows UV light to go through to cure the underlying imprint resist.

In the third step (Figure 3.5 (c)), imprinted substrate was prepared in a roll-to-roll manner to produce such substrates in large quantities. A detailed description of the roll-to-roll imprinting process is included in Chapter 4 experimental section. A systematic study of the imprinting process has been conducted, showing that web tension, PDMS mechanical properties and feature dimensions need to be optimized to in order to replicate the pattern from the PDMS stamp to the substrate with high fidelity [102].

In the fourth step (Figure 3.5 (d)), different inks were delivered sequentially into their designated receivers. Inks were dried and annealed before the next ink deposition. Inkjet printing was used as the printing method. After printing was completed, the device was measured electronically and analyzed using scanning electron microscopy (SEM) to characterize the film morphology. Then the original pattern and the printing process were further optimized according to the results until the desired electrical performance is achieved.

To guarantee the reproducibility of the process and the device performance, several factors need to be considered in the design of a process flow including choice of ink materials, interaction between different layers, device architecture and compatibility with roll-to-roll process.

The choice of ink materials is critical to achieve an excellent device performance. When the ink enters a capillary channel or flows along the lip of a device cavity, the flow distance highly depends on the surface tension, viscosity and solvent evaporation rate of the ink [103-

[105]. Typically, lower surface tension, lower viscosity and less volatile solvent lead to a longer flow distance. A long enough flow distance of the conductive ink is essential to establish a connection network within a circuit especially for large-area applications. Besides, the inkjet printing process has placed certain requirements on the fluid properties of the ink to ensure a stable ink delivery [65]. Besides, the thickness profile of the dried film within the receiver is related to the ink's surface tension and viscosity, which can be adjusted by varying the concentration or adding additives.

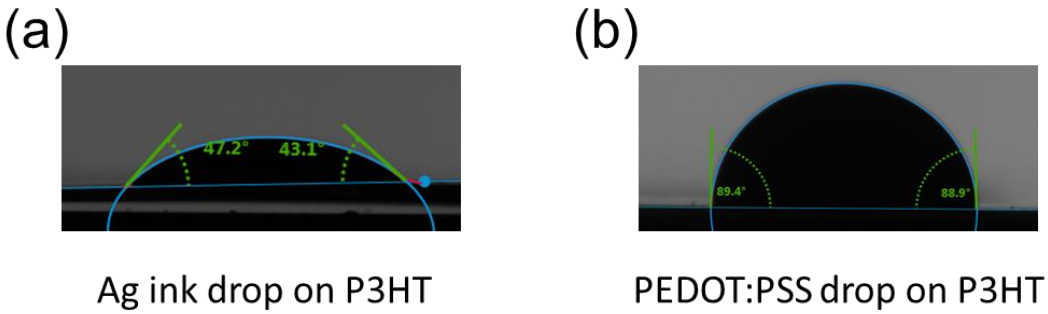

Figure 3.6 The contact angles of (a) Ag ink and (b) PEDOT:PSS ink on P3HT film

Apart from the fluid properties, the electrical properties of the dried film also significantly influence the final device electrical performance. A precursor-based particle-free Ag ink [106] was employed to print the electrodes because the ink can be converted into a conductive Ag film at around 90 °C, which is compatible with plastic substrates. Conducting polymers such as Poly(3,4-ethylene dioxythiophene):poly(styrene sulfonate) (PEDOT:PSS) and poly(3-hexylthiophene) (P3HT) are also frequently used in SCALE because they exhibit good conductivity after annealed at around 100 °C. Conducting

polymer inks are also preferred due to their inherent flexibility since we are targeting flexible circuits as the end product.

Both the designs of device structure and the process flow are critical in SCALE. When making a multilayer device, the bottom film may dissolve in the ink deposited on top of it, causing performance degradation or even short circuit. This can be avoided by carefully designing the deposition sequence or changing to similar materials. The design of the multilayer pattern on the substrate also needs to consider the flow distance of the ink and the morphology of the deposited film. The flow distance is determined not only by the ink properties, which has been discussed above, but also by the geometry of the capillary channel, the surface energy of the substrate and the ambient humidity. These parameters must be optimized and maintained during the fabrication process. For example, the contact angles of Ag ink and PEDOT:PSS ink are different on P3HT film. Ag ink is expected to have a longer flow distance than PEDOT:PSS ink due to its lower contact angle, which is displayed in Figure 3.6.

Since the ultimate goal is to transfer the whole fabrication process to roll-to-roll printing, all the processing steps should be compatible with roll-to-roll processing. From this point of view, inks with more volatile solvents are preferred since they dry faster at a low temperature. This feature can shorten the processing time. Besides, processing in vacuum environment should be avoided.

3.4 Current Progress of SCALE

In order to build a functional circuit, it is important to have the ability to manufacture each of the circuit components on the same platform by SCALE. Already, successful fabrication of discrete circuit elements including transistors, capacitors, and resistors on individual plastic sheets has been demonstrated by SCALE [1-3, 36, 103, 107]. Both the pattern design and the process flow of each type of circuit elements are being optimized aiming at achieving better electrical performances and/or increasing device density by reducing footprint.

3.4.1 Conductive lines

Conductive layers are required for almost all the electronic devices. However, patterning high aspect ratio metal lines has always been a technical bottleneck in printing because ink tends to spread on the substrate. Besides, it is also hard to print extremely thin lines (<10 μm) and lines with small separations. SCALE got around these problems by using capillary channels where the conductive ink could be confined very well within the channel. Deposition of the conductive film only occurs along the walls and bottoms of the channels, resulting in conductive lines with crisp edges. Then, the trench can be further filled by copper in order to form a high aspect ratio metal line.

To print conductive lines, a thin layer of particulate Ag film was deposited first inside the receivers and capillary channels (Figure 3.7 (b), (e) and (h)). The narrowest metal line that has been successfully deposited is as narrow as 500 nm [2], which can hardly be printed by other printing methods alone. A subsequent copper plating step was optional in order to

increase the conductance of the metal lines and to reduce the work function when necessary (Figure 3.7 (c), (f) and (i)) [103]. The copper plating recipe was further optimized [102] to achieve better reproducibility. Conductive lines with high resolution, high aspect ratio (height:width ~ 5:1) and low resistance per length (around 0.46 Ω/cm for a 10 μm line) can be reproducibly printed using this method [102].

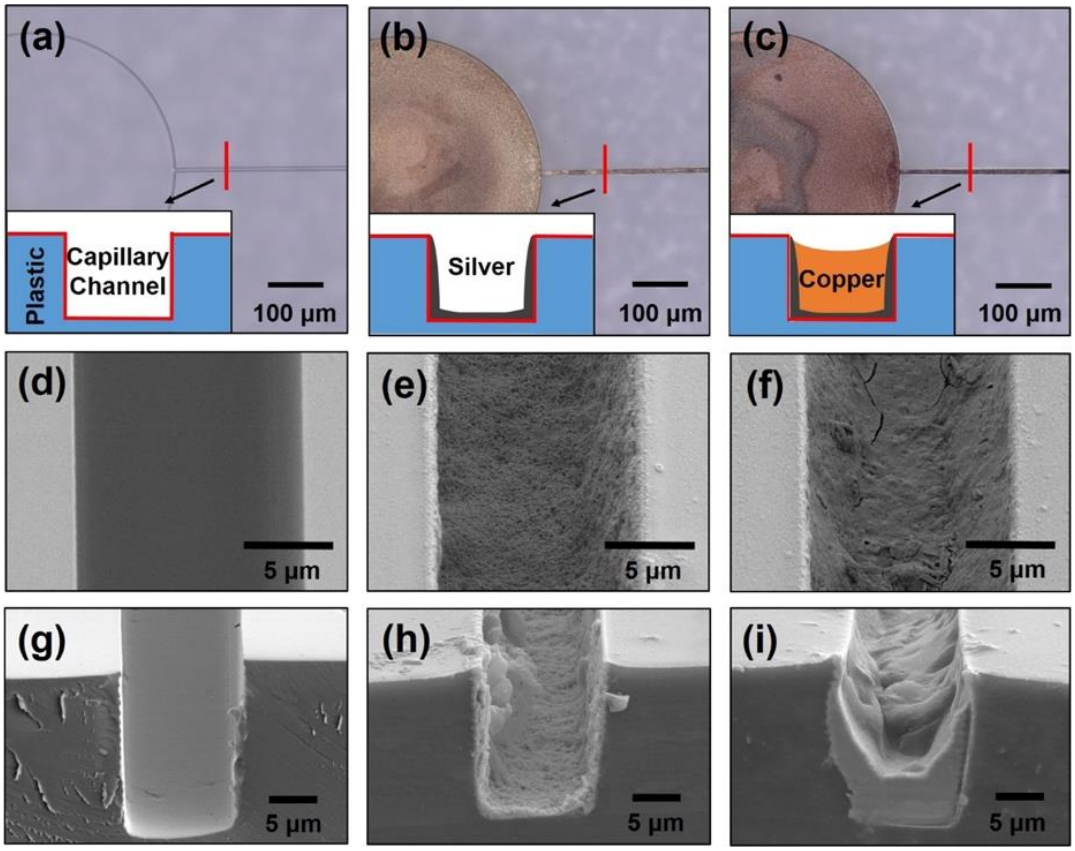

Figure 3.7. Microscopic images of printed conductors by the SCALE strategy (a,b,c) top view optical images of (a) imprinted substrate, (b) printed Ag film, and (c) electroless-plated Cu film. (d,e,f) corresponding topview SEM images of (d) the substrate, (e) Ag film, and (f) Cu film. (g, h, i) corresponding cross-sectional SEM images of (g) the substrate, (h) Ag film, and (i) Cu film. Adapted from [102]

Besides straight conductive lines, metal interconnects with right angle turns can also be printed using this method, which is much simpler and more efficient than writing the connected thin lines one by one by traditional digital printing methods. Interdigitated

electrodes with small and precise spacings can be achieved [108], which is discussed later in the capacitor part. Curved capillary conductors has also been demonstrated, showing the potential of making printed spiral antennae. Research is going on in exploring the flow mechanism and influencing factors of flow distance in an open microfluidic channel [105]. These investigations can help us optimize the printing conditions to increase the flow distance and have better control of conductive film deposition.

3.4.2 Resistors

Printed resistors are widely used for adjusting signal level, reducing current flow, dividing voltage and heating. Usually a printed resistor consists of two layers, one resistive layer and one conductive layer to realize external connections. In SCALE, a printed resistor employed a coplanar structure (Figure 3.8) with the two Ag electrodes and the resistive carbon black layer on the same plane [1]. The measured resistance of this SCALE resistor is around 64 kΩ. A new design of resistor used PEDOT:PSS as the resistive material and incorporated two-tier junctions to achieve unidirectional liquid flow. Self-aligned resistors were printed with resistance over 100 kΩ [109]. Overall, SCALE provides a reliable route to manufacture printed resistors in a roll-to-roll compatible way. But a printed resistors with a wide range of resistance have not been demonstrated in SCALE.

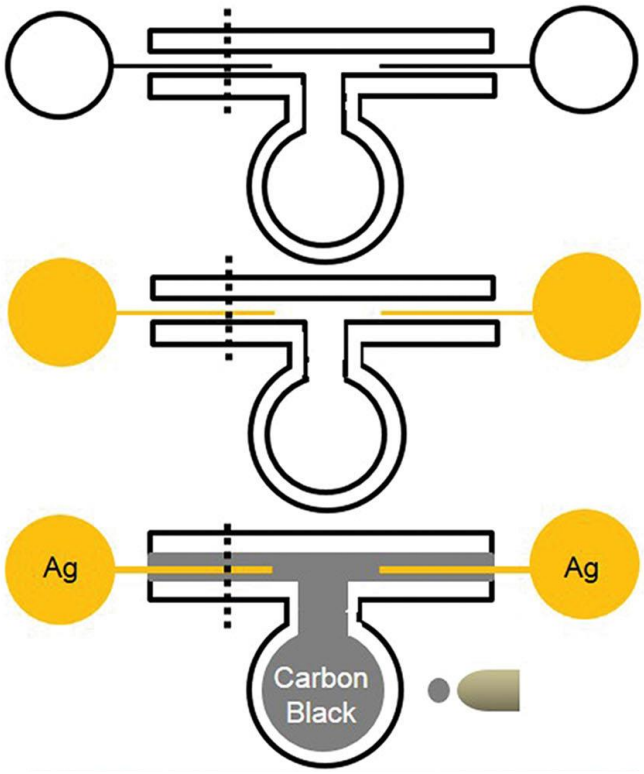

Figure 3.8 Schematic plot of the printing process of a resister by the SCALE strategy. Adapted from [1]

3.4.3 Capacitors

Capacitor is another essential component of a circuit which can store electrical energy. Printed capacitors are frequently used in voltage multipliers, signal filters and temporary batteries [23, 45, 110]. As has been discussed in the 3.4.1, interdigitated electrodes with small separations can be easily printed via the SCALE strategy. Utilizing ion-gel as the dielectric layer, a printed capacitor with interdigitated electrode was printed. Ion-gel is a gel electrolyte composed of an ionic liquid [EMIM]:[TFSI] and a copolymer. Electrical double layers formed at the interfaces of the ion-gel and both electrodes due to the existence of mobile ions within the gel, which allowed printed capacitors to use coplaner electrodes and simplified the printing process [19, 111]. Graphene was chosen as the electrode material due

to its high conductivity, large specific surface area and good electrochemical stability [79, 108, 112]. Self-aligned capacitors were printed with a large specific capacitance (268 μF·cm^{-2}), excellent mechanical durability and high yield (100%).

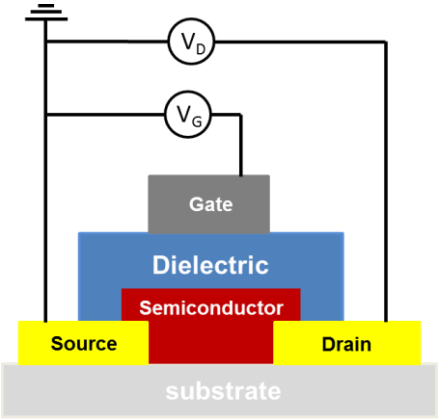

Figure 3.9. Device structure of a bottom contact, top gate thin film transistor

3.4.4 Transistors

Transistors are the basis of logic circuits. Thin film transistors (TFTs), which are three-terminal devices similar to metal-oxide-semiconductor field effect transistors (MOSFETs), can be fabricated by additive manufacturing methods. A thin film transistor has the semiconductor, dielectric, and electrode materials deposited additively as thin films on a variety of substrates such as glass or polyimide films [113]. The basic device structure of thin film transistor is shown in Figure 3.9. The dielectric layer separates the semiconductor layer from the gate electrode. TFT utilizes a capacitively coupled gate dielectric layer to control the current through the semi-conductor layer [113]. The voltage applied to the gate electrode controls the concentration of carriers and the current in the semiconductor layer. These carriers form an accumulation layer at the semiconductor/dielectric interface. When

a bias is also applied on the drain electrode, a current driven by the corresponding electric field will flow across the accumulation layer turning the device on. As the gate bias increases, the current will also increase due to the elevated carrier concentration.

There are three main parameters to evaluate TFTs' performance, mobility, ON/OFF ratio and threshold voltage. Mobility is a measure of how fast carriers can move within the semiconductor thin film under an applied electric field; The ON/OFF ratio denotes the ability of switching the current, and a large ON-OFF ratio is desirable for fabricating integrated circuits. The threshold voltage, VT, physically represents the transition between ON/OFF regimes. The importance of these parameters is evident through the use of TFTs in LCD displays. The switching of the pixel requires quick charging and discharging processes. The charges need to be held on the pixel until next signal arrives. Therefore, the requirements for a TFT switch in LCD are as follows, on/off ratio > 10^6, and mobility of at least 1 $cm^2/V{\cdot}s$. [114].

Transistors are the basis of modern logic circuits and are frequently used to amplify or switch electronic signals. However, high-performance transistors are harder to achieve using printing methods than other device because fabricating transistors have higher requirements for materials registration and film quality. The quality of the printed films, especially the semiconductor layer, has a significant influence on the device performance. Formulating a high-performance semiconducting ink is essential for printing functional transistors. Besides, it has been reported that the operating frequency of printed transistors is limited by the parasitic capacitance, which is the capacitance between the gate and drain [115]. The switching speed can be increased by minimizing the size of the drain electrode or

by improving the layer-to-layer alignment to reduce the overlap between the gate and the drain electrode. As has been discussed above, SCALE strategy is capable of patterning sub-micron electrodes using inkjet printing and improving materials registration by self-alignment. It is promising to improve the operating speed of fully printed transistors via the SCALE strategy.

Several designs of transistors printed via the SCALE strategy has been reported [1-3, 36]. The first reported transistor design (Figure 3.10 (a)) utilized a side-gated device structure with ion-gel as the dielectric layer and P3HT (poly(3-hexylthiophene)) as the semiconductor. [1] The fully-printed transistor achieved a mobility of 0.8 $cm^2 \cdot V^{-1}s^{-1}$. However, the long gate distance retards ion transport in the ion-gel layer and slows down the switching of the transistor [116]. So, the transistor design based on a side-gated structure was further improved by shrinking the width of the source and drain electrodes down to less than 1 μm and reducing the distance between the gate and the semiconductor channel down to less than 5 μm in a subsequent report [2]. This improved side-gated transistor design is shown in (Figure 3.10 (b)). To further reduce the spatial separation between the gate electrode and semiconductor, top-gate thin film transistors were designed and printed using the SCALE method, shown in Figure 3.10 (c) [3]. The change from side-gate to top-gate in design significantly decreased hysteresis and sweep rate dependence from 50 to 500 $mV \cdot s^{-1}$. Other than P3HT, carbon nanotube has also been employed as the semiconductor material in fabrication of printed transistors in SCALE [36]. All the processing steps in transistor fabrication are compatible with roll-to-roll printing. These successful

demonstrations of fully-printed thin film transistors by SCALE show the promising future of mass-production of printed transistors.

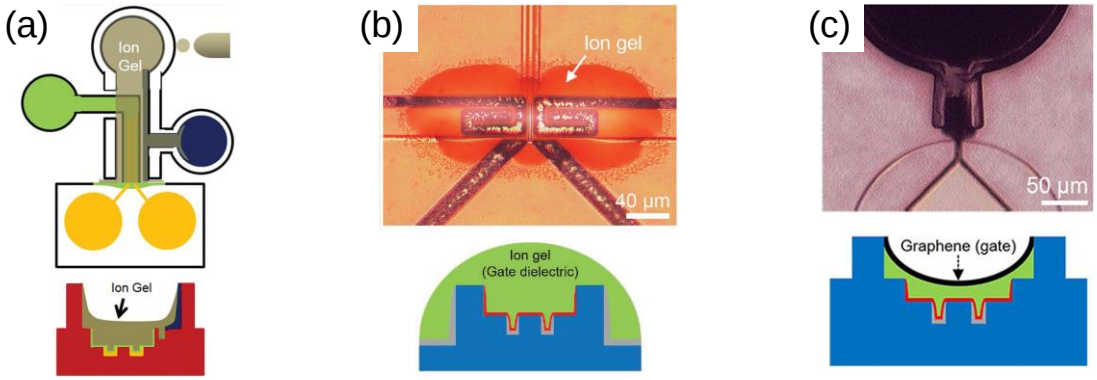

Figure 3.10 Comparison of several transistor designs based on the SCALE strategy. (a) The first side-gated transistor design reported in [1]. (b) The second side-gated transistor design with narrow gate-to-channel distance reported in [2]. (c) a top-gated transistor design reported in [3]

3.5 Existing challenges with SCALE

The first challenge with SCALE is to demonstrate resistors with resistances over many orders of magnitude without changing its overall footprint. Previously, it has been shown that SCALE can be used to make a variety of discrete electronic components, but it has never been shown that SCALE can produce resistors with a wide range of resistances using roll-to-roll methods. Key to this effort is the choice of printable resistive materials and the manipulation of the conductivity over a large range.

The second challenge with SCALE is to stack layers on top of one another without undesirable electrical shorts. A vertically stacked structure is preferred sometimes due to the larger contact area between layers, which leads to larger currents or capacitance than a horizontal, coplanar structure. The challenging part of making SCALE devices in a vertically stacked structure via the SCALE process lies in preventing shorts. This is because in such structures the middle layers are thin and can have pinholes, causing

undesirable contact between the top and bottom layers. An additional complication that can lead to shorting is uncontrolled spreading of ink into channels or cavities that have already received ink or that are intended to be devoid of ink.

The third challenge with SCALE is to improve the electrical performance of the self-aligned transistors. The plastic substrates cannot withstand a temperature higher than 120 ºC, which limits the usage of some high mobility semiconductors that require high temperature processing. So, finding a high-performance semiconductor ink that can be processed at a low temperature is one bottle neck of producing transistors. Besides, the performance of top-gated transistor is limited by the dewetting of the ink for the top electrode on the dielectric layer.

The last challenge is to transfer the SCALE process from bench-top experiments to large scale manufacturing. Successful production of imprinted plastic substrates in large quantities has been successfully demonstrated [102]. The next step is to integrate digital printheads into the roll-to-roll line. Aligning the printheads to the receivers on a moving web is another technical challenge. A digital alignment system with the help of image recognition can be employed to drive the movement of the web and the printheads.

These challenges limit the ability of SCALE to produce a fully-printed circuit, which contains a variety of basic building blocks and connections between devices. Further investigation is needed to tackle these limitations, which requires new designs of material systems, device patterns and process flows.

Chapter 4

Self-Aligned Inkjet Printing of Resistors and Low-Pass RC Filters on Roll-to-Roll Imprinted Plastics

4.1 Introduction

Chapter 3 shows that successful fabrication of discrete circuit elements including transistors, capacitors, and resistors on individual plastic sheets has been demonstrated by SCALE [1-3, 36, 103, 107]. However, the use of SCALE and roll-to-roll processing to create resistors with resistances over many orders of magnitude has not been demonstrated. As resistors are ubiquitous electronic building blocks, this is a crucial challenge for the

---

An adapted version of this chapter is published as

Cao, M., Jochem, K., Hyun, W. J., Francis, L. F., & Frisbie, C. D. (2018). Self-aligned inkjet printing of resistors and low-pass resistor–capacitor filters on roll-to-roll imprinted plastics with resistances ranging from 10 to 106 Ω. *Flexible and Printed Electronics*, *3*(4), 045003.

ultimate goal of roll-to-roll printing of complete circuits. Indeed, printed resistors have been realized utilizing screen printing [77, 117-119], stencil printing [120], aerosol jet printing [73] and inkjet printing [100, 121-123], but these fabrication procedures were not completely compatible with self-alignment and/or roll-to-roll processing. Thus, in this paper we focus on demonstrating SCALE-based, roll-to-roll approaches to creating resistors with resistances spanning many orders of magnitude.

Key to this effort is the choice of printable resistive materials. Poly(3,4-ethylene dioxythiophene):poly(styrene sulfonate) (PEDOT:PSS), which has been widely used as both a conductive and a resistive material in printed electronics, is an ideal material due to its adjustable resistivity and good printability. It has been reported that the resistivity of PEDOT:PSS films deposited from the commercial PH1000 ink (Heraeus) can be decreased by adding a small amount of high boiling point solvents such as dimethyl sulfoxide (DMSO) and ethylene glycol (EG) [124-125]. Jung, et al. reported inkjet-printed resistors using PEDOT:PSS PH1000 inks [100]. They modified the film resistivity by varying the concentration of DMSO added into the solution. Also, Ali et al. increased the resistivity of PEDOT:PSS films from 48 to 210 mΩ·cm by blending poly(methyl methacrylate)(PMMA) into PH1000 PEDOT:PSS ink [101]. Though not explored here, carbon based inks can also be used to print the resistive layer. Chang, et al. blended high (Dupont 5036) and low (Dupont 7082) resistivity carbon materials and achieved a resistance range from 3.3 kΩ/□ to 800 kΩ/□ using screen printing [118].

In order to make resistors having resistance ranging over orders of magnitude, but with the same spatial footprint, which is important for circuit layout considerations, this chapter introduces a two-pronged strategy in which the distance between printed electrodes was

changed in concert with alterations of the PEDOT:PSS ink formulation to adjust resistivity, as just described. Resistors on plastic substrates were achieved with resistances varying from 10-10^6 Ω. The resistors were robust to bending strains of up to 1% and to thousands of repeated electrical measurements. To test dynamic performance, low-pass *RC* (resistor-capacitor) filters were printed. The fabrication of *RC* filters by inkjet printing was first reported by Varahramyan and colleagues [110, 126-127]. Then, Castro, et al. demonstrated all-inkjet-printed low-pass filters with cutoff frequency from 82 Hz to 740 Hz by applying printed organic thin-film transistors [128]. Here, fully printed low-pass *RC* filters are demonstrated with cutoff frequencies over three orders of magnitude by varying the resistance. Collectively, the results demonstrate that the SCALE process has excellent potential for self-aligned printing of resistors and *RC* filters necessary for building more advanced electronic systems on flexible substrates.

4.2 Experimental Section

4.2.1 Silicon master template fabrication

The silicon master template was fabricated by two rounds of traditional photolithography. (a) Patterning the recessed receivers and channels for electrodes: A 4-in silicon wafer was heated at 115 ºC for 1 min to remove the water molecules on the top surface. Then the wafer was treated in a hexamethyldisilazane (HMDS) atmosphere for 4 min. A layer of photoresist (Microposit S1813, Dow) was spin-coated onto the silicon wafer at 3000 rpm for 30 s. The wafer was soft-baked at 115 ºC for 1 min and then exposed to UV light for 5 s under a photomask designed for the electrodes. The wafer was developed in a mixture of Microposit 351 (Dow) and deionized water (1:5 v/v) for 30 s. The exposed

area of the wafer was dry etched down to a depth of 7 μm in a deep trench etcher (SLR 770). The photoresist was then washed off by acetone and the wafer was immersed in Piranha solution (H_2SO_4 and H_2O_2, 1:1) for 20 min at 120 ºC to clean the residual photoresist. (b) Patterning the raised ink receivers: SU-8 2010 photoresist (MicroChem) was spin-coated onto the same silicon wafer at 500 rpm for 5 s and then at 2000 rpm for 30 s, followed by baking at 65 ºC for 3 min and 95 ºC for 7 min. The photoresist was then exposed to UV light for 24 s through the photomask designed for the raised walls. The exposed wafer was heated at 65 ºC for 1 min and 95 ºC for 7 min. The wafer was immersed in 1-methoxy-2-propanyl acetate for 5 min to develop the photoresist and then rinsed with isopropyl alcohol. Lastly, the wafer was baked at 180 ºC for 10 min.

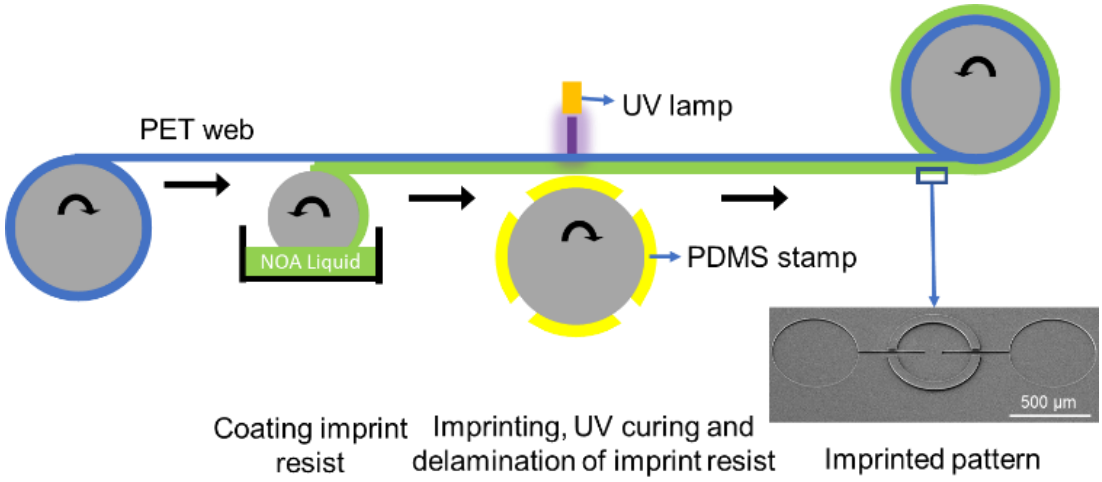

Figure 4.1. Schematic illustration of roll-to-roll imprinting of receivers, capillary channels, and device cavities for the SCALE process. The imprint material (green) is a cross-linkable liquid that is cured by UV illumination while the web is in contact with the PDMS stamp roll, as shown.

4.2.2 PDMS stamp fabrication

The silicon master template was first silane-treated in a vacuum chamber overnight with trichloro(1H,1H,2H,2H-perfluorooctyl)silane (Aldrich). A curing agent and PDMS

monomer (Sylgard 184, Dow Corning) were mixed in a weight ratio of 1:10 and then poured onto the silicon master template. The PDMS was first cured at 70 ºC for 2 h in an oven. Then the PDMS stamp was peeled off from the silicon wafer, followed by heating at 120 ºC for 2 h and at 215 ºC for another 2 h to enhance the mechanical durability.

4.2.3 Roll to roll imprinting of the flexible substrates

The imprinting of the flexible substrates was performed on a roll-to-roll machine (Carpe Diem Technologies). The PDMS stamps were glued to a piece of silicone coated PET sheet and cured at 45 ºC for 1 day. The PET sheet with the PDMS stamps on it was then wrapped around the imprinting drum and clamped in place. A pre-cleaned PET web, which was used as the flexible substrate, was coated with a liquid layer of UV-curable imprint resist (Norland Optical Adhesive 73, Norland Products) to a thickness of 25 μm by reverse gravure coating. The web then passed at 10 cm/min and 18 N web tension to the imprint drum where the PDMS molds were pressed into the NOA layer. A high intensity UV light cured the resist coating while it was still in contact with the stamp. The web with the imprinted layer was then delaminated from the PDMS stamp roll and spooled up.

4.2.4 Ink preparation

The resistive inks were prepared following the compositions listed in Table 4.1. Two types of PEDOT:PSS inks (Clevios PH1000 and Clevios AI4083) were purchased from Heraeus. Ethylene glycol was purchased from Sigma Aldrich. Isopropyl alcohol (10 vol%) was added to reduce the surface tension. The inks were sonicated for 15 min and filtered through a 5 μm pore filter before each use. The ion-gel ink was prepared by mixing an

ionic liquid (1-ethyl-3-methylimidazolium bis(trifluoromethylsulfonyl)imide, [EMIM][TFSI]), a triblock copolymer (poly (styrene-b-ethyl acrylate-b-styrene), SEAS) and *n*-butyl acetate to a weight ratio of 8:2:90.

4.2.5 Device fabrication

For printing the resistor, a reactive silver ink [106] was delivered into the ink receivers by inkjet printing followed by a 3-min annealing process at 100 ºC in air to generate the two electrodes. Then the PEDOT:PSS ink was also inkjet-printed into the round ink receiver in the center of the device to cover the gap between the two electrodes followed by drying at 100 ºC in air for 10 min, resulting in a 1-μm thick PEDOT:PSS film. For printing the *RC* filter, the interdigitated electrodes and the connection wires were also printed from the reactive silver ink. Then the PEDOT:PSS ink and the ion-gel ink were delivered respectively into their raised receivers and were annealed at 100 ºC for 10 min in air together. A piezoelectric nozzle (Microfab) with an orifice of 80 μm was used for the inkjet printing. A unipolar waveform was applied during the jetting with a rise time of 5 μs, a dwell time of 20 μs, a down time of 5 μs, a driving voltage of 120 V and a frequency of 1000 Hz. 8 nL of the silver ink (20 drops) was delivered into each of the ink receiver and 27 nL of the PEDOT:PSS ink (70 drops) was delivered into the corresponding ink receiver.

4.2.6 Characterization

The optical images of the devices were taken by an optical microscope (Keyence). Film thickness profiles were measured by a Tencor P-7 profilometer. The surface tensions were measured by a pendant drop shape analyzer (Kruss). The resistivities of the PEDOT:PSS

films were measured via the Van der Pauw method on spin-coated PEDOT:PSS films on square glass slides. To calculate the resistance, current-voltage curves were measured

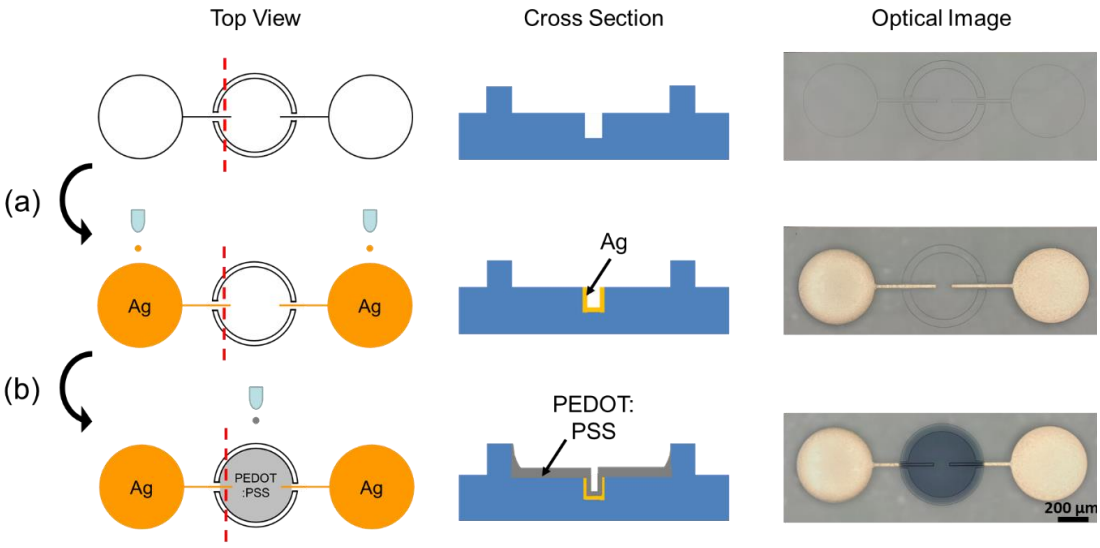

Figure 4.2. Top-view (left) and cross-sectional (middle) illustrations and optical images (right) for the fabrication of a resistor via the SCALE process. The cross-sectional illustrations show the topographic profile along the red dashed lines in the top-view illustrations. (a) When the silver ink is delivered to the receivers by inkjet printing, the ink is patterned into the channels by capillary action and forms electrodes after thermal annealing. (b) PEDOT:PSS ink is delivered to the center ink receiver to form a resistive layer between the electrodes.

under a N_2 atmosphere using two source meters (Keithley 236 and 237). For the electrical characterization of the *RC* filter, the input signals were generated by a waveform generator (Agilent 33512B). The output voltages were acquired with a digital oscilloscope (Tektronix TDS3014C). The capacitance of the printed ion-gel capacitor was measured by an impedance analyzer (HP4192A LF).

4.3 Roll-to-roll Imprinting and Printing Resistors

Figure 4.1 illustrates the roll-to-roll process to prepare the imprinted substrates for resistors. Prior to the roll-to-roll imprinting process, a silicon master template (Figure 4.3 a) was prepared by traditional photolithography methods, and the patterns were transferred

to PDMS stamps (Figure 4.3 (b, c)). The PDMS stamps were secured around an imprinting drum in the roll-to-roll machine. When the PET web, which was pre-coated with a layer of UV curable imprint resist, passed through the imprinting drum at a speed of 10 cm/min, the PDMS stamps were pressed into the imprint coating to create the capillary channels and connected receivers. At the same time, the imprint layer was cured by a high intensity UV light. The imprinted web was peeled off from the PDMS stamps and collected by a rewind drum. The channels (20 μm wide and 7 μm deep), receivers (500 μm in diameter and 7 μm deep) and ink receivers (500 μm in diameter and 10 μm above the plane) were successfully replicated onto flexible substrates from the silicon master template, which is shown by the tilted scanning electron microscopy (SEM) image in Figure 4.1. Compared with our previous SCALE resistor design [1], this new design reduced the device area from 2.8 mm^2 to 1.0 mm^2. Further reductions should be possible in future designs with smaller receivers.

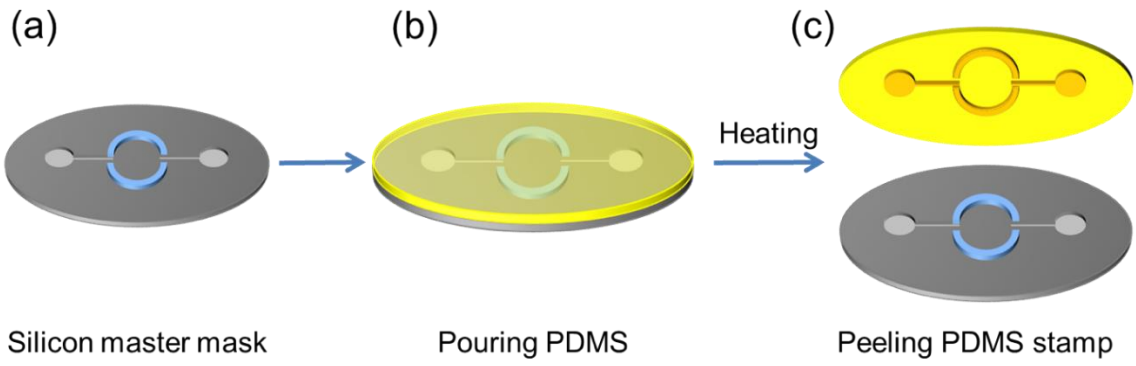

Figure 4.3. Schematic illustration for preparation of PDMS stamps. (a) Silicon master template prepared by photolithography. (b) Pouring PDMS onto the silicon template. (c) Peeling off the PDMS stamp after thermal curing.

Figure 4.2 shows the printing steps of a resistor on the imprinted substrate. To generate electrodes (Figure 4.2 (a)), a particle free silver ink [106] was delivered into the two ink receivers on both sides by inkjet printing. The silver ink wicked into the capillary channels,

and then formed conductive silver films in the channels connected to the receivers upon annealing. Compared with directly writing the electrodes by conventional inkjet printing,

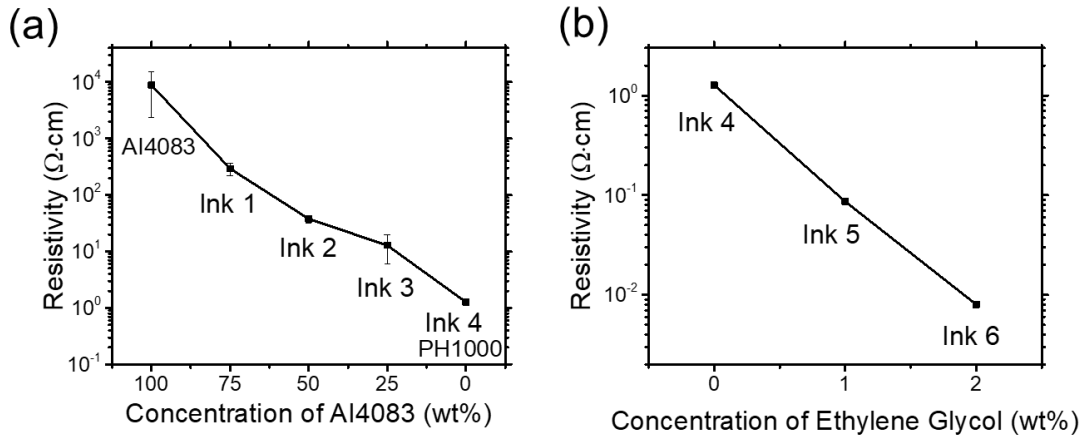

Figure 4.4. (a) Resistivity of PEDOT:PSS films printed from a mixture of PH1000 and AI4083 for different mixing ratios. Error bars represent one standard deviation. (b) Resistivity of PEDOT:PSS films versus the weight fraction of ethylene glycol in the PH1000 ink. Note that the error bars (one standard deviation) are not visible in this panel as they are smaller than the data points.

the SCALE process (1) increased resolution by preventing lateral spreading of the silver ink, (2) provided straight electrodes with highly smooth edges, and (3) simplified registration of the two electrodes with respect to each other, i.e., precise nozzle alignment was not required to produce the two electrodes with the desired spacing and co-linear alignment. To deposit the resistor layer and complete the device, PEDOT:PSS ink was delivered into the center ink receiver, bridging the two electrodes (Figure 4.2 (b)).

4.4 Variation of the Resistance

To manipulate the total electrical resistance (*R*) of the device, the resistive film was deposited using a mixture of two types of PEDOT:PSS solutions (purchased from Heraeus) with different intrinsic resistivities: PH1000 (resistivity: 1.3 Ω·cm) and AI4083 (resistivity: 8800 Ω·cm). Figure 4.4 a shows the PEDOT:PSS film resistivity measured in Van der

Pauw geometry as a function of the mixing ratio of the two inks. The film resistivity increases with the concentration of AI4083 and can be controlled in a wide range from 1 to 300 Ω·cm by the mixing ratio. Moreover, the resistivity can be further adjusted by the addition of ethylene glycol (EG) into the PH1000 solution. It is proposed in the literature that the addition of ethylene glycol induces a conformational change of the PEDOT chains from coiled to linear or to an expanded-coil conformation [125, 129]. This change leads to enhanced charge carrier transport within the PEDOT:PSS film and results in a lower resistivity. As shown in Figure 4.4 (b), the resistivity of the PEDOT:PSS film printed from the PH1000 ink decreases from 1 to 0.008 Ω·cm with the addition of only 2 wt% of ethylene glycol. Therefore, the resistivity of the printed PEDOT:PSS film can be changed over five orders of magnitude by simply modifying the ink formulation.

Table 4.1 Composition of PEDOT:PSS ink formulations

Ink #	PH1000 (wt%)	AI4083 (wt%)	Ethylene glycol (wt%)
Ink 1	25	75	0
Ink 2	50	50	0
Ink 3	75	25	0
Ink 4	100	0	0
Ink 5	99	0	1
Ink 6	98	0	2

All inks were modified with 10 vol% isopropyl alcohol.

In addition to controlling the electrical resistivity, another way to manipulate the device resistance is controlling the distance between the two electrodes. For facile control of the resistance with the electrode separation *L* (Figure 4.5 (a)), the film uniformity is important because a linear relationship between the resistance and the electrode separation can be

expected when the film thickness is uniform in the center ink receiver. However, the resistive layer printed using the as-received PEDOT:PSS solution shows significant thickness variation, as evident in the profile (Figure 4.5 (b)). To improve the thickness uniformity, isopropyl alcohol (IPA) was added to the PEDOT:PSS solutions to reduce the surface tension of the inks. As previously reported, Xing, et.al. suggested that the addition of IPA into the PEDOT:PSS inks led to a film with a flatter top surface in a confined groove due to a reduction in the ink surface tension [48]. The surface tension of PH1000 was measured without and with IPA, as shown in Figure 4.5 (c). The surface tension of the ink decreases with the IPA content because IPA has a much lower intrinsic surface tension (23 mN/m) than the aqueous PH1000 ink (68.5 mN/m). As a result, the PEDOT:PSS film

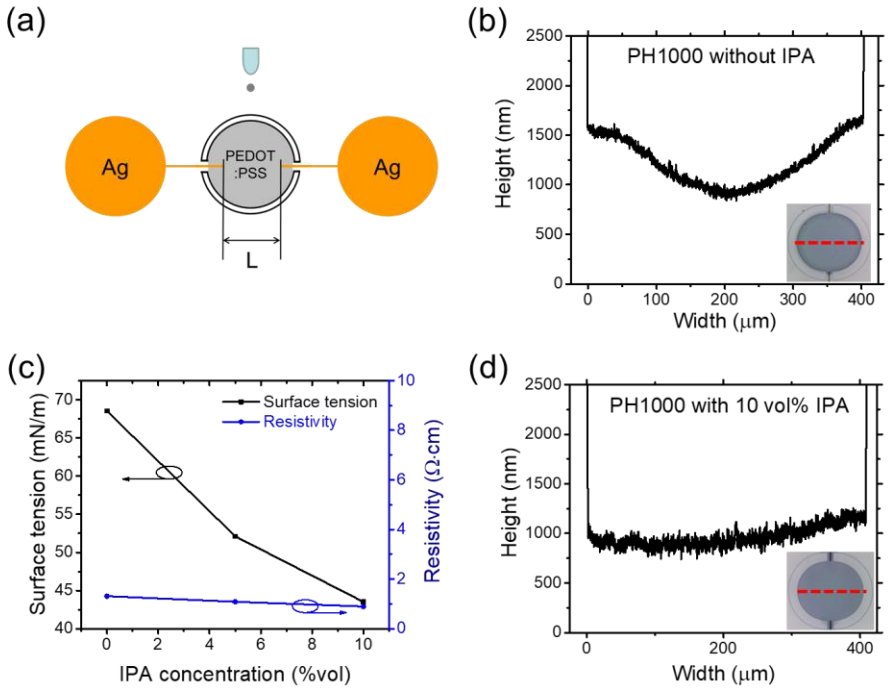

Figure 4.5 (a) Sketch defining the electrode separation L. (b) Thickness profile of the PEDOT:PSS film (in the ink receiver) printed using (b) as-received PH1000 and (d) a mixture of PH1000 and isopropanol (9:1 vol/vol). The profiles were taken along the red dashed lines shown in the inset optical images. (c) Surface tension of PH1000 inks blended with isopropyl alcohol and resistivity of PEDOT:PSS films printed using these inks.

exhibits significantly improved thickness uniformity after the addition of IPA to the ink (Figure 4.5 (d)) while the film resistivity remains almost unchanged (Figure 4.5 (c)).

The relationship between the resistance and the electrode separation (L) was explored for various resistance ranges by employing different PEDOT:PSS ink formulations (Table 1) modified with IPA (10 vol% in the inks). Figures 4.6 (a-f) display the plots of the resistance as a function of L for devices fabricated with different inks. Each data point represents the average and the standard deviation for 20 devices, and 600 devices in total were fabricated with a yield of 100%. The standard deviations of resistance were all less than 15% and could be further reduced upon optimization of the printing precision to achieve better thickness control of the PEDOT:PSS film. The results demonstrate that the resistance increases linearly with the electrode separation and the linear relationship holds well for all the resistance ranges with R^2 higher than 0.9. Typical current-voltage curves of printed resistors covering all the resistance ranges indicate good linear response (Figure 4.7). We found that the resistors could withstand a maximum current of 5 mA. Finally, a resistance range over five orders of magnitude from 57 Ω to 1.3 MΩ was achieved with good repeatability.

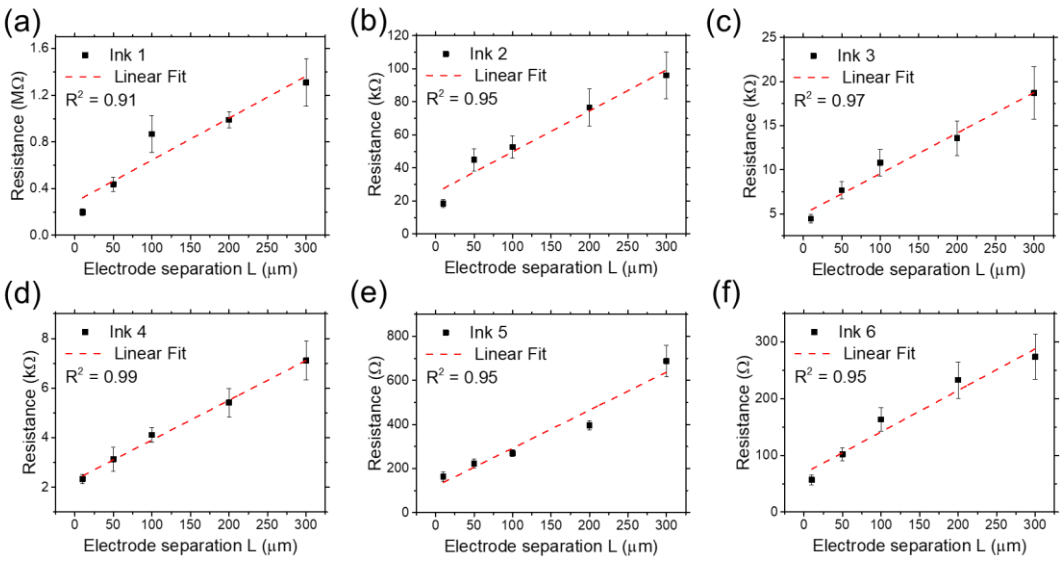

Figure 4.6. (a)-(f) Resistance as a function of L for resistors printed with different ink formulations (see Table 1). The red dashed line shows the linear fit of the five data points in each figure.

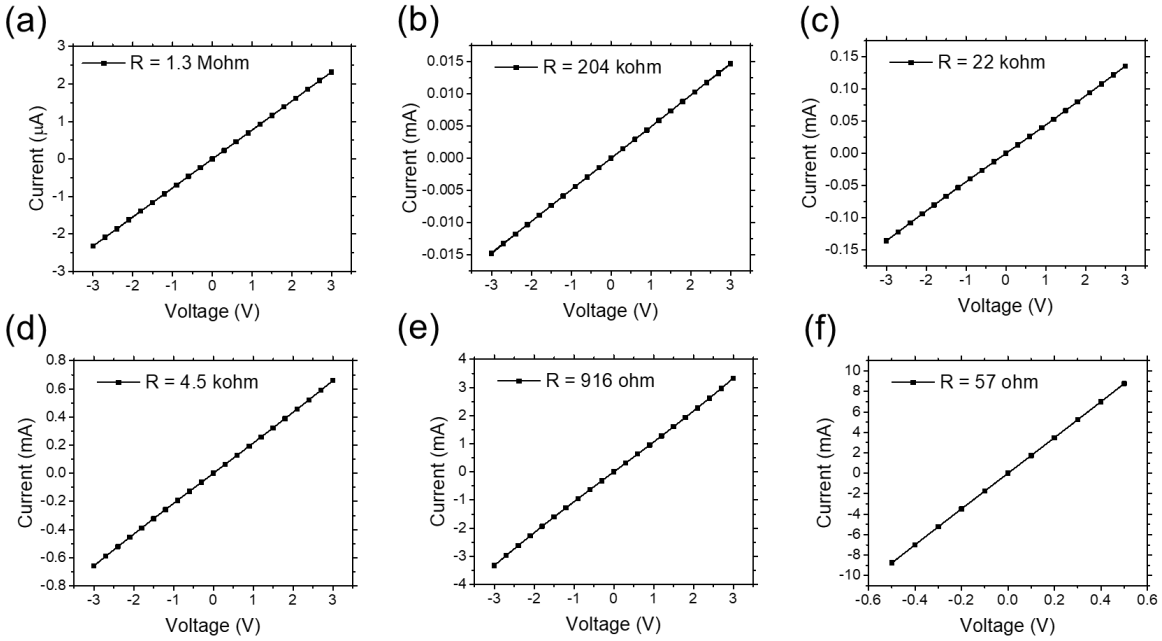

Figure 4.7. Current-voltage characteristics of a printed resistor of (a) 1.3 MΩ, (b) 204 kΩ, (c) 22 kΩ, (d) 4.5 kΩ, (e) 916 Ω, and (f) 57Ω.

4.5 Device Stability

To investigate the mechanical flexibility of the printed resistors (Figure 4.8 (a)), a bending test (Figure 4.8 (b)) was performed with a bending radius of 1 cm (tensile strain of about 0.8%). The device resistance was monitored during the bending test and did not exhibit a significant change over 5000 bending cycles, as shown in Figure 4.8 (c), revealing excellent tolerance to bending. Moreover, the operational stability was examined by acquiring standard current-voltage curves of the resistors repeatedly. The resistance values are plotted against the number of measurements in Figure 4.8 (d). Typical resistors retained over 96% of their original resistance after 1000 measurements, showing good long-term operational stability.

4.6 Low-Pass *RC* Filters

To examine dynamic behavior, low-pass *RC* filters employing the printed resistors (Figure 4.9 (a)) were demonstrated. The capacitor of the *RC* filter was also fabricated via the SCALE process using a previously reported procedure [107]. The underlying silver electrodes are in a co-planar interdigitated structure with six digits in total. A gel electrolyte composed of an ionic liquid [EMIM]:[TFSI] and a copolymer (see experimental), was employed as the dielectric material due to its high specific capacitance, excellent printability at room temperature, and good mechanical integrity [19, 111]. The capacitance of an individual printed capacitor is shown as a function of frequency in Figure 4.10. The maximum operating voltage is approximately 3V. Figure 4.9 (b) shows an optical image of a completed *RC* filter.

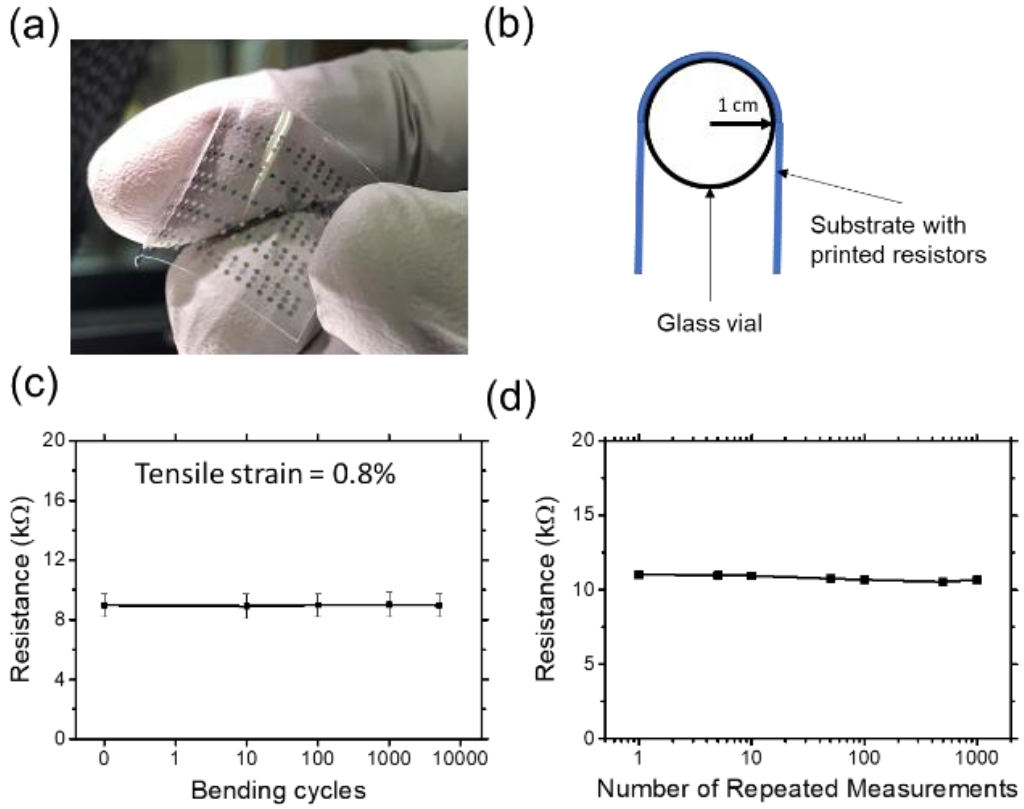

Figure 4.8 (a) Photograph of a 20 × 5 array of printed resistors on a PET substrate. (b) A schematic drawing of the bending test along the length of the resistors with a bending radius of 1 cm. (c) The resistance changes with bending cycles for the printed resistors. The averages and the standard deviations show the results collected from 5 devices. (d) The resistance changes with the number of repeated IV measurements of one device.

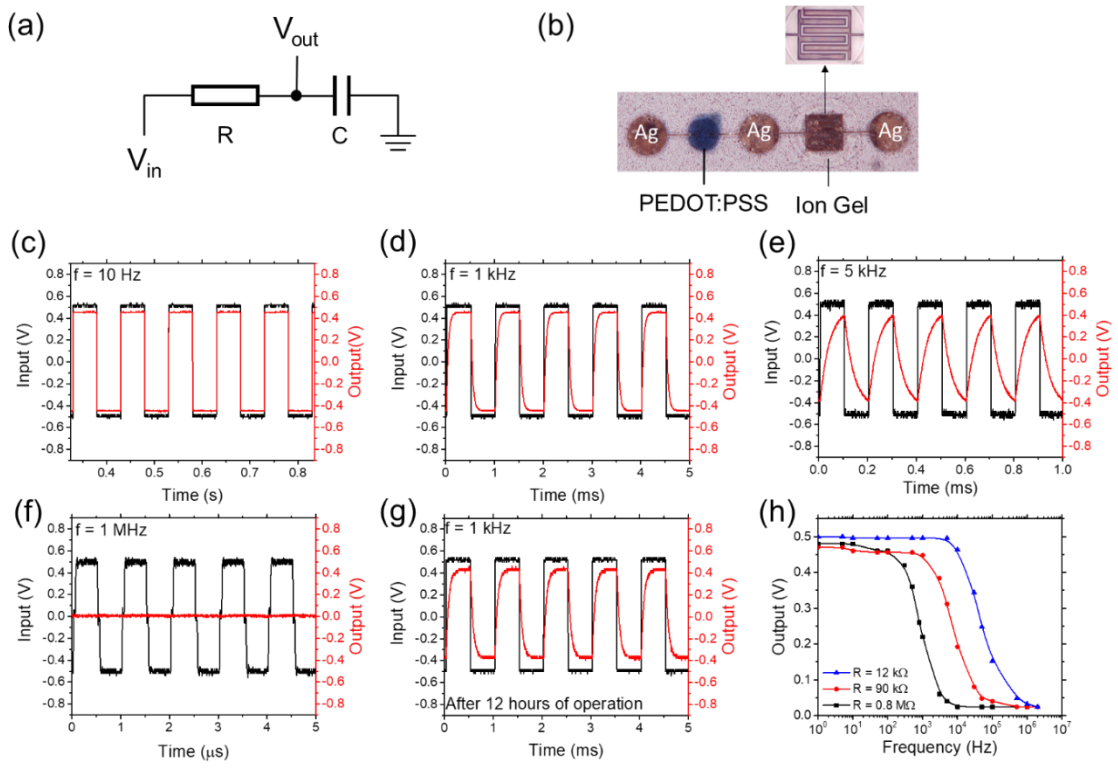

Figure 4.9 (a) Equivalent circuit of the printed low-pass RC filters. (b) Optical image of a completed RC filter with a PEDOT:PSS resistor and an ion-gel capacitor. Transient response of a RC filter with a resistor of 90 kΩ under a square wave input at frequencies of (c) 10 Hz, (d) 1 kHz, (e) 5 kHz, (f) 1 MHz, and (g) 1 kHz after 12 hours of continuous operation. (h) Frequency response of printed low-pass RC filters with resistors of 0.8 MΩ, 90 kΩ and 12 kΩ.

The transient response of the *RC* filter was measured by applying a square wave input signal and collecting the output signal using a digital oscilloscope. Figures 4.9 (c-f) show the transient responses of the *RC* filter consisting of a 90 kΩ resistor and a 0.45 nF capacitor at different frequencies. For an ideal low-pass *RC* filter, the output voltage within the time domain can be predicted by

$$V_{out} = V_{in}\left(1 - e^{-\frac{t}{RC}}\right) \qquad (1)$$

where V_{in}, R, C, and t are the input voltage, resistance, capacitance, and time, respectively[130]. *RC* is the time constant, which is 40.5 μs in this case. When the *RC* constant

is much smaller than the period of the input signal, that is, at a low frequency (f = 10 Hz, Figure 4.9 (c), the waveform of the output signal matches the input signal very well and $V_{out} \approx V_{in}$. The output signal follows the input signal well up to 1 kHz (Figure 4.9 (d)). At 5 kHz, the period of the input signal is small enough to be comparable to the *RC* constant, so the amplitude of the output voltage starts to diminish (Figure 4.9 (e)). When the frequency is further increased, the amplitude of the output voltage drops significantly until no output waveform is observed at 1 MHz (Figure 4.9 (f)). The results show that the dependence of the transient responses on the input frequency is in good agreement with the theoretical prediction, indicating that printed low-pass *RC* filters via the SCALE process are fully functional and rationally designed. In addition, an operational stability test was performed on the *RC* filter. As shown in Figure 4.9 (g), the transient response of the device shows negligible change after 12 h of continuous operation at a frequency of 1 kHz under inert atmosphere, indicating good long-term operational stability.

To demonstrate the tunability of the cutoff frequency, low-pass *RC* filters were fabricated using resistors with different resistances (12, 90, 800 kΩ), as shown in Figure 4.9 (h). A low-pass *RC* filter allows signals with frequencies below the cutoff frequency to pass through with little to no attenuation, while suppressing or blocking the ones with higher frequencies. The cut-off frequency is defined as

$$f_c = \frac{1}{2\pi RC} \qquad (2)$$

at which the amplitude of the output voltage is reduced to $V_{out} = V_{in}/\sqrt{2}$ [130]. The theoretical cutoff frequencies are compared with the experimental cutoff frequencies estimated from the frequency response curves (Figure 4.9 (h)), as summarized in Table 4.2 The results show that the measured cutoff frequencies agree well with the calculated cutoff

frequencies, demonstrating that varying the resistance is a reliable way to tailor the cutoff frequency of the printed low-pass *RC* filter. The cutoff frequency can be adjusted over two orders of magnitude from 400 Hz to 27 kHz simply by changing the resistance.

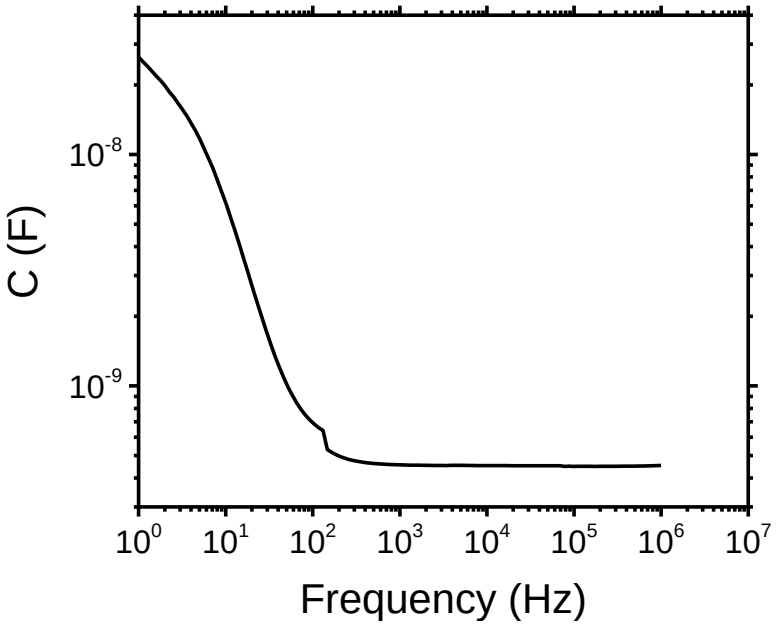

Figure 4.10 Plot of the capacitance of an individual printed capacitor as a function of frequency

Table 4.2 Experimentally estimated and theoretically calculated cut-off frequencies of the printed *RC* filters

Resistance	**Capacitance**	**Cut-off frequency from experiments**	**Cut-off frequency calculated theoretically**
12 kΩ	5.00×10^{-10} F	26.8 kHz	26.5 kHz
90 kΩ	4.54×10^{-10} F	4.3 kHz	3.9 kHz
0.8 MΩ	4.59×10^{-10} F	477 Hz	434 Hz

4.7 Conclusion

In this work, we demonstrated self-aligned inkjet printed resistors on roll-to-roll imprinted flexible substrates with resistances ranging over five orders of magnitude. Changes in resistance within one order of magnitude were achieved by varying the separation of the two electrodes, while larger changes were made by blending the PEDOT:PSS PH1000 ink with ethylene glycol or PEDOT:PSS AI4083 ink. A linear relationship was observed between the resistance and the electrode separation, indicating precise control of the resistance. The printed flexible resistors exhibited high mechanical durability and outstanding operational stability. Inkjet-printed low pass RC filters with predictable and stable dynamic performance were also successfully fabricated using the SCALE process. The cut-off frequency was varied over two orders of magnitude by simply changing the resistance of the resistor. The SCALE method appears to be a promising way to facilitate the fabrication of flexible resistors by roll-to-roll processing. Future work will focus on shrinking the size of the receivers to further reduce the footprint and integrating the resistors into flexible circuits.

Chapter 5

Inkjet-Printed, Self-Aligned Organic Schottky Diodes on Imprinted Plastic Substrates

5.1 Introduction

Previous chapters have shown that a variety of printed circuit elements fabricated via the SCALE strategy have been reported to have good electrical performance. However, a multilayer device with a stacked structure such as a diode has been hard to achieve using the SCALE process.

Diodes are ubiquitous elements in electronic circuits that can be used in a vast range of applications, including radio frequency identification (RFID) tags [52], energy harvesting devices [131] and wireless communication [132]. Organic Schottky diodes based on polymer

semiconductors have attracted considerable attention in the printed electronics field due to the relatively simple device structure compared to a PN junction diode [133-136]. A typical printed organic Schottky diode consists of a semiconductor thin film sandwiched between two electrode layers forming one ohmic contact and one Schottky contact depending on the work function of the electrodes. A diode conducts appreciable current only in one direction due to the existence of the asymmetric energy barrier at the Schottky contact. Printing is regarded as a very promising way to make diodes in large quantities, [137] and several reports have appeared on printed diodes [23, 131, 135, 138-142]. However, fully printed diodes in a roll-to-roll compatible process are much less frequently reported [51, 54, 135]. Finding a reliable process to fabricate fully printed diodes in large quantities still remains a challenge.

A vertically stacked structure is preferred for printed diodes due to the larger contact area between the metals and the semiconductor, which leads to larger forward-bias currents than a horizontal, coplanar structure. The challenging part of making printed diodes in a vertically stacked structure via the SCALE process lies in preventing a short between the top and bottom electrodes. This is because in such structures the semiconductor layers are thin and can have pinholes. An additional complication that can lead to shorting is uncontrolled spreading of ink into channels or cavities that have already received ink or that are intended to be devoid of ink, as will be clarified below.

This chapter discusses a roll-to-roll compatible printing method to fabricate self-aligned, fully printed diodes on plastic substrates using SCALE. The diode is based on a Ag/P3HT/PEDOT vertical stack. An Ag thin film serves as the bottom electrode, forming a Schottky contact with the P3HT (poly(3-hexylthiophene)) semiconducting layer on top

of it. PEDOT:PSS (poly(3,4-ethylenedioxythiophene) polystyrene sulfonate) is chosen as the top electrode material since it forms an ohmic contact with the P3HT layer. The capillary network design of the diode includes several flow control structures to achieve precise ink flow, which is a key point to avoid electrical shorts and to improve device performance. Employing this new strategy, we have achieved fully printed diodes on polyethylene terephthalate (PET) with rectification ratios up to 5×10^4. The results of bending tests indicate excellent mechanical durability of the printed diodes. Overall, it appears promising to scale-up the whole fabrication process to roll-to-roll printing in order to facilitate low-cost, large scale manufacturing of printed diodes.

5.2 Experimental Section

5.2.1 Silicon master template

The silicon master template was prepared by three cycles of photolithography and dry etching on a 4-in silicon wafer (Figure 5.1). (1) In the first patterning cycle, the receiver pattern shared by the semiconductor layer and the top electrode was created on the silicon wafer. A silicon wafer was dried at > 100 ºC on a hot plate and then immersed in a hexamethyldisilazane (HMDS) atmosphere. A layer of positive photoresist (Microposit S1813) was deposited onto the wafer by spin-coating at 2000 rpm for 30 s followed by soft-baking at 115 ºC for 1 min. The wafer was then exposed to ultraviolet light for 6 s in a photo aligner under a photomask and immersed in a diluted solution of developer (Microposit 351 (Dow):H_2O = 1:5 by volume) for 40 s to remove the photoresist in the exposed area. A plasma etcher (STS) was used to etch the exposed area down to a depth of

4 μm. The wafer was then washed by acetone, methanol, and isopropyl alcohol in sequence to strip off the photoresist. (2) The second patterning cycle created the ink receiver and the capillary channel for the bottom Ag electrode. The silicon wafer from the last step was heated at 200 ºC for 5 min and treated in a HMDS atmosphere again. Then, a layer of positive photoresist (AZ9260, MicroChemicals) was spin-coated onto the wafer (300 rpm for 10 s then 2000 rpm for 60 s) to achieve a thickness of about 10 μm. After pre-baking at 110 ºC for 165 s, the wafer was aligned to the photomask for the second layer in the same photo aligner and exposed to UV light for 42 s. The wafer was then washed in a mixture of AZ400K (Merck Performance Materials) and H_2O (AZ400K:H_2O=1:4) for 4 min to remove the exposed part of the photoresist. The exposed area of the silicon wafer was then dry etched to a depth of 5 μm by the plasma etcher (STS). To remove the rest of the AZ 9260 photoresist layer, the wafer was immersed in heated 1165 resist remover (Dow) for 1 h. (3) In the third cycle, the receivers and capillary channels designed to connect this single diode to other devices were patterned using a similar procedure as the second cycle except for the etching step. A plasma deep trench etcher (SLR 770) was employed instead of the STS etcher in the third cycle to obtain indented features with vertical walls and a depth of 10 μm. The wafer was further cleaned in a Piranha solution (H_2SO_4 and H_2O_2, 1:1; WARNING: Piranha solution is highly oxidizing and corrosive!!) to dissolve any residual photoresist.

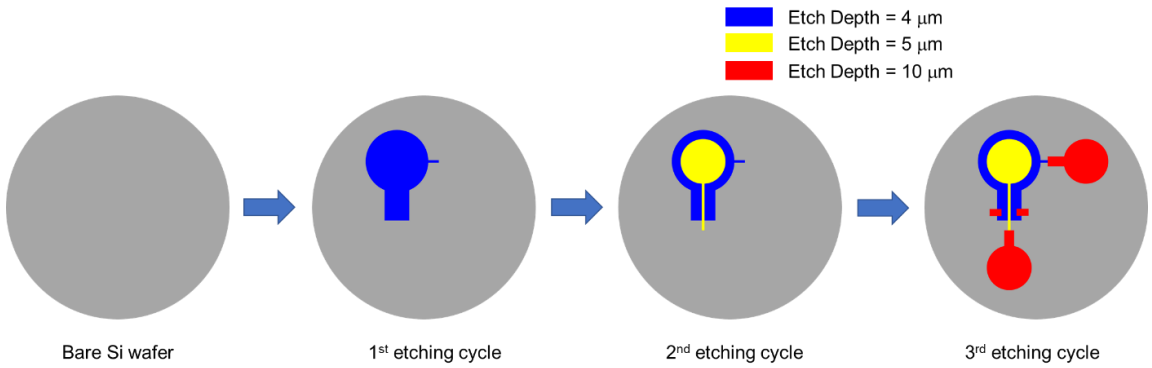

Figure 5.1 Schematic drawing for preparation of silicon master template through three cycles of photolithography and etching

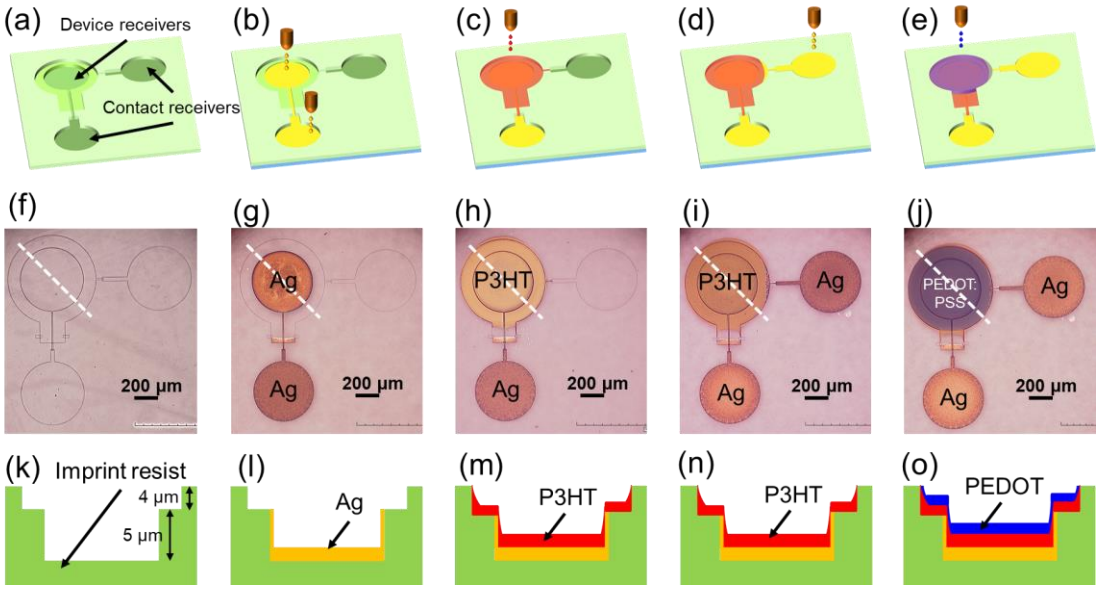

Figure 5.2 Schematic illustration of the printing process of a diode using the SCALE process showing (a) the as-prepared imprinted substrate, (b) Ag electrode printing, (c) P3HT ink printing, (d) side Ag electrode printing and (e) top PEDOT:PSS electrode printing with the corresponding top view optical images (f)-(j), and the schematic cross sections (k)-(o) along the white dashed line.

5.2.2 Imprinted flexible substrates

The patterns on the silicon master template were first transferred to a flexible PDMS (polydimethylsiloxane) stamp. The wafer was pre-treated in a trichloro(1H,1H,2H,2H-perfluorooctyl)silane vapor to facilitate the peeling off process of the PDMS stamp. The PDMS elastomer and the curing agent (Sylgard 184, Dow Corning) were mixed to a weight ratio of 10:1 and the mixture was poured slowly on top of the silicon master template. Then the PDMS was heated to 70 ºC in an oven and kept at that temperature for 1 h. After the PDMS layer was fully cured and solidified, it was peeled from the silicon template followed by a post-annealing at 100 ºC for 30 min in an oven.

A PET sheet was pre-cleaned by isopropyl alcohol. A layer of UV-crosslinkable imprint resist (NOA73: Norland Optical Adhesive 73) was coated on the PET sheet. Then the PDMS stamp was pressed into the imprint resist, which was illuminated by an ultra-violet light for 2 h. After the imprint resist solidified, it adhered firmly to the PET sheet. The PDMS stamp was then delaminated from the imprint resist, resulting in pattern transfer. The imprinted NOA73-PET laminate served as the substrate for printing devices.

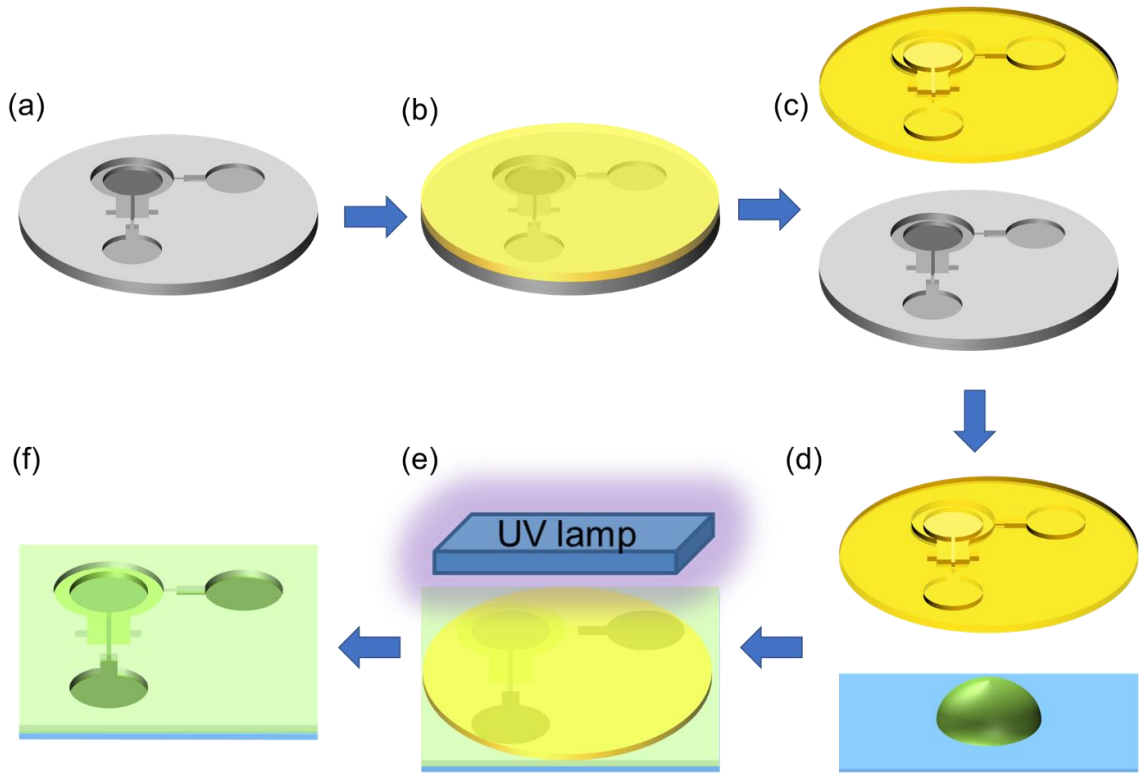

Figure 5.3. Schematic illustration for preparation of imprinted substrates. (a) Silicon master template shown in Figure 5.1. (b) Casting PDMS over the silicon template. (c) Remove the thermally cured PDMS stamp. (d) Coating imprint resist onto a piece of PET substrate. (e) Pressing the PDMS stamp into the resist coating and Curing with UV light. (f) An imprinted substrate with patterns after the delamination of the PDMS stamp

5.2.3 Ink preparation and inkjet printing of diodes

The particle-free Ag ink was purchased from Electroninks. The P3HT ink was prepared by dissolving P3HT in dicholorobenzene to various concentrations (25, 37.5 and 50 mg/ml). The PEDOT:PSS ink was prepared by mixing a commercial PEDOT:PSS ink (PH1000, Heraeus) with ethylene glycol (6 wt%) to improve the conductivity [125].

All the inks were inkjet printed using an inkjet nozzle (Microfab) with an 80 μm orifice in ambient air, according to the sequence shown in Figure 5.2. A particle-free Ag ink (Electroninks, Inc) was first printed into two recievers (Figure 5.2 (b)) and annealed at 100 ºC for 3 min on a hotplate. Then P3HT ink was deposited on top of the Ag film in the

device reciever (Figure 5.2 (c)) and heated at 120 ºC for 30 min in a N_2 atmosphere in a glovebox. Then the particle-free Ag ink was delivered into the side, contact receiver to form the connection to the top electrode (Figure 5.2 (d)) and dried. Finally, the top electrode was printed using the PEDOT:PSS ink (Figure 5.2 (e)) and annealed at 120 ºC for 10 min in a glovebox.

5.2.4 Characterization

Optical images were taken with a Hirox high-resolution optical microscope. All the SEM images were taken with a JEOL 6500 scanning electron microscope (SEM). The current-voltage (I-V) curves were measured at a probe station with Keithley 236 and 237 source meters. A signal generator (Agilent 33512B) was utilized to apply the sine waves to the diodes, and an oscilloscope (Tektronix TDS3014C) was employed to measure the input and output signals.

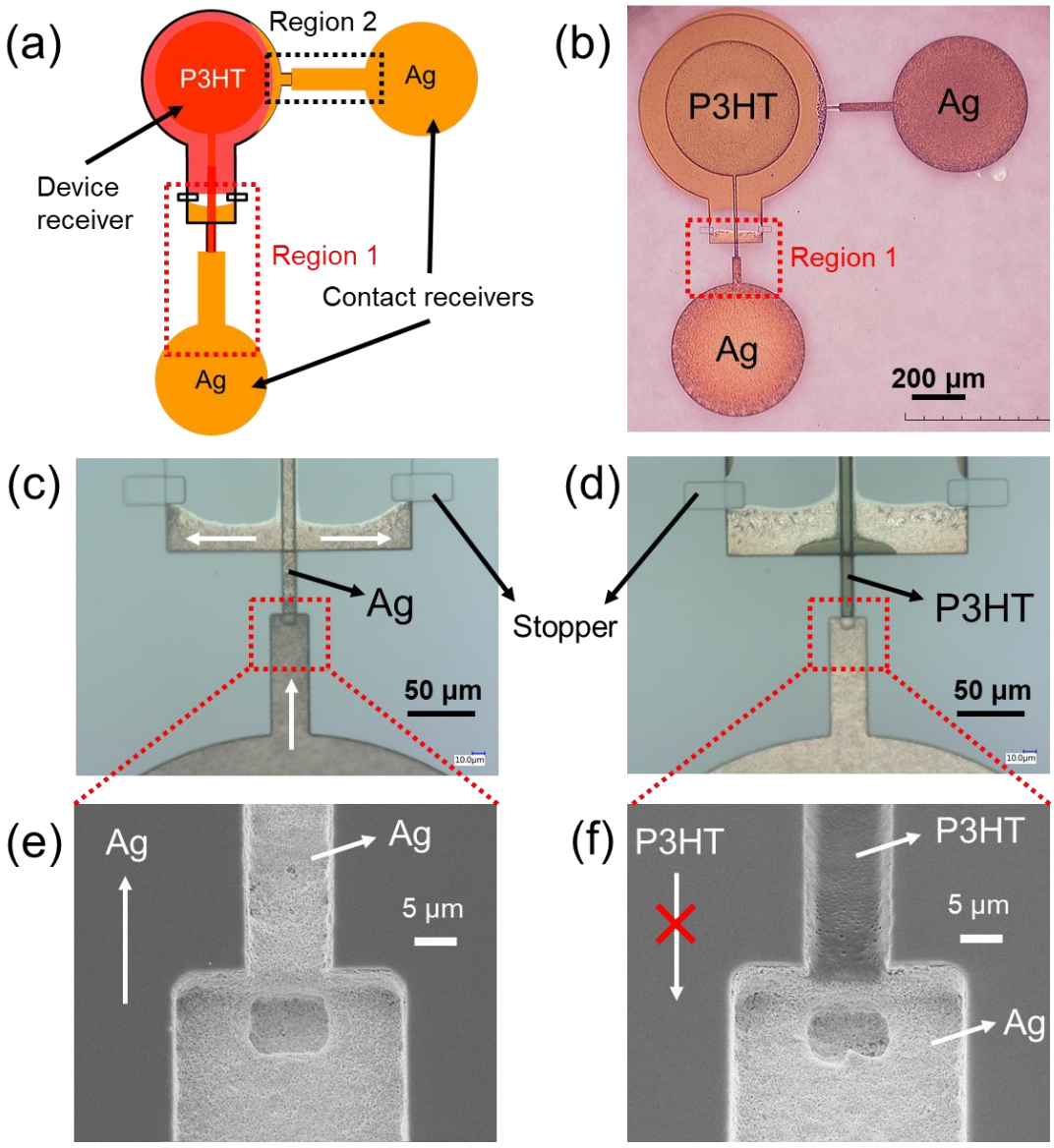

Figure 5.4 Optical and SEM images of an unfinished diode showing details of the *microfluidic* diodes and the flow stoppers. (a) A top view scheme and (b) an optical image of a partially completed printed diode. Two regions of interest are highlighted. (c,d) Enlarged optical images for Region 1 after depositing the Ag film (c) and the P3HT film (d). (e, f) Slightly tilted SEM images for the red dotted regions in (c) and (d), correspondingly.

Figure 5.2 shows an overview of the printing process for diodes via the SCALE strategy. For example, Figures 5.2 (a, f and k) display the 3D schematic, the corresponding top view optical image of an imprinted pattern, and the device cross-section along the dotted line. The preparation process of the imprinted substrates is discussed in detail in the Supporting Information (Figure 5.1 and 5.3). In this paper, a *contact receiver* is defined as a circular depression where inks are delivered in order to form an external contact pad for a device; a *device receiver* is a circular cavity in which the delivered ink dries and forms an active layer of a device. The diode was mainly constructed within the two concentric device receivers shown on the upper left corner of Figures 5.2 (a-j). The smaller receiver (diameter = 500 μm, depth = 5 μm) for the bottom Ag electrode was depressed within the larger receiver (diameter = 700 μm, depth = 4 μm) designed for the semiconductor and the top electrode. The other two contact receivers and the capillary channels connected to them served as the external connection to the bottom and top electrodes, so the diode could be integrated into a circuit. The depth of these contact receivers and the capillary channels was 10 μm because a larger depth facilitates a longer capillary flow distance, which is preferrable for external connections.

The printing process is depicted schematically in Figures 5.2 (b – e). First, a particle-free Ag ink was delivered into the device receiver and contact receiver (Figure 5.2 (b)) and then dried on a hot plate in air to form the bottom electrode and the external connection to the bottom electrode (Figures 5.2 (g), (l)). The device receiver and contact receiver were connected through a capillary channel (width = 10 - 30 μm) with a two-tier junction, whose structure and function are discussed later.

5.3 Design and Fabrication of Printed Diodes

In the next step, P3HT ink was printed into the larger device receiver over the Ag film (Figure 5.2 (c)) and the ink flowed into a wide channel (width = 100 μm) to fully cover the underlying Ag film (Figures 5.2 (h), (m)). After drying and annealing of the P3HT film, the same particle-free Ag ink was printed into the contact receiver on the right side (Figure 5.2 (d)). The adjoining capillary channel that connected to the P3HT-filled device receiver contained a two-tier junction. Thus, Ag ink could flow via the channel onto the circular P3HT film and form a crescent-shaped contact along the circular ink receiver lip (Figure 5.2 (i)). Lastly, PEDOT:PSS ink was printed into the same receiver as the P3HT ink (Figure 5.2 (e)) and annealed to form the top electrode (Figures 5.2 (j), (o)). The PEDOT:PSS also covered the crescent-shaped Ag film on top of P3HT to make an external connection to the top electrode (Figure 5.2 (j)).

5.4 Flow Control Structures

To fabricate a diode in a vertically stacked structure using the SCALE process, precise control of the ink flow in the imprinted capillary network is critical to avoid short circuits and to improve reproducibility. We incorporated two types of ink flow control structures, namely flow stoppers and *microfluidic* diodes, into the capillary network to regulate ink flows and subsequent film deposition. Figure 5.4 (a) shows the flow control structures in two regions of interest in a schematic drawing of a printed diode from top view. Figure 5.4 (b) displays the corresponding top view optical image. Enlarged optical images of Region 1 are shown in Figures 5.4 (c, d) to show the design details clearly. Region 2 is shown in Figure 5.5 and will be discussed later.

A flow stopper is a rectangular depression [3]. Two stoppers were introduced along the wide channel connected to the P3HT receiver (Figures 5.4 (c, d)). The stoppers (depth = 10 μm) were deeper than the wide P3HT channel (depth = 4 μm), thus creating an edge along the flow path of the Ag ink and obstructing further flow along the side walls of the wide channel. When the Ag ink was delivered to the contact receiver at the bottom of the image, the ink passed the microfluidic diode, bifurcated along the walls on both sides at the intersection of the wide P3HT channel and the narrow channel and then was stopped by the rectangular depressions due to contact line pinning at the sharp edge. Without the stoppers, the Ag ink might flow along the side walls of the wide P3HT channel and into the adjoining P3HT receiver, in which the Ag film along the side wall couldn't be fully

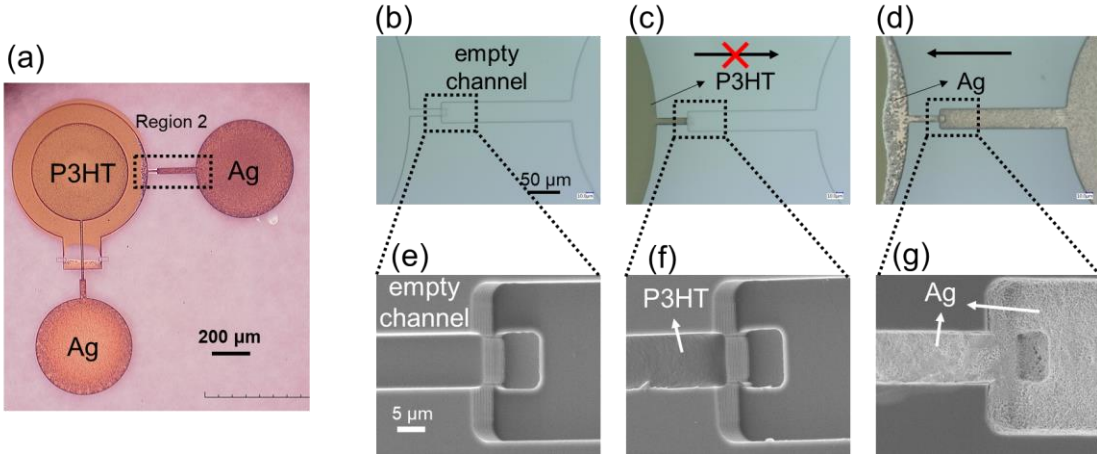

Figure 5.5. Role of microfluidic diode in Region 2. (a) Optical image of a partially completed printed diode showing the second microfluidic diode in Region 2. (b-d) Zoom in optical images of Region 2 showing (b) the empty channels, (c) the pinning effect of P3HT ink and (d) the formation of the crescent shaped Ag film. (e-g) corresponding tilted SEM images of the black dotted boxes in (b-d).

covered by the P3HT film. Since PEDOT:PSS shared the device receiver with P3HT, the uncovered Ag film along the side wall would be in contact with the PEDOT:PSS layer, causing shorting defects.

The second type of ink flow control structures was the *microfluidic* diode. A microfluidic diode consists of two adjoining open capillary channels: a narrow, shallow channel abutting a wide, deep channel (Figure 5.4 (e, f)). This junction provides unidirectional ink transport that only allows the ink to flow from the deeper channel to the shallower one but halts the flow in the opposite direction due to the Gibbs criterion that governs flow over edges and steps [109]. The microfluidic diode in Region 1 is displayed in Figures 5.4 (c, d) marked by red dotted boxes. Ag ink delivered to the contact receiver flowed through the junction to make connection to the Ag delivered nearly simultaneously to the device receiver. A granular Ag film was deposited uniformly in the microfluidic diode and in the two receivers. The tilted SEM image in Figure 5.4 (e) shows the high quality Ag film in the microfluidic diode. In the next step, P3HT ink was delivered to the device receiver, covering the bottom Ag electrode. Excess P3HT ink flowed out of the receiver and down the capillary, but was pinned at the junction (Figure 5.4 (d)). The SEM image in Figure 5.4 (f) clearly shows that the deposition of P3HT stopped at the junction. Interestingly, this also indicates that the underlying Ag film does not disturb the flow control function of the microfluidic diode. Crucially, the microfluidic diode prevented the P3HT ink from flowing over the Ag contact pad, which is important for clear device definition and integration into circuits.

Figure 5.5 (a) shows the microfluidic diode in Region 2 on the right side of the device in the black dotted box. Figures 5.5 (b - d) display the top view optical images of the junction before printing, after P3HT deposition, and after the second Ag deposition, respectively. Excess P3HT ink delivered to the device receiver (as described above) flowed into the narrow capillary but stopped precisely at the junction (Figures 5.5 (c, f)). After the

P3HT film dried, the Ag ink delivered subsequently to the contact receiver on the right flowed through the junction over the P3HT film in the narrow channel and into the circular lip on the right side of the device receiver. The deposited Ag film formed a crescent shape on the lip because the hydrophobicity of the P3HT surface inhibited the ink from flowing and spreading farther. Thus, this second microfluidic diode blocked P3HT ink from flowing over the external contact but then allowed the Ag ink to pass the junction to add the necessary connection to the top device electrode, namely PEDOT, delivered to the device receiver at the last step (see Figure 5.2 (e)). PEDOT:PSS ink has a higher surface tension than Ag and P3HT ink [109]. So, the PEDOT:PSS ink was confined within its receiver very well and didn't enter the adjacent narrow capillary channels filled with Ag (and partially with P3HT). Taking advantage of the difference of surface tension of the inks

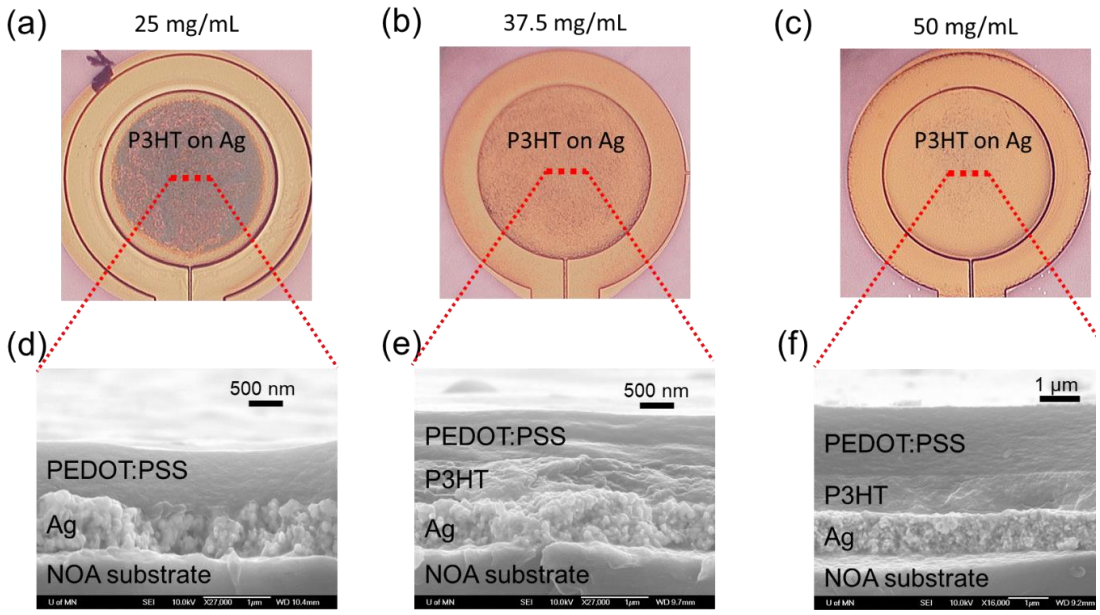

Figure 5.6. (a-c) top view optical images of annealed P3HT films deposited using inks with a P3HT concentration of (a) 25 mg/mL, (b) 37.5 mg/mL and (c) 50 mg/mL. (d-f) cross-sectional SEM images for completed devices taken along the red dashed lines shown in (a-c)

prevents undesirable contact between the top and bottom electrodes. This is one reason why PEDOT:PSS was placed on the top instead of at the bottom.

The thickness of the P3HT film has a significant influence on the device performance and yield. Figure 5.6 shows the P3HT film deposited from inks with concentrations varied from 25 mg/ml to 50 mg/ml. Figures 5.6 (a - c) show the top view optical images of the P3HT film over the bottom Ag electrode. To characterize the thickness of P3HT films, completed devices were cut across the P3HT receivers along the red dashed lines after printing the top PEDOT:PSS electrodes. Cross-sectional SEM images taken at the center point of the P3HT receiver are shown in Figures 5.6 (d - f). When a 25 mg/ml P3HT ink was used, the underlying Ag film was not fully covered by the P3HT film. Most of P3HT deposited along the edge because the ink wet the sidewalls of the receiver, leaving a thin and non-uniform P3HT film covering the Ag electrode in the center. A P3HT layer is barely visible between the Ag and PEDOT:PSS films in Figure 5.6 (d). As a result, all devices fabricated with 25 mg/ml P3HT inks were shorted, indicating that this concentration was too low to deposit a thick enough P3HT film. When the ink concentration increased to 37.5 mg/ml, the Ag electrode was fully covered by a P3HT film with a thickness of 528 nm at the center. The yield of functional diodes printed with the 37.5 mg/ml P3HT ink was around 22%, which was not satisfactory for a reliable process. When a P3HT ink of 50 mg/ml was used, the film thickness at the center of the device receiver increased to 950 nm, resulting in a raised yield up to 90%. The boost in yield upon increasing ink concentration could be explained by the thinning of the P3HT film at the edge of the Ag-coated device receiver, see Figure 5.2 (n). The P3HT film covering the vertical wall at the edge of the device receiver was much thinner than the P3HT film over the center of the receiver. Using a

P3HT ink with a concentration of 37.5 mg/mL had a higher possibility of leaving a P3HT film that was too thin at the edge of the receiver to cover the underlying Ag film, leading pinholes and shorts. Consequently, P3HT inks with a concentration of 50 mg/ml were used for diode printing and further device tests. The humidity when printing the diodes was also critical to the yield; high humidity led to undesirable wetting of the P3HT ink outside the device receiver, resulting in a thinner P3HT film in the device receiver. A relative humidity around 20% was needed to guarantee a high yield.

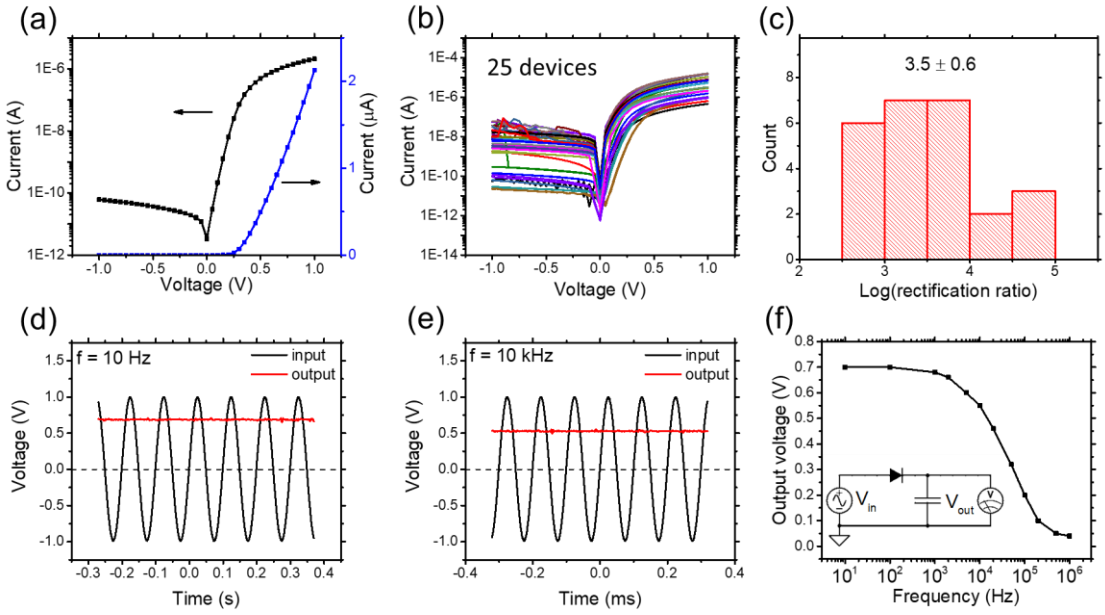

Figure 5.7. Static and dynamic electrical performances of printed diodes (a) IV characteristic of a printed diode. (b) IV curves collected from 25 printed diodes and (c) histogram of log(rectification ratio) of these devices. (d-) dynamic performance of a rectifier circuit (shown in the inset image in (f)) at an input frequency of (d) 10 Hz and (e) 10 kHz. (f) Output voltage as a function of input frequency for the rectifier circuit in the inset image. The capacitor connected in series with the diode is 1 μF.

5.5 Electrical Performance

Figure 5.7 presents the electrical performance of printed diodes using P3HT inks with a concentration of 50 mg/ml. Figure 5.7 (a) plots the I-V characteristic of a printed diode

when sweeping the voltage applied to the top PEDOT:PSS electrode from -1 V to 1 V and grounding the bottom Ag electrode. No measurable hysteresis was observed. Figure 5.7 (b) overlays the I-V curves of 25 printed diodes to evaluate the reproducibility of the process, and the calculated rectification ratios were measured to be $10^{3.5 \pm 0.6}$, which is summarized in a histogram (Figure 5.7 (c)). The variation in device performance could be further improved by better control of the ink delivery process and the substrate wetting condition.

In order to assess the printed diode as a rectifier, a simple circuit was employed for dynamic measurements in which a printed diode was connected in series with a commercial

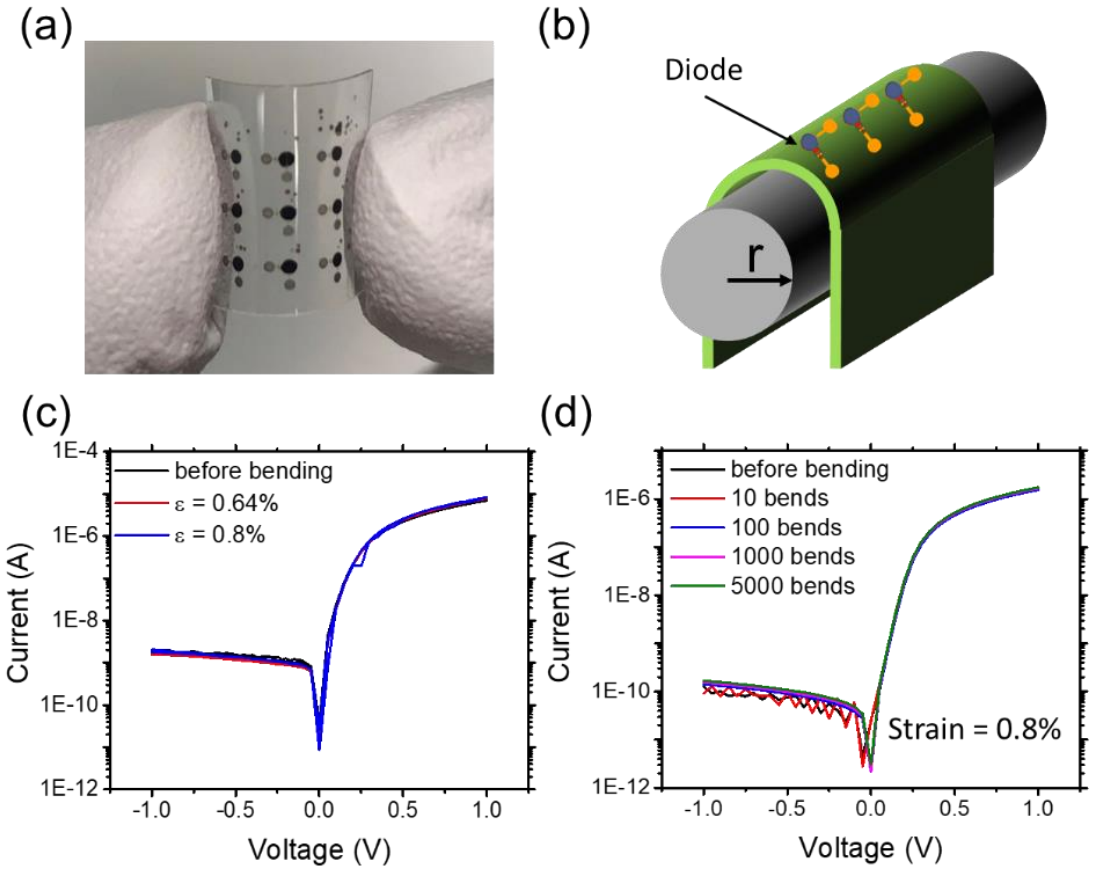

Figure 5.8. (a) Photo of a bended 3 × 3 array of printed diode on a piece of imprinted substrate. (b) A 3D schematic illustration of a bending test over a glass vial. (c) IV curves measured on a bended diode as the tensile strain increases from 0 to 0.8%. (d) IV curves collected after repeated bending cycles from 0 to 5000 bends.

capacitor (C = 1 μF). The measurement circuit is shown in the inset plot in Figure 5.7 (f). Under a 10 Hz, 1 V peak-to-peak oscillating input signal, an output DC voltage of 0.7 V was obtained (Figure 5.7 (d)), which demonstrates a maximum 70% rectification efficiency. A DC output voltage of 0.55 V was maintained when the input frequency rose to 10 kHz without any AC ripples (Figure 5.7 (e)). The frequency response of the output of the rectifier circuit is plotted in Figure 5.7 (f), indicating that the printed diodes rectified an AC signal with a frequency as high as 100 kHz.

As shown in Figure 5.8 (a), an array of diodes was printed on a flexible substrate. The mechanical durability of the printed diodes was investigated by measuring the I-V characteristics under various bending conditions, as shown schematically in Figure 5.8 (b). The device was first tested in situ when wrapped around a glass vial with a bending radius of 1.25 or 1 cm, which correspond to a tensile strain of 0.64% or 0.8%. The electrical performance was unchanged under a tensile strain up to 0.8% (Figure 5.8 (c)). Then the device was bent repeatedly over a glass vial to a tensile strain of 0.8 % and the electrical performance was tracked, Figure 5.8 (d). After 5000 bend cycles, there were no appreciable changes in the electrical performance, demonstrating excellent mechanical durability. Printed P3HT and PEDOT:PSS films are inherently flexible, but it was easier for the Ag film to crack under a tensile strain due to its granular nature. So, the resilience to bending of an individual device depended primarily on the quality and thickness of the deposited Ag film.

5.6 Conclusion

Fully printed and flexible diodes were fabricated via the SCALE strategy that utilizes capillarity, differential wetting, and edge pinning to control liquid flows. Diodes with a rectification ratio as high as 5×10^4 were achieved with this process, and printed diodes on flexible substrates demonstrated excellent mechanical durability in bending tests. Overall, this work demonstrates a reliable way to fabricate flexible diodes by printing. We anticipate that the process design described here can also be utilized for other electronic components with a vertically stacked structure such as capacitors and crossovers. Furthermore, the integration of the diodes into simple AC power rectifiers suggests that these devices can be employed in fully printed RFID tags and sensors by the SCALE method, which will be the subject of future work.

Chapter 6

Future Work

6.1 Reducing the Overall Device Footprint

In traditional microelectronic manufacturing area, the development of integration density follows a trend known as the Moore's law. The number of transistors on a silicon chip doubles every two years. Higher integration density has always been the pursuit of semiconductor industry because it indicates higher chip functionality. Although printed devices are much larger in size compared with electronic elements on a chip, device density is still a big concern in printed electronics field considering the fabrication cost. So, one possible direction of future work in SCALE will focus on miniaturization of printed devices. This goal can be realized by both shrinking the size of the receivers and optimizing the pattern design.

6.1.1 Shrinking the size of receivers

In the work showcased in the preceding chapters, both ink and device receivers have diameters around or above 500 μm, which is large in size compared to the capillary channels. On one hand, using these large receivers greatly relax printing tolerance; On the other hand, these large receivers significantly increase the total area taken by each device. Scaling down ink receivers which don't serve as active layers in a device is an easier approach since the size of ink receivers doesn't have a significant impact on device performance. For example, if the ink receiver diameter in the printed resistor discussed in Chapter 4 shrinks from 500 μm to 100 μm, the total footprint can be reduced by 40%.

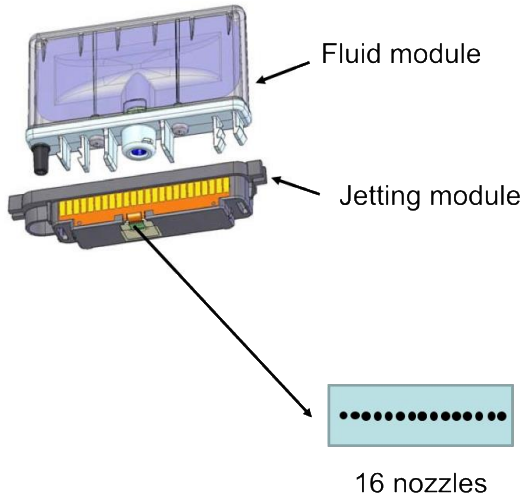

Figure 6.1 Dimatix printhead

The nozzle (Microfab) used in Chapter 4 and 5 has an orifice diameter of 80 μm, which delivers ink drops with a diameter of around 90 μm. Printed dots are around 220 μm after the spreading and drying of drops on the substrate, which is too large for 100 μm receivers. In order to achieve a higher resolution, a nozzle with a smaller orifice is preferred for

targeting smaller receivers. Dimatix printhead, another type of piezoelectric printhead, has an orifice of 21 μm. Figure 6.1 shows the structure of a Dimatix printhead. Utilizing Dimatix printhead for printing can reduce the diameter of the printed dots to around 50 μm with 26 μm drops. The relationship between the orifice opening and drop size is summarized in Table 6.1. It is promising to reduce the receiver size down to 100 μm by utilizing a printhead with a smaller orifice and a more precise digital alignment system.

One challenge with utilizing printheads with smaller orifice is that they have a higher tendency of clogging by the dried ink. In SCALE, inks are formulated to facilitate low-temperature (< 120 °C) drying due to the processing temperature requirement of the plastic substrate. Besides, fast drying is preferred when building a continuously running roll-to-roll printing line. Inks with more volatile solvents are preferred since they dry faster at a low temperature. This feature can shorten the processing time. Considering these two preferences, solvents with low boiling point and good volatility at low temperature are frequently used in ink formulations. However, particle accumulation or film deposition within and around the nozzle caused by fast drying may clog or partially clog the orifice. As a result, the ejected drops are misaligned with the targeted receiver. Satellite drops may also be generated in this process. So, printing through smaller orifices puts a higher requirement for the ink formulation, which may limit the range of available inks. For example, printing polymer particle-based PEDOT:PSS PH1000 ink (Heraeus) may cause nozzle clogging for the 21 μm orifice. Another PEDOT:PSS ink (P Jet HC from Heraeus) is available designed for jetting from small orifice, but the film conductivity deposited by

this ink is lower than the PH1000 ink. There may be a tradeoff between printability and electrical performance in ink formulating.

Table 6.1 Comparison between Microfab and Dimatix printheads

Printhead	**Microfab**	**Dimatix**
Orifice diameter	80 μm	21 μm
Droplet diameter	~ 90 μm	~26 μm
Droplet volume	~380 pl	~10 pl
Printed dot diameter	~ 220 μm	~ 50 μm

6.1.2 Optimizing the pattern design

Another method to reduce the footprint is by optimizing the pattern layout for each electrical element. For example, changing the planar layout of a printed capacitor into a stack structure can reduce the area taken by a device for the same capacitance. Sharing the ink receiver between different devices (Figure 6.2) can both reduce the footprint and the waste of metal materials. Taking advantage of ink flow control structures introduced in Chapter 5 is also a good route. Figures 6.3 (a) and (e) show the design for a design in a previous report [1] and a new design of crossover structures. The new design significantly shrinks the device footprint by utilizing microfluidic diodes to eliminate the “box” marked by red arrows in Figures 6.3 (a)) designed to bifurcate the flow of epoxy. Figure 6.3 (b-d) depicts the printing process of the new crossover structure.

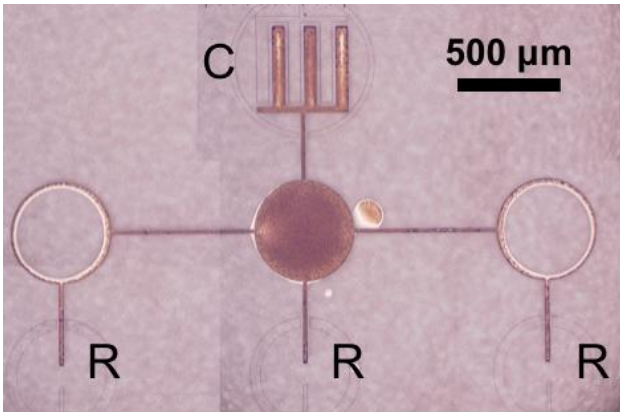

Figure 6.2 A interconnect structure designed to connect three resistors and one capacitor. The interconnect can be printed by only deliver Ag ink in one receiver.

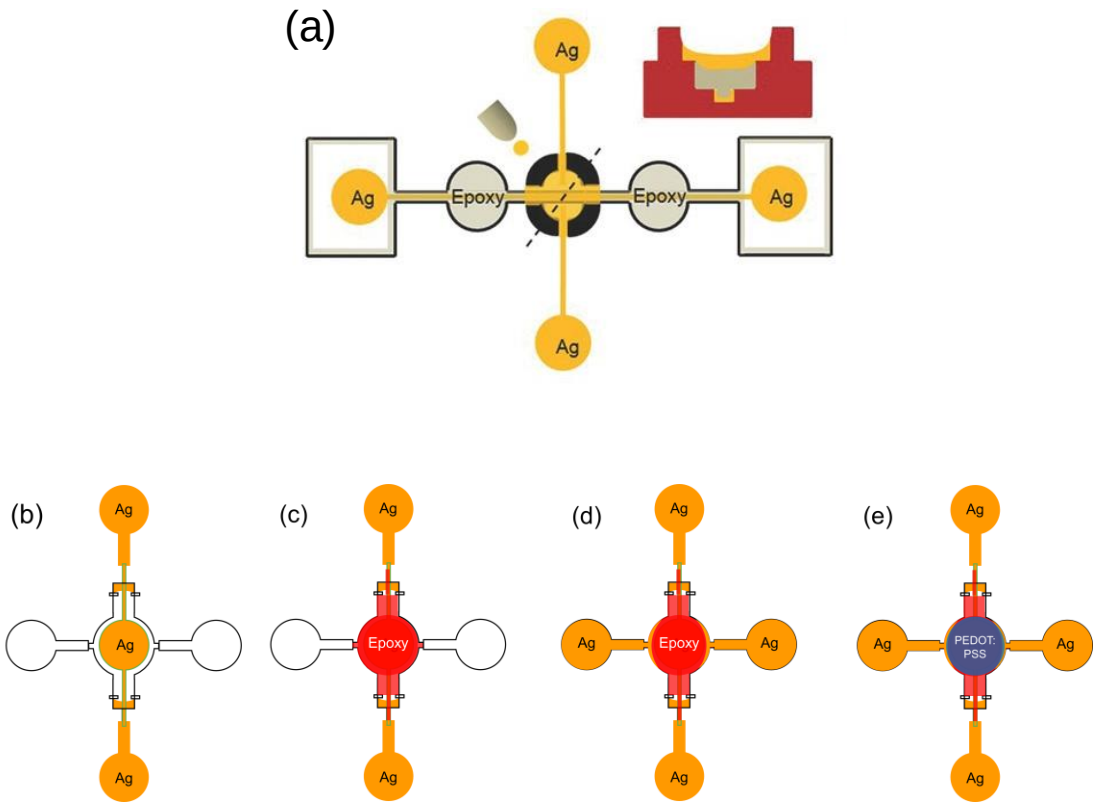

Figure 6.3 Comparison of the previous crossover structure design and the new design. (a) crossover structure design by SCALE in [1]. (b-e) fabrication process of a crossover junction based on the new design. (b) printing the bottom silver electrode and external connections. (c) printing the insulating epoxy layer. (d) printing the Ag connections on both sides. (e) printing the top PEDOT electrode to connect the two Ag electrodes on both sides.

6.2 New Design for a Stack Structure in SCALE

In SCALE, complex topography is patterned on the surface of the plastic substrate to guide the ink flow. Although this feature improves printing resolution and materials registration, it also introduces another short circuit problem when printing a multilayer device in a vertically stacked structure.

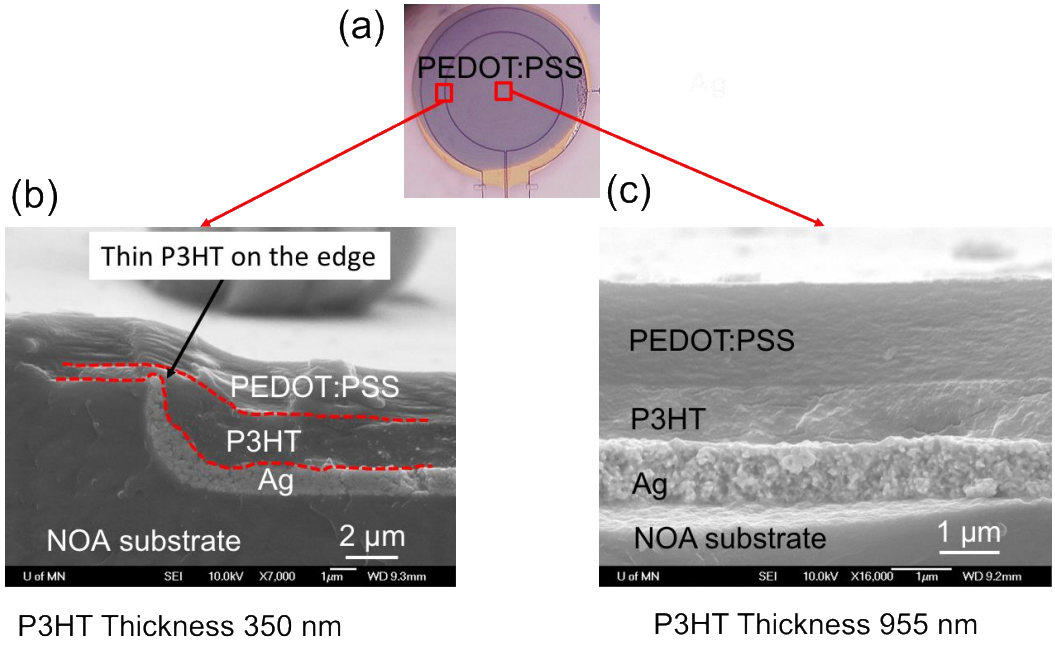

Figure 6.4 Thinning of P3HT film at the edge of the ink receiver observed in the diode design in chapter 5. (a) a top view optical image of a completed diode. (b,c) Cross-sectional SEM image taken at the corresponding marked red boxes in (a) for film stack at (b) the edge of the Ag receiver and (c) the center of the Ag receiver.

The design of printed diodes by SCALE, as has been shown in the preceding chapters, has two concentric circular ink receivers with different radii, resulting in a staggered cavity. When ink dries inside the cavities and deposits a thin film along the wall, the P3HT film covering the vertical wall at the edge of the device receiver (Figure 6.4 (b)) was much thinner than the P3HT film over the center of the receiver (Figure 6.4 (c)). For example,

for a printed diode, in order to retain the device footprint without degrading the performance, a thinner semiconductor is preferred in the stack structure to increase the forward current. But further reduction of the P3HT film thickness by reducing the concentration may lead to electrical shorts at the edge of the inner receiver.

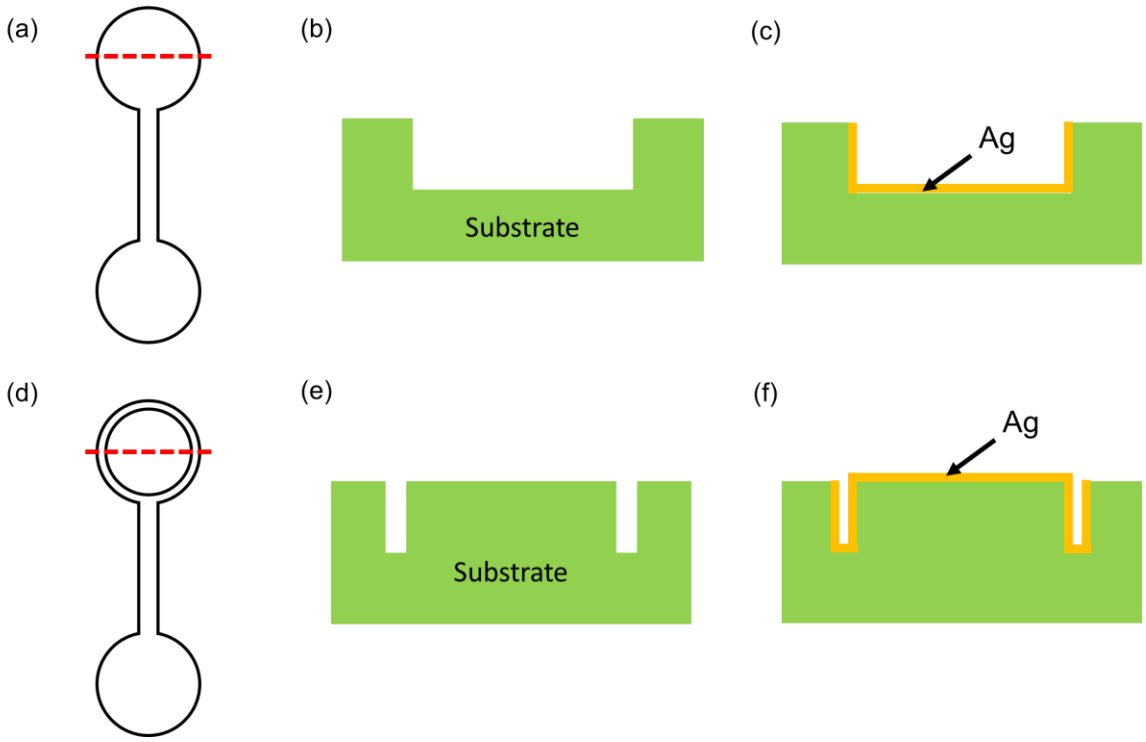

Figure 6.5 Comparison between an indented receiver and an infinite receiver. (a,b,c) plots of an indented receiver from (a) top view, (b) cross sectional view along the red dashed line, and (c) cross sectional view after deposition of a silver layer. (d,e,f) plots of an infinite receiver from (d) top view, (e) cross sectional view along the red dashed line, and (f) cross sectional view after deposition of a silver layer.

In order to tackle this issue, a new design is proposed for printing a device in a stack structure by introducing an “infinite receiver”. In this design, circular trenches are utilized instead of indented reservoirs to build the device receivers (Figure 6.5 (d, e)). The center of the device receiver is at the same level as the rest of the substrate, which reduces the

elevation change on the surface and eliminates the edge of the stagger structure in the previous design. Circular trenches have the same functions with the indented reservoirs. When ink is only deposited in the inner circle and spreads within it, the drop is confined within the circle due to the edge pinning effect. If the same ink is fed into the circular trench from another ink receiver connected to it right after the ink delivery to the inner circle, the ink merges with the drop in the inner circle and form a continuous film after drying (shown in Figure 6.5 (f)) connecting the inner circle to the trench and further to the external contact pad. The film within the inner circle serves as the bottom electrode. When the subsequent layer (e.g. P3HT for a diode) is deposited, dried film can fill the trenches and planarize the surface, thus reducing the thickness variation due to film thinning at the edge.

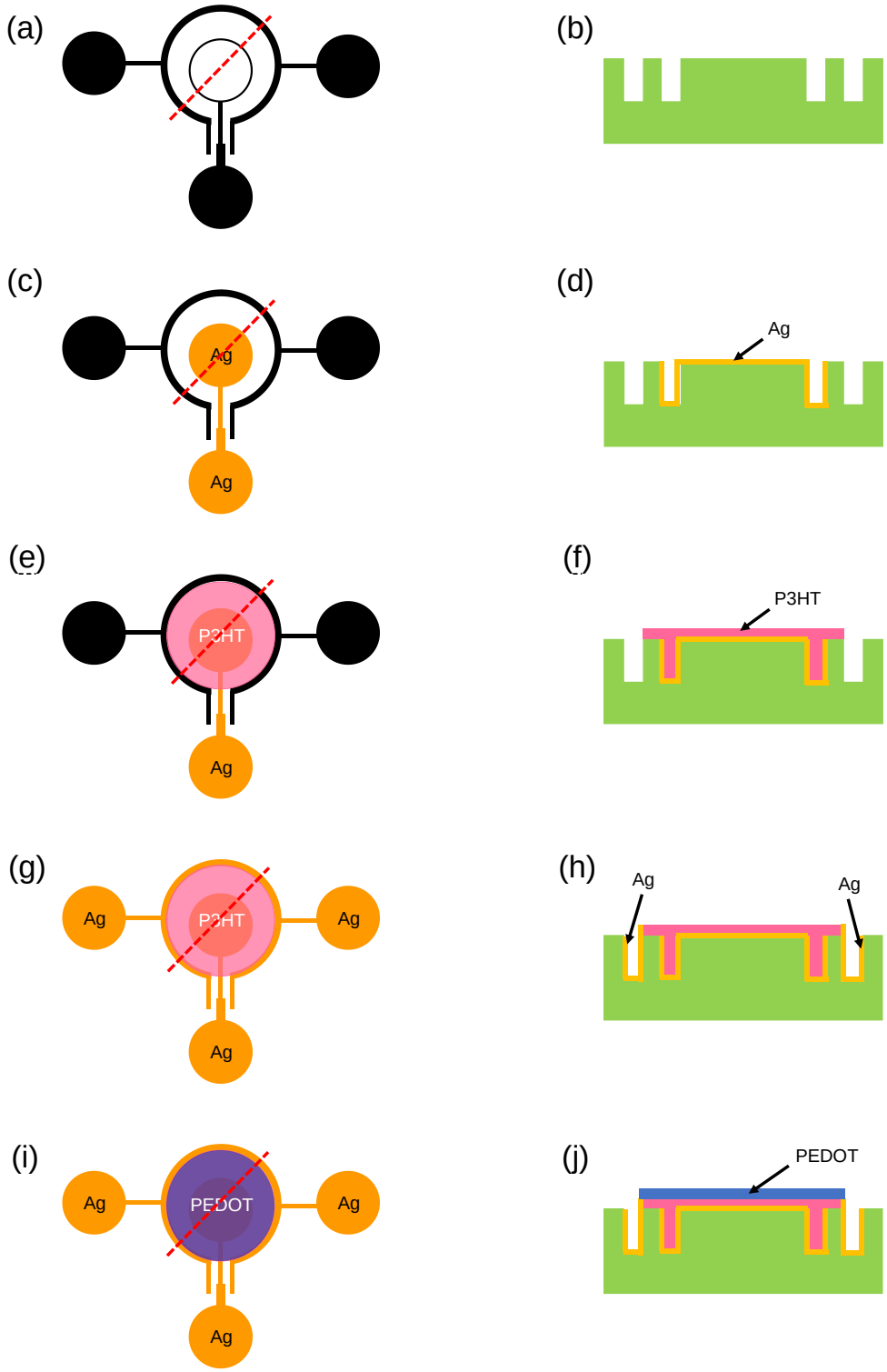

Figure 6.6. Schematic illustration of the printing process of a diode using the new design showing (a) the as-prepared imprinted substrate with all black area indented below the surface. (b) printing Ag electrode in the infinite ink receiver, (c) printing P3HT ink, (d) printing side Ag electrodes, (e) printing top PEDOT:PSS electrode, and the schematic cross sections (b, d, f, h, j) along the white dashed line.

Figure 6.6 shows the printing process of a diode utilizing this new infinite reservoir design schematically from the top and cross-sectional view. The two concentric indented device receivers in the previous diode design in Chapter 5 were replaced by infinite device receivers in Figure 6.6 (a). In Figure 6.6 (a, c, e), all the black areas are indented. The ink receivers were kept as indented receivers to feed ink into the capillary channels. In the first printing step shown in Figure 6.6 (c) and (d), the particle-free Ag ink was delivered to the infinite device receiver on the top and the ink receiver on the bottom. The ink in the circular trench and the drop in the center of the top device receiver merged together into one bead. After the ink dried and formed a silver film, these two receivers were electronically connected. The circular Ag film in the top device receiver served as the bottom electrode of a diode. Then, a 50 mg/ml P3HT ink was printed into the larger infinite device receiver to cover the Ag film (Figure 6.6 (e) and (f)). The P3HT ink used here shared the same formulation with the one mentioned in Chapter 5. After drying and annealing of the P3HT film, the P3HT film filled the circular trench around the smaller Ag device receiver. Then, the same Ag ink was delivered into the two ink receivers on the left and right side (Figure 6.6 (g) and (h)). The Ag ink entered the circular trench defining the P3HT device receiver. This trench is designed to both confine the P3HT ink and to provide external connections to the top PEDOT:PSS electrode, which was deposited in the next printing step. In the last printing step, the high conductivity PEDOT:PSS ink similar to the one used in Chapter 5 was delivered into the P3HT device receiver as the top electrode (Figures 6.6 (i) and (j)) since P3HT shared its device receiver with PEDOT:PSS to minimize the device size. The PEDOT:PSS film connected with the Ag film in the circular trench around the PEDOT:PSS device receiver due to the small overlap of these two films at the receiver edge. So, a printed

diode is completed. The cross-sectional SEM images (Figure 6.7 (b) and (c)) show that the P3HT film thickness at the edge (1.6 μm) is thicker than that at the center (0.74 μm) of the Ag device receiver. This new design is expected to achieve planarization of the middle layer to facilitate the deposition of the subsequent layers and to avoid short circuits.

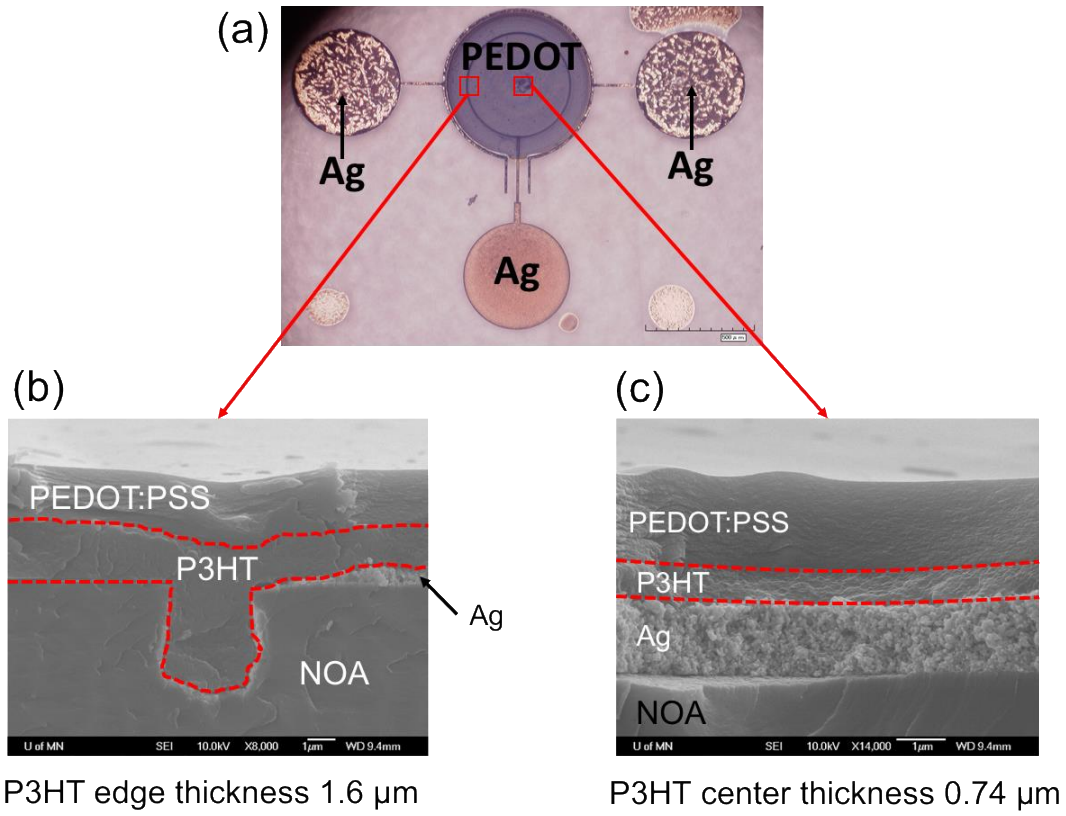

Figure 6.7 P3HT thickness variation across the Ag device receiver. (a) a top view optical image of a completed diode. (b,c) Cross-sectional SEM image taken at the corresponding marked red boxes in (a) for (b) at the edge of the Ag receiver and (c) at the center of the Ag receiver

The dimension of the circular trench of the Ag device receiver was further optimized and the results were shown in (Figures 6.8 (a) and (b)). In Figure 6.8 (a), the trench has a width of 7.3 μm, which is too wide for the P3HT layer to completely fill the trench. When the trench width was decreased to 3 μm, the trench was filled by P3HT, resulting in an

almost flat P3HT top surface (Figure 6.8 (b)), making it easier for depositing the subsequent layer. The P3HT film in and over the trench was labeled and separated with red dashed lines in the cross-section SEM image in Figure 6.8 (b), indicating the planarization of the trench which was coated with a thin silver layer. The silver film on the edge of the infinite device receiver was fully covered by a P3HT film with a thickness of around 1.6 μm, which was thicker than the P3HT (~ 740 nm) over the center of the Ag device receiver. The comparison is displayed by cross-sectional SEM images taken at the edge and the center of the Ag device receiver in Figure 6.8 (b) and (c). So, the application of infinite device receivers can help prevent the film thinning at the edge of the receiver and eliminate the short circuit problem caused by the poor coverage of the Ag film.

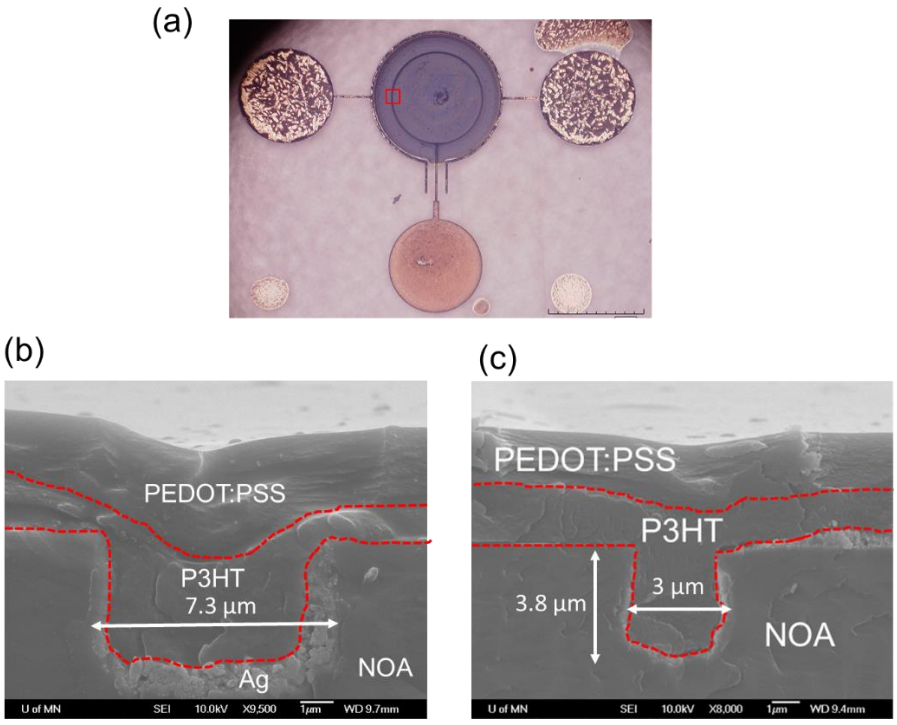

Figure 6.8 The impact of circular trench width of the Ag receiver on the filling of P3HT in the trench. (a) a top view optical image of a completed diode. (b,c) Cross sectional SEM image taken at the marked red box in (a) for (b) channel width = 7.3 μm and (c) channel width = 3 μm

The electrical performance of this printed diode based on the new design was evaluated and the IV curve was displayed in Figure 6.9. The diode exhibited a rectification ratio of 10^4 and no hysteresis was detected. The reverse current was lower compared to the previous result in Chapter 5 because the leakage current was reduced by the elimination of the edge thinning of the P3HT film. It is promising to further increase the forward current level by utilizing a P3HT ink with a lower concentration to reduce the P3HT film thickness.

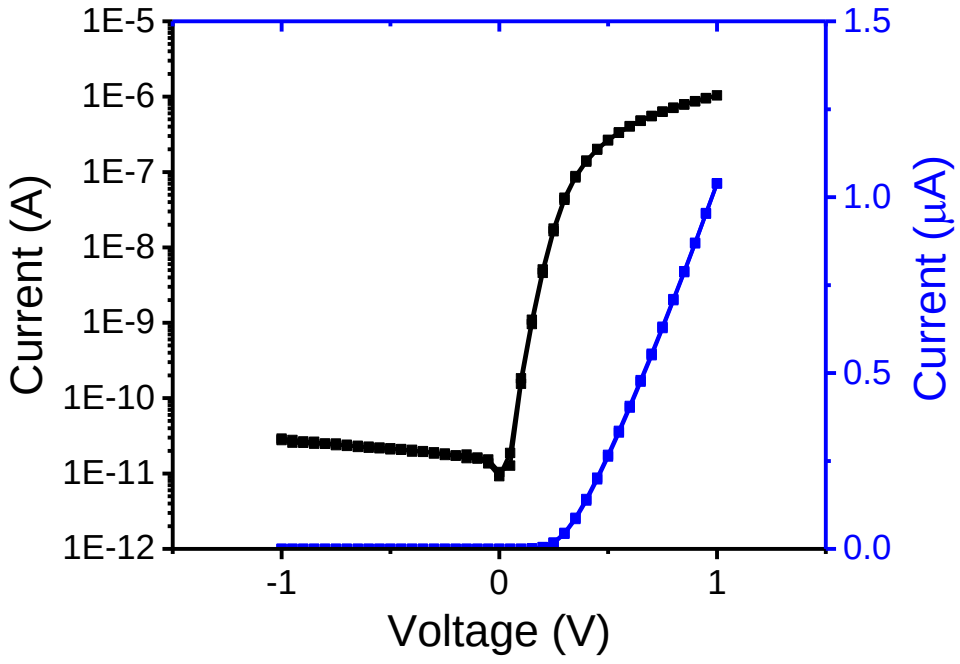

Figure 6.9 IV characteristic of a printed diode.

There are many advantages of this new design with infinite device receivers. First, this design utilizes infinite receivers to reduce the thickness variation of the P3HT film, making it possible to further reduce the film thickness to achieve a higher forward current without causing short circuits. Second, the idea of using infinite receiver helps with planarization of the patterned surface, which is very important for the fabrication of a multilayer device.

So, this idea can also be utilized in the design of other electronic components with a vertically stacked structure such as capacitors, transistors and crossovers. Third, preparation of the silicon master template of this design only takes two patterning cycles instead of three cycles in the previous design. So, the fabrication process is simpler.

The existing challenge of using this new design to print diodes is to boost up the yield. The yield of functional devices was around 50%. One possible reason leading to this low yield is that the contact between the top PEDOT:PSS electrode and the external Ag contact along the edge of the infinite device receiver is not very solid, resulting in open circuit issue sometimes. Further optimization of the pattern design is needed to form a more reliable contact and to improve the yield.

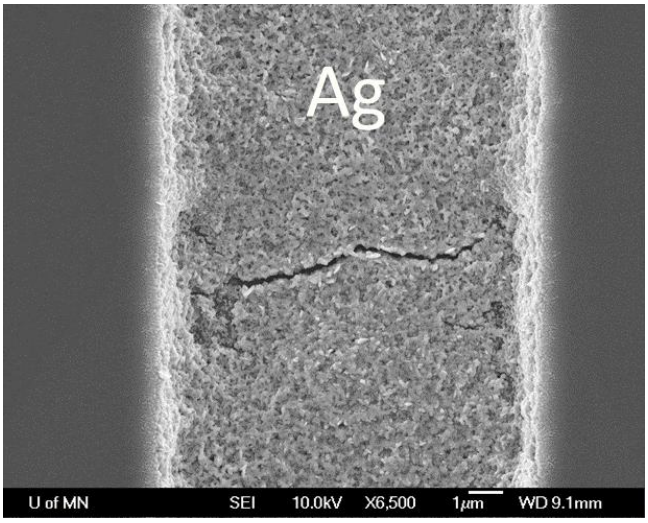

Figure 6.10 Cracking of Ag film deposited within a capillary channel

6.3 Improving Mechanical Durability

With the aim of fabricating flexible electronic circuits, the endurance to bending cycles is an important metric for devices printed via the SCALE method. Most of the polymer

materials used are robust to bending because they benefit from their intrinsic flexibility. But particulate Ag films, which are also frequently used in SCALE, suffer from poor flexibility. Ag films thicker than 1 μm in SCALE cannot withstand a tensile strain more than 1%. Figure 6.10 shows the crack of a Ag film inside the channel after bended to a tensile strain of 1% along the channel. This is also a problem with roll-to-roll printed circuits because completed devices are collected in a roll by a rotating drum at last. So, improving the flexibility of printed Ag films is the key point of realizing real flexible circuits. To meet the requirement of flexibility, it is necessary to modify the Ag layer.

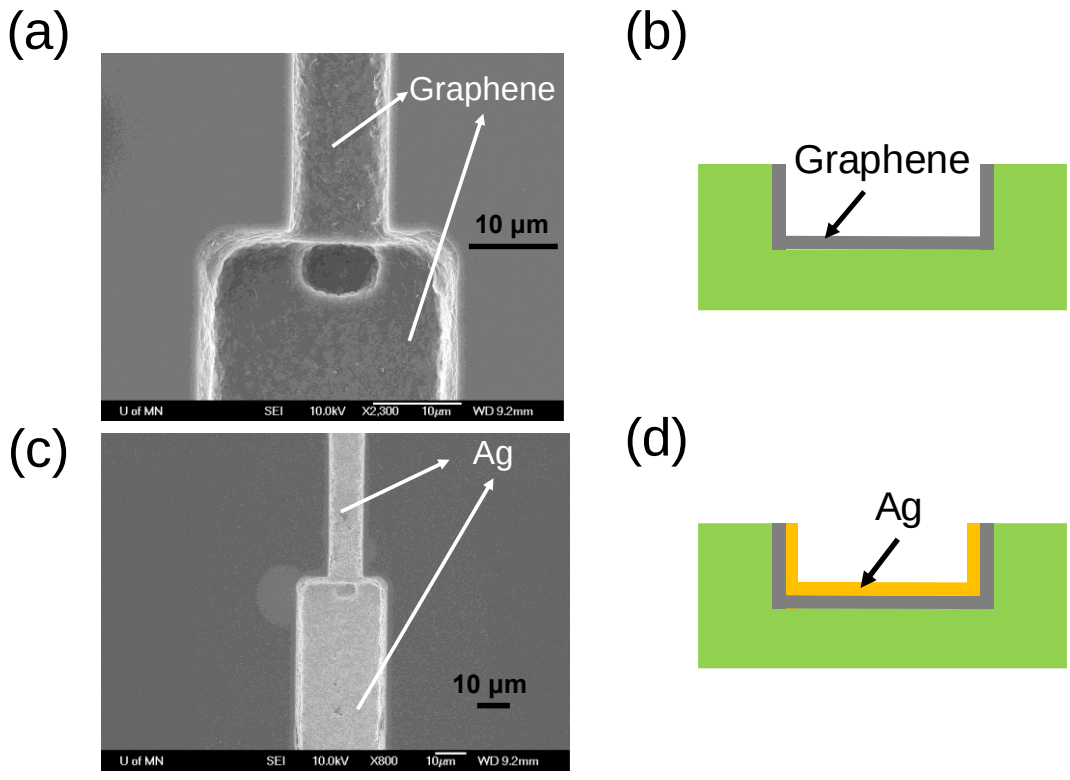

Figure 6.11 Top view SEM images and schematic crosssections of printed microfluidic channels with graphene and silver. (a) top view SEM image and (b) plot of the crosssection of a printed graphene film. (c) top view SEM image and (d) plot of the crosssection of the Ag film printed on top of the graphene film.

One possible route is to print a layer of graphene under the Ag layer as a buffer layer to improve the flexibility. Graphene is also a printable conductive material that can be used as electrodes [108]. Graphene ink is formulated by dissolving both graphene sheets and ethyl cellulose in cyclohexanone [143]. Compared with Ag films, graphene films are less conductive due to the existence of the organic binders and have a higher work function (around 5 eV). So, graphene is not suitable to replace Ag for printing the electrode of a diode with P3HT as the semiconductor layer directly. But it makes a good electrode for printed capacitors. Before the printing of Ag ink, graphene ink was delivered into the ink receivers designed for the Ag ink followed by a drying step and a photonic sintering step to reduce the amount of organic binders. A dense graphene film was coated uniformly inside the channel, shown in Figure 6.11 (a). Then the particle-free Ag ink was delivered into the same ink receiver. The Ag ink spread over the graphene film and flowed into the channel, forming a Ag layer right on top of the graphene layer after a drying and annealing step. After bending the Ag/graphene laminate to a tensile strain of 1%, no cracking of the Ag film was visible in the top view SEM image (shown in Figure 6.11 (c)). Possible reasons for this flexibility improvement of the Ag film are that (1) The graphene film acts as an underlying buffer layer and releases the tensile stress; (2) The Ag film becomes thinner because the deposition of graphene film makes the channel shallower; (3) The underlying graphene film changes the morphology of the Ag film, making it more resilient to bending. More investigations are required to clarify the real reason for the improvement, and the impact of the graphene film on the device performance also needs to be explored before this method can be applied in device fabrication.

Using a compound material consisting of graphene or silver and a polymer network is another promising route to solve this problem. Conductive fillers are imbedded in a flexible network to improve the conductivity of the film and at the same time retain its flexibility. Electrical properties can be tuned by adjusting the ratio between the filler and the polymer. Incorporating this material into SCALE process might be harder than the other route of simply laminating two layers. The first step is to formulate an inkjet printable ink based on a mixture of conductive fillers and a polymer, which may require extra efforts.

6.4 Circuit Integration

It has been demonstrated that SCALE is capable of fabricating multiple essential building blocks in a circuit. In chapters 4 and 5, the successful fabrication of printed *RC* filters and the integration of the diodes into simple AC power rectifiers suggest that these devices can be employed in fabricating a functional circuit by the SCALE method, which is another direction of future work and also the ultimate goal of the SCALE process.

In the near future, envisioned applications include fully printed RFID tags and sensors, which are relatively simple circuit. Using simple printed components, strain sensors, humidity sensors and temperature sensors can be realized.

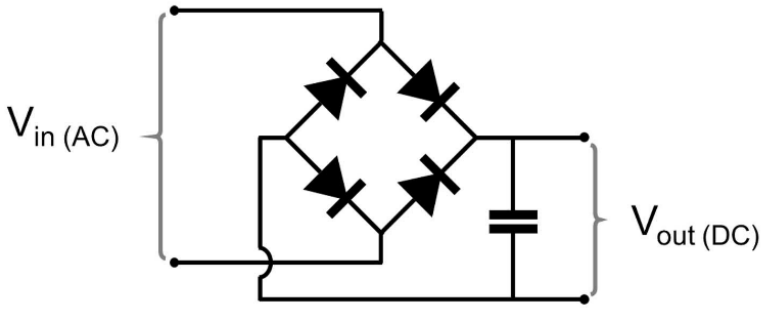

Figure 6.12 Circuit of a full wave bridge rectifier

For mass production of flexible integrated using SCALE, it is essential to minimize the performance variation of printed devices from batch to batch and to improve the yield by having better control of the printing process. Because each individual device contributes to the overall performance of the circuit. Besides, the process flow for each individual component needs modification to accommodate the fabrication requirement of other devices. For example, a full wave rectifier consists of four diodes (Figure 6.12) in which two diodes are connected head to tail. So, the top electrode of one diode needs to be printed together with the bottom electrode of the diode connected to it, which gives rise to a fabrication challenge. Overall, SCALE is a promising route to realize large-scale manufacturing of fully-printed functional circuits.

References:

(1) Mahajan, A.; Hyun, W. J.; Walker, S. B.; Rojas, G. A.; Choi, J. H.; Lewis, J. A.; Francis, L. F.; Frisbie, C. D. A Self-Aligned Strategy for Printed Electronics: Exploiting Capillary Flow on Microstructured Plastic Surfaces. *Adv. Electron. Mater.* **2015,** *1* (9), 1500137.

(2) Hyun, W. J.; Zare Bidoky, F.; Walker, S. B.; Lewis, J. A.; Francis, L. F.; Frisbie, C. D. Printed, Self-Aligned Side-Gate Organic Transistors with a Sub-5 μm Gate–Channel Distance on Imprinted Plastic Substrates. *Adv. Electron. Mater.* **2016,** *2* (12), 1600293.

(3) Hyun, W. J.; Secor, E. B.; Zare Bidoky, F.; Walker, S. B.; Lewis, J. A.; Hersam, M. C.; Francis, L. F.; Frisbie, C. D. Self-aligned capillarity-assisted printing of top-gate thin-film transistors on plastic. *Flexible and Printed Electronics* **2018,** *3* (3), 035004.

(4) Council, N. R. *The Flexible Electronics Opportunity*, National Academies Press: 2015.

(5) Ivanova, O.; Williams, C.; Campbell, T. Additive Manufacturing (AM) and Nanotechnology: Promises and Challenges. *Rapid Prototyping. J.* **2013,** *19* (5), 353-364.

(6) Thompson, S. E.; Parthasarathy, S. Moore's law: the future of Si microelectronics. *Materials Today* **2006,** *9* (6), 20-25.

(7) Bihar, E.; Wustoni, S.; Pappa, A. M.; Salama, K. N.; Baran, D.; Inal, S. A fully inkjet-printed disposable glucose sensor on paper. *npj Flexible Electronics* **2018,** *2* (1), 30.

(8) Yao, S.; Zhu, Y. Wearable Multifunctional Sensors Using Printed Stretchable Conductors Made of Silver Nanowires. *Nanoscale* **2014,** *6* (4), 2345-2352.

(9) Wataru, H.; Shingo, H.; Takayuki, A.; Seiji, A.; Kuniharu, T. Wearable, Human-Interactive, Health-Monitoring, Wireless Devices Fabricated by Macroscale Printing Techniques. *Adv. Funct. Mater.* **2014,** *24* (22), 3299-3304.

(10) Street, R. A.; Wong, W. S.; Ready, S. E.; Chabinyc, M. L.; Arias, A. C.; Limb, S.; Salleo, A.; Lujan, R. Jet Printing Flexible Displays. *Mater. Today* **2006,** *9* (4), 32-37.

(11) Street, R. A.; Ng, T. N.; Schwartz, D. E.; Whiting, G. L.; Lu, J. P.; Bringans, R. D.; Veres, J. From Printed Transistors to Printed Smart Systems. *Proc. IEEE* **2015,** *103* (4), 607-618.

(12) Yeo, W. H.; Kim, Y. S.; Lee, J.; Ameen, A.; Shi, L.; Li, M.; Wang, S.; Ma, R.; Jin, S. H.; Kang, Z.; Huang, Y.; Rogers, J. A. Multifunctional Epidermal Electronics Printed Directly Onto the Skin. *Adv. Mater.* **2013,** *25* (20), 2773-2778.
(13) Corea, J. R.; Lechene, P. B.; Lustig, M.; Arias, A. C. Materials and Methods for Higher Performance Screen-Printed Flexible MRI Receive Coils. *Magn. Reson. Med.* **2017,** *78* (2), 775-783.
(14) Das, R.; He, X.; Ghaffarzadeh, K. Flexible, Printed and Organic Electronics 2019-2029: Forecasts, Players & Opportunities. *IDTechEx* **2019**.
(15) Perelaer, J.; de Gans, B. J.; Schubert, U. S. Ink-jet Printing and Microwave Sintering of Conductive Silver Tracks. *Advanced Materials* **2006,** *18* (16), 2101-2104.
(16) Jeong, S.; Woo, K.; Kim, D.; Lim, S.; Kim, J. S.; Shin, H.; Xia, Y.; Moon, J. Controlling the thickness of the surface oxide layer on Cu nanoparticles for the fabrication of conductive structures by ink-jet printing. *Advanced Functional Materials* **2008,** *18* (5), 679-686.
(17) Speakman, S. P.; Rozenberg, G. G.; Clay, K. J.; Milne, W. I.; Ille, A.; Gardner, I. A.; Bresler, E.; Steinke, J. H. High performance organic semiconducting thin films: Ink jet printed polythiophene [rr-P3HT]. *Organic Electronics* **2001,** *2* (2), 65-73.
(18) Shen, W.; Zhao, Y.; Zhang, C. The preparation of ZnO based gas-sensing thin films by ink-jet printing method. *Thin Solid Films* **2005,** *483* (1), 382-387.
(19) Cho, J. H.; Lee, J.; Xia, Y.; Kim, B.; He, Y.; Renn, M. J.; Lodge, T. P.; Frisbie, C. D. Printable Ion-Gel Gate Dielectrics for Low-Voltage Polymer Thin-Film Transistors on Plastic. *Nat. Mater.* **2008,** *7* (11), 900-906.
(20) Calvert, P. Inkjet Printing for Materials and Devices. *Chem. Mater.* **2001,** *13* (10), 3299-3305.
(21) Gans, B. J. D.; Duineveld, P. C.; Schubert, U. S. Inkjet Printing of Polymers: State of the Art and Future Developments. *Adv. Mater.* **2004,** *16* (3), 203-213.
(22) Scheideler, W. J.; Kumar, R.; Zeumault, A. R.; Subramanian, V. Low-Temperature-Processed Printed Metal Oxide Transistors Based on Pure Aqueous Inks. *Adv. Funct. Mater.* **2017,** *27*, 1606062.

(23) Ng, T. N.; Schwartz, D. E.; Mei, P.; Kor, S.; Veres, J.; Bröms, P.; Karlsson, C. Pulsed Voltage Multiplier Based on Printed Organic Devices. *Flexible and Printed Electronics* **2015,** *1* (1), 015002.
(24) Bucella, S. G.; Salazar-Rios, J. M.; Derenskyi, V.; Fritsch, M.; Scherf, U.; Loi, M. A.; Caironi, M. Inkjet Printed Single-Walled Carbon Nanotube Based Ambipolar and Unipolar Transistors for High-Performance Complementary Logic Circuits. *Adv. Electron. Mater.* **2016,** *2* (6), 1600094.
(25) Sirringhaus, H.; Kawase, T.; Friend, R. H.; Shimoda, T.; Inbasekaran, M.; Wu, W.; Woo, E. P. High-Resolution Inkjet Printing of All-Polymer Transistor Circuits. *Science* **2000,** *290* (5499), 2123-2126.
(26) Ng, T. N.; Wong, W. S.; Chabinyc, M. L.; Sambandan, S.; Street, R. A. Flexible image sensor array with bulk heterojunction organic photodiode. *Appl. Phys. Lett.* **2008,** *92* (21), 213303.
(27) Kawase, T.; Sirringhaus, H.; Friend, R. H.; Shimoda, T. Inkjet Printed Via-Hole Interconnections and Resistors for All-Polymer Transistor Circuits. *Adv. Mater.* **2001,** *13* (21), 1601-1605.
(28) Ng, T. N.; Mei, P.; Schwartz, D. E.; Kor, S.; Krusor, B.; Veres, J.; Bröms, P.; Eriksson, T.; Wang, Y.; Hagel, O.; Karlsson, C. In *Additive printing of organic complementary circuits for temperature sensor tag*, SPIE Organic Photonics + Electronics, SPIE: 2015; p 6.
(29) Tobjörk, D.; Kaihovirta, N. J.; Mäkelä, T.; Pettersson, F. S.; Österbacka, R. All-printed low-voltage organic transistors. *Org. Electron.* **2008,** *9* (6), 931-935.
(30) Khan, Y.; Pavinatto, F. J.; Lin, M. C.; Liao, A.; Swisher, S. L.; Mann, K.; Subramanian, V.; Maharbiz, M. M.; Arias, A. C. Inkjet-Printed Flexible Gold Electrode Arrays for Bioelectronic Interfaces. *Adv. Funct. Mater.* **2016,** *26* (7), 1004-1013.
(31) Whiting, G. L.; Arias, A. C. Chemically modified ink-jet printed silver electrodes for organic field-effect transistors. *Appl. Phys. Lett.* **2009,** *95* (25), 253302.
(32) Lessing, J.; Glavan, A. C.; Walker, S. B.; Keplinger, C.; Lewis, J. A.; Whitesides, G. M. Inkjet Printing of Conductive Inks with High Lateral Resolution on Omniphobic "RF Paper" for Paper-Based Electronics and MEMS. *Adv. Mater.* **2014,** *26* (27), 4677-4682.

(33) Zirkl, M.; Sawatdee, A.; Helbig, U.; Krause, M.; Scheipl, G.; Kraker, E.; Ersman, P. A.; Nilsson, D.; Platt, D.; Bodö, P.; Bauer, S.; Domann, G.; Stadlober, B. An All-Printed Ferroelectric Active Matrix Sensor Network Based on Only Five Functional Materials Forming a Touchless Control Interface. *Adv. Mater.* **2011,** *23* (18), 2069-2074.
(34) Homenick, C. M.; James, R.; Lopinski, G. P.; Dunford, J.; Sun, J.; Park, H.; Jung, Y.; Cho, G.; Malenfant, P. R. L. Fully Printed and Encapsulated SWCNT-Based Thin Film Transistors via a Combination of R2R Gravure and Inkjet Printing. *ACS Appl. Mater. Interfaces* **2016,** *8* (41), 27900-27910.
(35) Lee, H.-H.; Chou, K.-S.; Huang, K.-C. Inkjet printing of nanosized silver colloids. *Nanotechnology* **2005,** *16* (10), 2436.
(36) Song, D.; Zare Bidoky, F.; Hyun, W. J.; Walker, S. B.; Lewis, J. A.; Frisbie, C. D. All-Printed, Self-Aligned Carbon Nanotube Thin-Film Transistors on Imprinted Plastic Substrates. *ACS Appl. Mater. Interfaces* **2018,** *10* (18), 15926-15932.
(37) Hyun, W. J.; Secor, E. B.; Kim, C. H.; Hersam, M. C.; Francis, L. F.; Frisbie, C. D. Scalable, Self-Aligned Printing of Flexible Graphene Micro-Supercapacitors. *Adv. Energy Mater.* **2017**, 1700285.
(38) Gubbi, J.; Buyya, R.; Marusic, S.; Palaniswami, M. Internet of Things (IoT): A vision, architectural elements, and future directions. *Future Generation Computer Systems* **2013,** *29* (7), 1645-1660.
(39) Park, S.; Jayaraman, S. Enhancing the quality of life through wearable technology. *IEEE Eng. Med. Biol. Mag.* **2003,** *22* (3), 41-48.
(40) Bonato, P. Advances in wearable technology and applications in physical medicine and rehabilitation. *J. Neuroeng. Rehabil.* **2005,** *2* (1), 2.
(41) Quintero, A. V.; Molina-Lopez, F.; Smits, E. C. P.; Danesh, E.; van den Brand, J.; Persaud, K.; Oprea, A.; Barsan, N.; Weimar, U.; de Rooij, N. F.; Briand, D. Smart RFID label with a printed multisensor platform for environmental monitoring. *Flexible and Printed Electronics* **2016,** *1* (2), 025003.
(42) Windmiller, J. R.; Wang, J. Wearable Electrochemical Sensors and Biosensors: A Review. *Electroanalysis* **2013,** *25* (1), 29-46.
(43) Rogers, J. A.; Bao, Z. Printed plastic electronics and paperlike displays. *J. Polym. Sci., Part A: Polym. Chem.* **2002,** *40* (20), 3327-3334.

(44) Arias, A. C.; Daniel, J.; Krusor, B.; Ready, S.; Sholin, V.; Street, R. All-additive ink-jet-printed display backplanes: Materials development and integration. *Journal of the Society for Information Display* **2007,** *15* (7), 485-490.
(45) Gaikwad, A. M.; Steingart, D. A.; Ng, T. N.; Schwartz, D. E.; Whiting, G. L. A flexible high potential printed battery for powering printed electronics. *Appl. Phys. Lett.* **2013,** *102* (23), 233302.
(46) Braam, K.; Subramanian, V. A Stencil Printed, High Energy Density Silver Oxide Battery Using a Novel Photopolymerizable Poly(acrylic acid) Separator. *Adv. Mater.* **2015,** *27* (4), 689-694.
(47) Cao, X.; Lau, C.; Liu, Y.; Wu, F.; Gui, H.; Liu, Q.; Ma, Y.; Wan, H.; Amer, M. R.; Zhou, C. Fully Screen-Printed, Large-Area, and Flexible Active-Matrix Electrochromic Displays Using Carbon Nanotube Thin-Film Transistors. *ACS Nano* **2016,** *10* (11), 9816-9822.
(48) Xing, R.; Wang, S.; Zhang, B.; Yu, X.; Ding, J.; Wang, L.; Han, Y. Inkjet Printed Polystyrene Sulfuric Acid-doped Poly(3,4-ethylenedioxythiophene) (PEDOT) Uniform Thickness Films in Confined Grooves through Decreasing the Surface Tension of PEDOT Inks. *RSC Adv.* **2017,** *7* (13), 7725-7733.
(49) Aminy, E. O.; Ana Claudia, A. Flexible photovoltaic power systems: integration opportunities, challenges and advances. *Flexible and Printed Electronics* **2017,** *2* (1), 013001.
(50) Zervos, H. Printed Electronics Market Update - Opportunities for the Printing Industry. **2016**.
(51) Jung, M.; Kim, J.; Noh, J.; Lim, N.; Lim, C.; Lee, G.; Kim, J.; Kang, H.; Jung, K.; Leonard, A. D.; Tour, J. M.; Cho, G. All-Printed and Roll-to-Roll-Printable 13.56-MHz-Operated 1-bit RF Tag on Plastic Foils. *IEEE Trans. Electron Devices* **2010,** *57* (3), 571-580.
(52) Semple, J.; Georgiadou, D. G.; Wyatt-Moon, G.; Gelinck, G.; Anthopoulos, T. D. Flexible diodes for radio frequency (RF) electronics: a materials perspective. *Semicond. Sci. Technol.* **2017,** *32* (12), 123002.
(53) Subramanian, V.; Frechet, J. M. J.; Chang, P. C.; Huang, D. C.; Lee, J. B.; Molesa, S. E.; Murphy, A. R.; Redinger, D. R.; Volkman, S. K. Progress Toward Development of

All-Printed RFID Tags: Materials, Processes, and Devices. *Proc. IEEE* **2005,** *93* (7), 1330-1338.
(54) Kang, H.; Park, H.; Park, Y.; Jung, M.; Kim, B. C.; Wallace, G.; Cho, G. Fully Roll-to-Roll Gravure Printable Wireless (13.56 MHz) Sensor-Signage Tags for Smart Packaging. *Sci. Rep.* **2014,** *4*, 5387.
(55) Bahadir, S. K.; Sahin, U. K. A Wearable Heating System with a Controllable e-Textile-Based Thermal Panel. *Wearable Technologies* **2018**, 175.
(56) Hussain, A. M.; Lizardo, E. B.; Torres Sevilla, G. A.; Nassar, J. M.; Hussain, M. M. Ultrastretchable and Flexible Copper Interconnect-Based Smart Patch for Adaptive Thermotherapy. *Advanced Healthcare Materials* **2015,** *4* (5), 665-673.
(57) Wallace, G. G.; Campbell, T. E.; Innis, P. C. Putting function into fashion: Organic conducting polymer fibres and textiles. *Fibers and Polymers* **2007,** *8* (2), 135-142.
(58) Rodrigues, L.; Mota, M. *Bioinspired Materials for Medical Applications*, Woodhead Publishing: 2016.
(59) Hong, Y. J.; Lee, H.; Kim, J.; Lee, M.; Choi, H. J.; Hyeon, T.; Kim, D.-H. Multifunctional Wearable System that Integrates Sweat-Based Sensing and Vital-Sign Monitoring to Estimate Pre-/Post-Exercise Glucose Levels. *Adv. Funct. Mater.* **2018,** *28* (47), 1805754.
(60) Wang, J.; Musameh, M. Carbon nanotube screen-printed electrochemical sensors. *Analyst* **2004,** *129* (1), 1-2.
(61) Lee, C.; Jug, L.; Meng, E. High strain biocompatible polydimethylsiloxane-based conductive graphene and multiwalled carbon nanotube nanocomposite strain sensors. *Appl. Phys. Lett.* **2013,** *102* (18), 183511.
(62) Yeom, C.; Chen, K.; Kiriya, D.; Yu, Z.; Cho, G.; Javey, A. Large-Area Compliant Tactile Sensors Using Printed Carbon Nanotube Active-Matrix Backplanes. *Adv. Mater.* **2015,** *27* (9), 1561-1566.
(63) Park, J.-U.; Hardy, M.; Kang, S. J.; Barton, K.; Adair, K.; Mukhopadhyay, D. k.; Lee, C. Y.; Strano, M. S.; Alleyne, A. G.; Georgiadis, J. G.; Ferreira, P. M.; Rogers, J. A. High-resolution electrohydrodynamic jet printing. *Nat. Mater.* **2007,** *6*, 782.
(64) Singh, M.; Haverinen, H. M.; Dhagat, P.; Jabbour, G. E. Inkjet Printing—Process and Its Applications. *Adv. Mater.* **2010,** *22* (6), 673-685.

(65) Francis, L. F. *Materials Processing: A Unified Approach to Processing of Metals, Ceramics and Polymers*, Academic Press: 2015.
(66) Derby, B. Inkjet Printing of Functional and Structural Materials: Fluid Property Requirements, Feature Stability, and Resolution. *Annual Review of Materials Research* **2010,** *40* (1), 395-414.
(67) Lee, J. S.; Kwack, Y.-J.; Choi, W.-S. Inkjet-Printed In2O3 Thin-Film Transistor below 200 °C. *ACS Appl. Mater. Interfaces* **2013,** *5* (22), 11578-11583.
(68) Kordás, K.; Mustonen, T.; Tóth, G.; Jantunen, H.; Lajunen, M.; Soldano, C.; Talapatra, S.; Kar, S.; Vajtai, R.; Ajayan, P. M. Inkjet Printing of Electrically Conductive Patterns of Carbon Nanotubes. *Small* **2006,** *2* (8-9), 1021-1025.
(69) Secor, E. B. Principles of aerosol jet printing. *Flexible and Printed Electronics* **2018,** *3* (3), 035002.
(70) Mahajan, A.; Frisbie, C. D.; Francis, L. F. Optimization of Aerosol Jet Printing for High-Resolution, High-Aspect Ratio Silver Lines. *ACS Appl. Mater. Interfaces* **2013,** *5* (11), 4856-4864.
(71) Hong, K.; Kim, S. H.; Lee, K. H.; Frisbie, C. D. Printed, sub-2V ZnO Electrolyte Gated Transistors and Inverters on Plastic. *Advanced Materials* **2013,** *25* (25), 3413-3418.
(72) Ha, M.; Seo, J.-W. T.; Prabhumirashi, P. L.; Zhang, W.; Geier, M. L.; Renn, M. J.; Kim, C. H.; Hersam, M. C.; Frisbie, C. D. Aerosol jet printed, low voltage, electrolyte gated carbon nanotube ring oscillators with sub-5 μs stage delays. *Nano letters* **2013,** *13* (3), 954-960.
(73) Ha, M.; Zhang, W.; Braga, D.; Renn, M. J.; Kim, C. H.; Frisbie, C. D. Aerosol-Jet-Printed, 1 Volt H-Bridge Drive Circuit on Plastic with Integrated Electrochromic Pixel. *ACS Appl. Mater. Interfaces* **2013,** *5* (24), 13198-13206.
(74) White, S. P.; Dorfman, K. D.; Frisbie, C. D. Label-Free DNA Sensing Platform with Low-Voltage Electrolyte-Gated Transistors. *Anal. Chem.* **2015,** *87* (3), 1861-1866.
(75) Cao, X.; Chen, H.; Gu, X.; Liu, B.; Wang, W.; Cao, Y.; Wu, F.; Zhou, C. Screen Printing as a Scalable and Low-Cost Approach for Rigid and Flexible Thin-Film Transistors Using Separated Carbon Nanotubes. *ACS Nano* **2014,** *8* (12), 12769-12776.

(76) Hyun, W. J.; Lim, S.; Ahn, B. Y.; Lewis, J. A.; Frisbie, C. D.; Francis, L. F. Screen Printing of Highly Loaded Silver Inks on Plastic Substrates Using Silicon Stencils. *ACS Appl. Mater. Interfaces* **2015,** *7* (23), 12619-12624.
(77) Ostfeld, A. E.; Deckman, I.; Gaikwad, A. M.; Lochner, C. M.; Arias, A. C. Screen printed passive components for flexible power electronics. *Sci. Rep.* **2015,** *5*, 15959.
(78) Serges, Z.; David, T. B.; Margit, H. Screen printed logic gates employing milled p-silicon as an active material. *Flexible and Printed Electronics* **2016,** *1* (3), 035002.
(79) Hyun, W. J.; Secor, E. B.; Hersam, M. C.; Frisbie, C. D.; Francis, L. F. High-Resolution Patterning of Graphene by Screen Printing with a Silicon Stencil for Highly Flexible Printed Electronics. *Adv. Mater.* **2015,** *27* (1), 109-115.
(80) Izdebska, J.; Thomas, S. *Printing on polymers: fundamentals and applications*, William Andrew: 2015.
(81) Nguyen, H. A. D.; Shin, K.-H.; Lee, D. Effect of process parameters on fidelity of printed line width in high resolution roll-to-roll gravure printing. *Jpn. J. Appl. Phys.* **2014,** *53* (5S3), 05HC04.
(82) Hrehorova, E.; Rebros, M.; Pekarovicova, A.; Bazuin, B.; Ranganathan, A.; Garner, S.; Merz, G.; Tosch, J.; Boudreau, R. Gravure Printing of Conductive Inks on Glass Substrates for Applications in Printed Electronics. *J. Display Technol.* **2011,** *7* (6), 318-324.
(83) Vornbrock, A. d. l. F.; Ding, J. M.; Sung, D.; Huai-Yuan, T.; Subramanian, V. In *Printing and scaling of metallic traces and capacitors using a laboratory-scale rotogravure press*, 2009 Flexible Electronics & Displays Conference and Exhibition, 2-5 Feb. 2009; 2009; pp 1-7.
(84) Rebros, M.; Hrehorova, E.; Bazuin, B. J.; Joyce, M. K.; Fleming, P. D.; Pekarovicova, A. In *Rotogravure printed UHF RFID antennae directly on packaging materials*, Proc TAGA 60th Annu. Tech. Conf, 2008; pp 16-19.
(85) Tuomikoski, M.; Suhonen, R.; Välimäki, M.; Maaninen, T.; Maaninen, A.; Sauer, M.; Rogin, P.; Mennig, M.; Heusing, S.; Puetz, J.; Aegerter, M. A. *Manufacturing of polymer light-emitting device structures*, SPIE: 2006; Vol. 6192.

(86) Noh, J.; Jung, M.; Jung, K.; Lee, G.; Lim, S.; Kim, D.; Kim, S.; Tour, J. M.; Cho, G. Integrable single walled carbon nanotube (SWNT) network based thin film transistors using roll-to-roll gravure and inkjet. *Org. Electron.* **2011,** *12* (12), 2185-2191.
(87) Krebs, F. C.; Fyenbo, J.; Jørgensen, M. Product integration of compact roll-to-roll processed polymer solar cell modules: methods and manufacture using flexographic printing, slot-die coating and rotary screen printing. *J. Mater. Chem.* **2010,** *20* (41), 8994-9001.
(88) Hösel, M.; Søndergaard, R. R.; Angmo, D.; Krebs, F. C. Comparison of Fast Roll-to-Roll Flexographic, Inkjet, Flatbed, and Rotary Screen Printing of Metal Back Electrodes for Polymer Solar Cells. *Adv. Eng. Mater.* **2013,** *15* (10), 995-1001.
(89) Tobjörk, D.; Aarnio, H.; Pulkkinen, P.; Bollström, R.; Määttänen, A.; Ihalainen, P.; Mäkelä, T.; Peltonen, J.; Toivakka, M.; Tenhu, H.; Österbacka, R. IR-sintering of ink-jet printed metal-nanoparticles on paper. *Thin Solid Films* **2012,** *520* (7), 2949-2955.
(90) Zhao, N.; Chiesa, M.; Sirringhaus, H.; Li, Y.; Wu, Y.; Ong, B. Self-aligned inkjet printing of highly conducting gold electrodes with submicron resolution. *J. Appl. Phys.* **2007,** *101* (6), 064513.
(91) Cao, X.; Wu, F.; Lau, C.; Liu, Y.; Liu, Q.; Zhou, C. Top-Contact Self-Aligned Printing for High-Performance Carbon Nanotube Thin-Film Transistors with Sub-Micron Channel Length. *ACS Nano* **2017,** *11* (2), 2008-2014.
(92) Choonee, K.; Syms, R. R. A. Multilevel Self-Aligned Microcontact Printing System. *Langmuir* **2010,** *26* (20), 16163-16170.
(93) Meissner, M. V.; Spengler, N.; Mager, D.; Wang, N.; Kiss, S. Z.; Höfflin, J.; While, P. T.; Korvink, J. G. Ink-jet printing technology enables self-aligned mould patterning for electroplating in a single step. *JMiMi* **2015,** *25* (6), 065015.
(94) Bidoky, F. Z.; Hyun, W. J.; Song, D.; Frisbie, C. D. Printed, 1 V electrolyte-gated transistors based on poly(3-hexylthiophene) operating at >10 kHz on plastic. *Appl. Phys. Lett.* **2018,** *113* (5), 053301.
(95) Wu, C.; Tetik, H.; Cheng, J.; Ding, W.; Guo, H.; Tao, X.; Zhou, N.; Zi, Y.; Wu, Z.; Wu, H.; Lin, D.; Wang, Z. L. Electrohydrodynamic Jet Printing Driven by a Triboelectric Nanogenerator. *Adv. Funct. Mater.* **2019,** *29* (22), 1901102.

(96) Sele, C. W.; von Werne, T.; Friend, R. H.; Sirringhaus, H. Lithography-Free, Self-Aligned Inkjet Printing with Sub-Hundred-Nanometer Resolution. *Adv. Mater.* **2005,** *17* (8), 997-1001.
(97) Bruno Michel; André Bernarda; Alexander Bietsch; Emmanuel Delamarche; Mattias Geissler; David Juncker; Hannes Kindb; Jean-Philippe Renaultc; Hugo Rothuizen; Heinz Schmid, P.; Schmidt-Winkeld; Stutz, R.; Wolf, H. Printing Meets Lithography: Soft Approaches to High-Resolution Patterning. *Chimia* **2002,** *56* (10), 527-542.
(98) Hendriks, C. E.; Smith, P. J.; Perelaer, J.; Berg, A. M. J. v. d.; Schubert, U. S. "Invisible" Silver Tracks Produced by Combining Hot-Embossing and Inkjet Printing. *Adv. Funct. Mater.* **2008,** *18* (7), 1031-1038.
(99) Pfohl, T.; Mugele, F.; Seemann, R.; Herminghaus, S. Trends in Microfluidics with Complex Fluids. *Chemphyschem* **2003,** *4* (12), 1291-1298.
(100) Jung, S.; Sou, A.; Gili, E.; Sirringhaus, H. Inkjet-Printed Resistors with a Wide Resistance Range for Printed Read-Only Memory Applications. *Org. Electron.* **2013,** *14* (3), 699-702.
(101) Ali, S.; Bae, J.; Lee, C. H. Design of Versatile Printed Organic Resistor Based on Resistivity (ρ) Control. *Appl. Phys. A* **2015,** *119* (4), 1499-1506.
(102) Jochem, K. S.; Suszynski, W. J.; Frisbie, C. D.; Francis, L. F. High-Resolution, High-Aspect-Ratio Printed and Plated Metal Conductors Utilizing Roll-to-Roll Microscale UV Imprinting with Prototype Imprinting Stamps. *Ind. Eng. Chem. Res.* **2018,** *57* (48), 16335-16346.
(103) Mahajan, A.; Hyun, W. J.; Walker, S. B.; Lewis, J. A.; Francis, L. F.; Frisbie, C. D. High-Resolution, High-Aspect Ratio Conductive Wires Embedded in Plastic Substrates. *ACS Appl. Mater. Interfaces* **2015,** *7* (3), 1841-1847.
(104) Lade, R. K.; Jochem, K. S.; Macosko, C. W.; Francis, L. F. Capillary Coatings: Flow and Drying Dynamics in Open Microchannels. *Langmuir* **2018,** *34* (26), 7624-7639.
(105) Kolliopoulos, P.; Jochem, K. S.; Lade, R. K.; Francis, L. F.; Kumar, S. Capillary Flow with Evaporation in Open Rectangular Microchannels. *Langmuir* **2019,** *35* (24), 8131-8143.
(106) Walker, S. B.; Lewis, J. A. Reactive Silver Inks for Patterning High-Conductivity Features at Mild Temperatures. *J. Am. Chem. Soc.* **2012,** *134* (3), 1419-21.

(107) Hyun, W. J.; Secor, E. B.; Kim, C. H.; Hersam, M. C.; Francis, L. F.; Frisbie, C. D. Scalable, Self-Aligned Printing of Flexible Graphene Micro-Supercapacitors. *Adv. Energy Mater.* **2017**.
(108) Hyun, W. J.; Secor, E. B.; Kim, C.-H.; Hersam, M. C.; Francis, L. F.; Frisbie, C. D. Scalable, Self-Aligned Printing of Flexible Graphene Micro-Supercapacitors. *Adv. Energy Mater.* **2017,** *7* (17).
(109) Hyun, W. J.; Kumar, S.; Francis, L. F.; Frisbie, C. D. Open-channel microfluidic diodes based on two-tier junctions. *Appl. Phys. Lett.* **2018,** *113* (19), 193701.
(110) Cui, T.; Liu, Y.; Chen, B.; Zhu, M.; Varahramyan, K. Printed Polymeric Passive *RC* filters and Degradation Characteristics. *Solid·State Electron.* **2005,** *49* (5), 853-859.
(111) Tang, B.; White, S. P.; Frisbie, C. D.; Lodge, T. P. Synergistic Increase in Ionic Conductivity and Modulus of Triblock Copolymer Ion Gels. *Macromolecules* **2015,** *48* (14), 4942-4950.
(112) Bae, S.; Kim, H.; Lee, Y.; Xu, X.; Park, J.-S.; Zheng, Y.; Balakrishnan, J.; Lei, T.; Ri Kim, H.; Song, Y. I.; Kim, Y.-J.; Kim, K. S.; Özyilmaz, B.; Ahn, J.-H.; Hong, B. H.; Iijima, S. Roll-to-roll production of 30-inch graphene films for transparent electrodes. *Nature Nanotechnology* **2010,** *5*, 574.
(113) Street, R. A. Thin-Film Transistors. *Adv. Mater.* **2009,** *21* (20), 2007-2022.
(114) Snell, A. J.; Mackenzie, K. D.; Spear, W. E.; LeComber, P. G.; Hughes, A. J. Application of amorphous silicon field effect transistors in addressable liquid crystal display panels. *ApPhy* **1981,** *24* (4), 357-362.
(115) Zare Bidoky, F.; Frisbie, C. D. Parasitic Capacitance Effect on Dynamic Performance of Aerosol-Jet-Printed Sub 2 V Poly(3-hexylthiophene) Electrolyte-Gated Transistors. *ACS Appl. Mater. Interfaces* **2016,** *8* (40), 27012-27017.
(116) Lee, S. W.; Kim, B. S.; Park, J. J.; Hur, J. H.; Kim, J. M.; Sekitani, T.; Someya, T.; Jeong, U. High performance foldable polymer thin film transistors with a side gate architecture. *J. Mater. Chem.* **2011,** *21* (46), 18804-18809.
(117) Numakura, D. In *Advanced Screen Printing "Practical Approaches for Printable & Flexible Electronics"*, 2008 3rd International Microsystems, Packaging, Assembly & Circuits Technology Conference, 22-24 Oct. 2008; 2008; pp 205-208.

(118) Chang, J.; Zhang, X.; Ge, T.; Zhou, J. Fully printed electronics on flexible substrates: High gain amplifiers and DAC. *Org. Electron.* **2014,** *15* (3), 701-710.
(119) Słoma, M.; Jakubowska, M.; Kolek, A.; Mleczko, K.; Ptak, P.; Stadler, A. W.; Zawiślak, Z.; Młożniak, A. Investigations on printed elastic resistors containing carbon nanotubes. *Journal of Materials Science: Materials in Electronics* **2011,** *22* (9), 1321-1329.
(120) Cheng, P. L.; Law, T. W.; Liu, C. K.; Chong, I. T.; Lam, D. C. C. In *Quantitative analysis of resistance of printed resistors*, 2nd International IEEE Conference on Polymers and Adhesives in Microelectronics and Photonics. , 23-26 June 2002; 2002; pp 205-210.
(121) Kang, B. J.; Lee, C. K.; Oh, J. H. All-inkjet-printed electrical components and circuit fabrication on a plastic substrate. *Microelectron. Eng.* **2012,** *97*, 251-254.
(122) Correia, V.; Mitra, K. Y.; Castro, H.; Rocha, J. G.; Sowade, E.; Baumann, R. R.; Lanceros-Mendez, S. Design and fabrication of multilayer inkjet-printed passive components for printed electronics circuit development. *Journal of Manufacturing Processes* **2018,** *31*, 364-371.
(123) Ionescu, C.; Svasta, P.; Vasile, A.; Bonfert, D. In *Investigations on organic printed resistors based on PEDOT:PSS*, 2012 IEEE 18th International Symposium for Design and Technology in Electronic Packaging (SIITME), 25-28 Oct. 2012; 2012; pp 85-89.
(124) Wang, G.; Tao, X.; Xin, J. H.; Fei, B. Modification of Conductive Polymer for Polymeric Anodes of Flexible Organic Light-Emitting Diodes. *Nanoscale Res. Lett.* **2009,** *4* (7), 613-617.
(125) Ouyang, J.; Chu, C. W.; Chen, F. C.; Xu, Q.; Yang, Y. High-Conductivity Poly(3,4-ethylenedioxythiophene):Poly(styrene sulfonate) Film and Its Application in Polymer Optoelectronic Devices. *Adv. Funct. Mater.* **2005,** *15* (2), 203-208.
(126) Chen, B.; Cui, T.; Liu, Y.; Varahramyan, K. All-Polymer *RC* Filter Circuits Fabricated with Inkjet Printing Technology. *Solid·State Electron.* **2003,** *47* (5), 841-847.
(127) Liu, Y.; Cui, T.; Varahramyan, K. All-polymer Capacitor Fabricated with Inkjet Printing Technique. *Solid·State Electron.* **2003,** *47* (9), 1543-1548.
(128) Castro, H. F.; Correia, V.; Sowade, E.; Mitra, K. Y.; Rocha, J. G.; Baumann, R. R.; Lanceros-Méndez, S. All-inkjet-printed low-pass filters with adjustable cutoff frequency

consisting of resistors, inductors and transistors for sensor applications. *Org. Electron.* **2016,** *38*, 205-212.
(129) Ouyang, J.; Xu, Q.; Chu, C.-W.; Yang, Y.; Li, G.; Shinar, J. On the mechanism of conductivity enhancement in poly(3,4-ethylenedioxythiophene):poly(styrene sulfonate) film through solvent treatment. *Polymer* **2004,** *45* (25), 8443-8450.
(130) Horowitz, P.; Hill, W. *The Art of Electronics*, 2nd edition ed.; New York, NY : Cambridge University Press: New York, NY, 1989; p 273-275.
(131) Sani, N.; Robertsson, M.; Cooper, P.; Wang, X.; Svensson, M.; Andersson Ersman, P.; Norberg, P.; Nilsson, M.; Nilsson, D.; Liu, X.; Hesselbom, H.; Akesso, L.; Fahlman, M.; Crispin, X.; Engquist, I.; Berggren, M.; Gustafsson, G. All-printed diode operating at 1.6 GHz. *Proceedings of the National Academy of Sciences* **2014,** *111* (33), 11943-11948.
(132) Facchetti, A. Printed diodes operating at mobile phone frequencies. *Proceedings of the National Academy of Sciences* **2014,** *111* (33), 11917-11918.
(133) Myny, K.; Steudel, S.; Vicca, P.; Genoe, J.; Heremans, P. An integrated double half-wave organic Schottky diode rectifier on foil operating at 13.56 MHz. *Appl. Phys. Lett.* **2008,** *93* (9), 093305.
(134) Güllü, Ö.; Aydoğan, Ş.; Türüt, A. Fabrication and electrical characteristics of Schottky diode based on organic material. *Microelectron. Eng.* **2008,** *85* (7), 1647-1651.
(135) Lilja, K. E.; Bäcklund, T. G.; Lupo, D.; Hassinen, T.; Joutsenoja, T. Gravure printed organic rectifying diodes operating at high frequencies. *Org. Electron.* **2009,** *10* (5), 1011-1014.
(136) Berggren, M.; Nilsson, D.; Robinson, N. D. Organic materials for printed electronics. *Nat. Mater.* **2007,** *6*, 3.
(137) Chu, Y.; Qian, C.; Chahal, P.; Cao, C. Printed Diodes: Materials Processing, Fabrication, and Applications. *Advanced Science* **2019,** *6* (6), 1801653.
(138) Rajbhandari, G.; Vanaraj, P. W.; Maskey, B. B.; Park, H.; Sapkota, A.; Jung, Y.; Majima, Y.; Cho, G. An Electroactive Binder in the Formulation of IGZO Ink to Print an IGZO-Based Rectifier for Harvesting Direct Current (DC) Power from the Near Field Communication (NFC) Signal of a Smartphone. *Adv. Electron. Mater.* **2018,** *4* (8), 1800078.

(139) Heljo, P. S.; Li, M.; Lilja, K. E.; Majumdar, H. S.; Lupo, D. Printed Half-Wave and Full-Wave Rectifier Circuits Based on Organic Diodes. *IEEE Trans. Electron Devices* **2013,** *60* (2), 870-874.
(140) Sun, Y.; Kim, H.-S.; Menard, E.; Kim, S.; Adesida, I.; Rogers, J. A. Printed Arrays of Aligned GaAs Wires for Flexible Transistors, Diodes, and Circuits on Plastic Substrates. *Small* **2006,** *2* (11), 1330-1334.
(141) Liu, Y.; Cui, T. Polymer-Based Rectifying Diodes on a Glass Substrate Fabricated by Ink-Jet Printing. *Macromol. Rapid Commun.* **2005,** *26* (4), 289-292.
(142) Mitra, K. Y.; Sternkiker, C.; Martínez-Domingo, C.; Sowade, E.; Ramon, E.; Carrabina, J.; Gomes, H. L.; Baumann, R. R. Inkjet printed metal insulator semiconductor (MIS) diodes for organic and flexible electronic application. *Flexible and Printed Electronics* **2017,** *2* (1), 015003.
(143) Secor, E. B.; Prabhumirashi, P. L.; Puntambekar, K.; Geier, M. L.; Hersam, M. C. Inkjet Printing of High Conductivity, Flexible Graphene Patterns. *The Journal of Physical Chemistry Letters* **2013,** *4* (8), 1347-1351.